

RWTH AACHEN UNIVERSITY

MASTER THESIS

---

**Sterile neutrino production  
mechanisms in the presence of  
non-standard interactions**

---

*Author:*

Aaroodd UJJAYINI  
RAMACHANDRAN

*Supervisor:*

Prof. Dr. Achim STAHL

*Co-supervisor:*

Dr. Werner RODEJOHANN

*A thesis submitted in fulfillment of the requirements  
for the degree of M. Sc. RWTH*

*in the*

Department of Physics

26th November, 2021



## *Abstract*

Active-sterile mixing is the simplest mechanism to produce sterile neutrinos in the early Universe. However, the generic production mechanism, known as the Dodelson-Widrow mechanism, is in tension with the astrophysical bounds coming from structure formation and X-ray observations. Thus, it is necessary to introduce new interactions to modify the DW production, as this mechanism is unavoidable if we assume non-zero mixing between neutrino flavours. In contrast to previous studies, we employ an effective field theory treatment to introduce non-standard neutrino interactions to the early Universe. We work out the details of scalar, pseudoscalar and axial vector self-interactions with heavy mediators. We find that the production of keV sterile neutrinos can be enhanced or suppressed depending on the non-standard interaction strength, and this helps the mechanism evade astrophysical constraints or move closer to future experimental sensitivities.



# Contents

<b>Abstract</b>	<b>iii</b>
<b>1 Introduction</b>	<b>1</b>
<b>2 Massive neutrinos</b>	<b>3</b>
2.1 Neutrino masses . . . . .	4
2.2 Neutrino oscillations . . . . .	7
2.2.1 Neutrino oscillations in vacuum . . . . .	10
2.2.2 Neutrino oscillations in a medium . . . . .	11
2.3 Sterile neutrino dark matter production mechanisms . . . . .	13
2.3.1 Non-resonant production . . . . .	15
2.3.2 Resonant production . . . . .	16
2.3.3 Production from scalar decays . . . . .	17
2.4 Experimental searches for sterile neutrino dark matter . . . . .	18
2.4.1 Single beta decay . . . . .	18
2.4.2 Electron capture decay . . . . .	19
2.5 Non-standard neutrino interactions . . . . .	20
2.5.1 Non-Standard neutrino Self-Interactions (NSSIs) . . . . .	21
<b>3 Dodelson-Widrow mechanism in presence of NSSIs</b>	<b>23</b>
3.1 Basic Dodelson-Widrow mechanism . . . . .	23
3.1.1 The sterile neutrino Boltzmann equation . . . . .	23
3.1.2 Active neutrino interaction rate in the Standard Model . . . . .	26
3.1.3 The Standard Model effective potential . . . . .	27
3.1.4 Numerical implementation of the Boltzmann equation . . . . .	28
3.2 Dodelson-Widrow mechanism in presence of NSSIs . . . . .	31
3.2.1 Non-standard neutrino self-interactions . . . . .	31
3.2.2 Non-standard self-interaction rate . . . . .	31
3.2.3 Non-standard self-interaction effective potential . . . . .	32
3.2.4 Numerical implementation . . . . .	33
3.2.5 Results and discussion . . . . .	34
Differential sterile neutrino production rate . . . . .	34
Sterile neutrino distribution function . . . . .	36
Sterile neutrino relic abundance . . . . .	40
Free streaming length . . . . .	44
<b>4 Conclusion and outlook</b>	<b>47</b>
<b>A Analytical solution of the Boltzmann equation</b>	<b>49</b>
A.1 Formal solution . . . . .	49
A.2 Calculation of relic abundance . . . . .	52

<b>B Calculation of non-standard neutrino self-interaction rate</b>	<b>55</b>
B.1 Total cross section . . . . .	57
B.2 Interaction rate . . . . .	58
<b>C Calculation of NSSI thermal potential</b>	<b>61</b>
C.1 Neutrino dispersion relation . . . . .	61
C.2 Effective potential . . . . .	62
C.3 Calculation of self-energy . . . . .	63
<b>Bibliography</b>	<b>67</b>
<b>Acknowledgements</b>	<b>75</b>

# List of Figures

2.1	Three-flavour oscillation parameters from global fit as of July 2020 [28].	7
2.2	Normal and Inverted mass hierarchy of active neutrinos. $0 - 2\pi$ represents CP-violating phase, $\delta_{CP}$ (Taken from [37]).	10
2.3	Evolution of dark matter yield with inverse temperature $x$ . The thick black line indicates the equilibrium yield $Y_{DM}^{\text{eq}}$ . Dashed coloured lines represent the freeze-in scenario and solid coloured lines represents the freeze-out scenario, where arrows point in the increasing coupling strength for the two processes (Taken from [43]).	15
2.4	Sterile neutrino distribution functions: Resonant and non-resonant production (Taken from [11]).	17
2.5	Sterile neutrino production via scalar decay (Taken from [11]).	18
a	Scalar freezes out.	18
b	Scalar freezes in.	18
2.6	Possible effect of sterile neutrino on beta decay spectrum. Dotted line represent the standard beta decay spectrum and red line represents the effect of a sterile neutrino with a mass, $m_s = 10$ keV and mixing angle $\sin^2 \theta = 0.2$ (Taken from [63]).	19
2.7	Effect of sterile neutrinos on electron capture in $^{163}\text{Ho}$ . Black line represent the standard case without sterile neutrinos and coloured line represents the various cases of non-zero sterile neutrino masses (Taken from [64]).	19
3.1	Effective number of relativistic degrees of freedom in the early Universe as a function of temperature. The dotted line indicate the entropic degrees of freedom. Decoupling of particles from the plasma at different temperatures are also shown (Taken from [78]).	26
3.2	$T$ Vs $C_a(T)$ for $a = e, \mu, \tau$ (Taken from [48]).	27
3.3	Self-energy contributions to effective potential. $f$ represents any fermion species in the background.	28
3.4	Sterile neutrino distribution function for the basic Dodelson-Widrow mechanism as a function of rescaled momentum $r$ . The Fermi-Dirac distribution is indicated as a blue line for comparison. The brown dotted line represents the ratio $f_{DW}/f_{FD}$ .	29
3.5	Sterile neutrino parameter space for the basic Dodelson-Widrow mechanism. Blue dot represent the benchmark point taken for Fig. 3.4. The black line corresponds to full dark matter abundance provided by the basic DW scenario. The grey lines represent the cocktail DM scenario, where only a fraction of the dark matter is produced by the basic DW mechanism. Experimental bounds featured in the plot are explained in Sec. 3.1.4.	30
3.6	NSSI contribution to the interaction rate.	32
3.7	NSSI contribution to the active neutrino self-energy.	33

3.8	Sterile neutrino production rate as a function of temperature $T$ for the Dodelson-Widrow mechanism in presence of a pseudoscalar NSSI. The thick black line corresponds to the basic DW scenario. The dashed black line corresponds to the NSSI strength that gives the correct abundance in the new production mechanism. NSSI strength $\epsilon$ is colour coded in the bar legend and $r = 1$ . . . . .	35
a	$m_\phi = 10 \text{ GeV}$ . . . . .	35
b	$m_\phi = 50 \text{ GeV}$ . . . . .	35
c	$m_\phi = 100 \text{ GeV}$ . . . . .	35
3.9	Sterile neutrino distribution function for the Dodelson-Widrow mechanism in presence of a scalar NSSI as a function of rescaled momentum $r = p/T$ . The black line corresponds to the basic DW scenario. NSSI strength $\epsilon$ is colour coded in the bar legend. . . . .	37
a	$m_\phi = 10 \text{ GeV}$ . . . . .	37
b	$m_\phi = 50 \text{ GeV}$ . . . . .	37
c	$m_\phi = 100 \text{ GeV}$ . . . . .	37
3.10	Sterile neutrino distribution function for the Dodelson-Widrow mechanism in presence of a pseudoscalar NSSI as a function of rescaled momentum $r = p/T$ . The black line corresponds to the basic DW scenario. NSSI strength $\epsilon$ is colour coded in the bar legend. . . . .	38
a	$m_\phi = 10 \text{ GeV}$ . . . . .	38
b	$m_\phi = 50 \text{ GeV}$ . . . . .	38
c	$m_\phi = 100 \text{ GeV}$ . . . . .	38
3.11	Sterile neutrino distribution function for the Dodelson-Widrow mechanism in presence of an axial vector NSSI as a function of rescaled momentum $r = p/T$ . The black line corresponds to the basic DW scenario. NSSI strength $\epsilon$ is colour coded in the bar legend. . . . .	39
a	$m_\phi = 10 \text{ GeV}$ . . . . .	39
b	$m_\phi = 50 \text{ GeV}$ . . . . .	39
c	$m_\phi = 100 \text{ GeV}$ . . . . .	39
3.12	Relic abundance parameter space for DW mechanism with the scalar NSSI. Figures in the right represent cocktail DM scenario with 10% relic abundance. NSSI strength $\epsilon_S$ is colour coded from 0.1 to 100 in the bar legend. The black line corresponds to the standard DW scenario. Beige (HUNTER), black (KATRIN/TRISTAN), and blue (ECHO) dashed lines represent experimental sensitivities. X-ray constraints for corresponding relic abundance shown in purple. . . . .	41
a	$m_\phi = 10 \text{ GeV}, \Omega_s h^2 = 0.12$ . . . . .	41
b	$m_\phi = 10 \text{ GeV}, \Omega_s h^2 = 0.012$ . . . . .	41
c	$m_\phi = 50 \text{ GeV}, \Omega_s h^2 = 0.12$ . . . . .	41
d	$m_\phi = 50 \text{ GeV}, \Omega_s h^2 = 0.012$ . . . . .	41
e	$m_\phi = 100 \text{ GeV}, \Omega_s h^2 = 0.12$ . . . . .	41
f	$m_\phi = 100 \text{ GeV}, \Omega_s h^2 = 0.012$ . . . . .	41
3.13	Relic abundance parameter space for DW mechanism with the pseudoscalar NSSI. Figures in the right represent cocktail DM scenario with 10% relic abundance. NSSI strength $\epsilon_P$ is colour coded from 0.1 to 100 in the bar legend. The black line corresponds to the standard DW scenario. Beige (HUNTER), black (KATRIN/TRISTAN), and blue (ECHO) dashed lines represent experimental sensitivities. X-ray constraints for corresponding relic abundance shown in purple. . . . .	42
a	$m_\phi = 10 \text{ GeV}, \Omega_s h^2 = 0.12$ . . . . .	42

b	$m_\phi = 10 \text{ GeV}, \Omega_s h^2 = 0.012$	42
c	$m_\phi = 50 \text{ GeV}, \Omega_s h^2 = 0.12$	42
d	$m_\phi = 50 \text{ GeV}, \Omega_s h^2 = 0.012$	42
e	$m_\phi = 100 \text{ GeV}, \Omega_s h^2 = 0.12$	42
f	$m_\phi = 100 \text{ GeV}, \Omega_s h^2 = 0.012$	42
3.14	Relic abundance parameter space for DW mechanism with the axial vector NSSI. Figures in the right represent cocktail DM scenario with 10% relic abundance. NSSI strength $\epsilon_A$ is colour coded from 0.1 to 100 in the bar legend. The black line corresponds to the standard DW scenario. Beige (HUNTER), black (KATRIN/TRISTAN), and blue (ECHO) dashed lines represent experimental sensitivities. X-ray constraints for corresponding relic abundance shown in purple.	43
a	$m_\phi = 10 \text{ GeV}, \Omega_s h^2 = 0.12$	43
b	$m_\phi = 10 \text{ GeV}, \Omega_s h^2 = 0.012$	43
c	$m_\phi = 50 \text{ GeV}, \Omega_s h^2 = 0.12$	43
d	$m_\phi = 50 \text{ GeV}, \Omega_s h^2 = 0.012$	43
e	$m_\phi = 100 \text{ GeV}, \Omega_s h^2 = 0.12$	43
f	$m_\phi = 100 \text{ GeV}, \Omega_s h^2 = 0.012$	43
3.15	Free streaming length as a function of $\epsilon$ . Grey areas in the plot represent regions excluded for warm dark matter. Scalar NSSI gives the same results as pseudoscalar NSSI and hence not included here.	45
a	Dodelson-Widrow mechanism with the pseudoscalar NSSI	45
b	Dodelson-Widrow mechanism with the axial vector NSSI	45
B.1	Non-standard contribution to the interaction rate	55
a	Feynman diagrams in the full theory	55
b	Feynman diagram in the NSSI	55
C.1	NSSI contribution to the self-energy	63



## Chapter 1

# Introduction

The Standard Model of particle physics is one of the most successful theories in the history of natural sciences. Despite its undeniable experimental successes in the past decades, we know that the Standard Model cannot be a complete theory of nature [1]. The Standard Model fails to explain what constitutes around 95% of the energy density of the observable universe: dark energy (69%) and dark matter (26%). In addition to these known unknowns, mathematical inconsistencies and challenges such as neutrino masses and matter-antimatter asymmetry compel us to go beyond the Standard Model to have a better understanding of the Universe.

Around 85% of the matter content (26% of the energy density) in the observable universe is invisible to us in the form of dark matter [2]. The concept of dark matter dates back to the early 20th century, before the Standard Model. Henri Poincaré coined the term “dark matter” (“matière obscure” in the original French) to comment on Lord Kelvin’s idea that dark bodies can explain the discrepancy between rotation and stellar mass of the Milky Way galaxy [3]. But, modern history of dark matter begins in 1933 when Swiss astronomer Fritz Zwicky published his paper on the dispersion of velocity in the Coma galaxy cluster [4]. Zwicky estimated the mass of the Coma cluster using the virial theorem. Combining the results with observation, he concluded that dark matter is present in a much greater amount than luminous matter.

The concept of dark matter has evolved considerably in the late 1900s [5]. Improvements in multi-messenger astronomy techniques helped to confirm the evidence of dark matter. In addition to rotation curves of spiral galaxies, the cosmic microwave background (CMB) measurements [2] and gravitational lensing studies of the Bullet cluster [6] provide strong evidence of the existence of dark matter. A good dark matter candidate is characterized by being stable, neutral, non-baryonic, and collisionless [7]. Additionally, it has to be compatible with bounds from the Big Bang nucleosynthesis and large scale structure formation. No Standard Model particle falls under the above criteria except neutrinos, which can be hot dark matter. However, limits on structure formation rule out neutrinos as the sole dark matter particle. Nonetheless, neutrinos and weak interactions are an interesting starting point for dark matter research. In fact, the heavy neutrino proposed by Lee & Weinberg [8] was one of the first dark matter candidates. *Weakly Interacting Massive Particles (WIMPs)* are one of the most studied species of dark matter. WIMPs naturally arise from supersymmetric extensions of the Standard Model, and an interaction strength similar to weak interaction gives the correct dark matter relic abundance. This coincidence, known as the *WIMP miracle*, led physicists to extensively search for WIMPs in a variety of experiments. However, there has been no evidence of any such particles so far [9]. Several other proposals are tailored for specific problems in the Standard Model. *Axion* [10], a light spin-0 scalar, could solve the strong CP problem. The main focus

of this work, *Sterile neutrinos* [11], is another well-motivated dark matter candidate that can explain massive neutrinos.

The neutrino oscillations, first predicted by Bruno Pontecorvo in 1957-1958 [12, 13] and later experimentally confirmed by several solar, atmospheric, and reactor neutrino experiments [14] prove that neutrinos possess a tiny but non-zero mass. Neutrinos are massless and left-handed in the Standard Model. But, if we extend the Standard Model with right-handed neutrinos, the See-saw mechanism provides an elegant way to explain active neutrino masses [15]. These right-handed neutrino fields, unrelated to weak interactions, gives more freedom in model building.

The right-handed partner of active neutrinos is referred to as *sterile neutrinos* because, unlike active neutrinos, they do not have weak interaction. But neutrino oscillation is a quantum mechanical process that is valid for all flavours. Thus, sterile and active neutrinos oscillate and mix with each other. This mixing is our gateway to the detection of sterile neutrinos. Direct neutrino mass experiments such as KATRIN [16], TRISTAN [17], ECHo [18], and HUNTER [19] can search for sterile neutrinos in the laboratory [20]. If discovered, sterile neutrinos with masses ranging from eV to TeV could solve various aspects of the neutrino puzzle. Sterile neutrinos in the keV mass range can act as a warm dark matter candidate [21]. Sterile neutrino dark matter produces a non-thermal momentum distribution, which can have non-trivial consequences on structure formation. This makes keV sterile neutrinos interesting from a phenomenological perspective. An unidentified X-ray line of 3.5 keV [22, 23] sparked a lot of interest in the sterile neutrino dark matter research. This line could be explained by the radiative decay of a sterile neutrino with a mass  $\approx 7.1$  keV. As there are no signs of thermal WIMPs yet, sterile neutrino dark matter provides a theoretically well-motivated and experimentally promising alternative. As we will show in this work, non-standard neutrino interactions could further enhance the keV sterile neutrino parameter space and provide better testability in future experiments.

This work focuses mainly on the non-resonant production of sterile neutrino dark matter. Chapter 2 provides an overview and motivation of sterile neutrinos. In Chapter 3, we will look closely at non-resonant production of sterile neutrinos, also known as the *Dodelson-Widrow Mechanism*, in the presence of *Non-Standard neutrino Self-Interactions (NSSIs)*. Conclusions are presented in Chapter 4 with outlook and possibilities for future work.

## Chapter 2

# Massive neutrinos

Neutrinos, first proposed by Wolfgang Pauli to explain  $\beta$ -decay [24], have always had a special place in the Standard Model. From being only massless fermion in the Standard Model to occasionally claiming faster-than-light status [25], Neutrinos were always troublemakers. We are still unsure whether they are Dirac or Majorana particles. However, we are sure that they oscillate between flavours and have a tiny yet non-zero mass. The neutrino oscillations, proposed by Bruno Pontecorvo in 1957 [12, 13] and experimentally confirmed after few decades by Super-Kamiokande [26] and SNO [27] collaborations, are the first solid evidence of physics beyond the Standard Model (BSM). We will study more about sterile neutrinos, a natural extension of the Standard Model and an elegant solution to the neutrino puzzle.

The Standard Model is a non-abelian gauge theory with  $SU(3)_C \times SU(2)_L \times U(1)_Y$  symmetry. Leptons in the Standard Model interact under Electroweak interactions, and quarks interact with both electroweak and strong forces. Field content of the Standard Model fermions are given in Table 2.1. If there exists a sterile neutrino, it would be a total singlet,  $(\mathbf{1}, \mathbf{1}, 0)$ , under the Standard Model gauge group. i.e., it does not interact with Strong ( $g$ ), weak ( $W, Z$ ) or electromagnetic ( $\gamma$ ) mediators. But, it could interact with Higgs scalar ( $H$ ) to couple with active neutrino sector to acquire mass.

	I	II	III	$SU(3)_C$	$SU(2)_L$	$U(1)_Y$
Leptons	$\begin{pmatrix} \nu_e \\ e \end{pmatrix}_L$	$\begin{pmatrix} \nu_\mu \\ \mu \end{pmatrix}_L$	$\begin{pmatrix} \nu_\tau \\ \tau \end{pmatrix}_L$	1	2	-1
	$e_R$	$\mu_R$	$\tau_R$	1	1	-2
Quarks	$\begin{pmatrix} u \\ d \end{pmatrix}_L$	$\begin{pmatrix} c \\ s \end{pmatrix}_L$	$\begin{pmatrix} t \\ b \end{pmatrix}_L$	3	2	+1/3
	$u_R$	$c_R$	$t_R$	3	1	+4/3
	$d_R$	$s_R$	$b_R$	3	1	-2/3

TABLE 2.1: Fermions in the Standard Model.

Bounds from global fits of cosmological observations [2] gives a limit

$$0.06 \text{ eV} < \sum m_\nu \leq 0.12 \text{ eV}$$

on the sum of active neutrino masses. Similarly, the global fit of neutrino experiments [28] provides the best-fit value for the mass square difference:

$$|\Delta m_{21}^2| = 7.42 \times 10^{-5} \text{ eV}^2, \quad |\Delta m_{32}^2| = 2.517 \times 10^{-3} \text{ eV}^2,$$

which translates to one neutrino mass eigenstate with a mass of at least 0.05 eV. In this chapter, we will give an overview of how this tiny but non-zero mass can be achieved and its consequences. We also give a brief overview of non-standard neutrino interactions, which would be useful for the rest of this work.

We mainly follow treatments given by Giunti [29] and the review on theory of neutrinos [15].

## 2.1 Neutrino masses

Fermions in the Standard Model acquire mass through the so-called *Higgs mechanism*. Left-handed doublets and right-handed singlets couple with Higgs Scalar  $\Phi = (\Phi^+, \Phi^0)^T$  through a Yukawa coupling.

$$\mathcal{L}_{e-\text{Yukawa}} = -y_e \bar{L} \Phi e_R + \text{h.c.} = -y_e (\bar{\nu}_L \Phi^+ + \bar{e}_L \Phi^0) e_R + \text{h.c.} . \quad (2.1)$$

As the Higgs scalar gets a vacuum expectation value  $\phi = (0, v)^T$  through spontaneous symmetry breaking, the first part of the Yukawa Lagrangian Eq. (2.1) goes away, and we can write down Dirac mass terms for fermions as

$$\mathcal{L}_{e-\text{mass}} = -y_e \bar{e}_L \Phi^0 e_R + \text{h.c.} = -m_e \bar{e}_L e_R + \text{h.c.} , \text{ where } m_e \equiv y_e v . \quad (2.2)$$

Not only fermion masses, but gauge boson masses are also generated via the Higgs mechanism. Vacuum expectation value is experimentally determined to be  $v = 246.22 \text{ GeV}$  [30]. However, this mass term Lagrangian is not gauge invariant as spontaneous breaking of symmetry changes  $SU(3)_C \times SU(2)_L \times U(1)_Y$  to  $SU(3)_C \times U(1)_{em}$ , which is what we observe in nature.

If we employ the same process to neutrinos by introducing a right-handed neutrino field  $N_R$ , we would get a Dirac mass term,

$$\mathcal{L}_D = -m_D \bar{\nu}_L N_R + \text{h.c.} , \text{ where } m_D \equiv y_\nu v \text{ is the Dirac mass of neutrino.} \quad (2.3)$$

Comparing Yukawa coupling  $y_\nu$  required for eV-scale active neutrino masses with other Yukawa couplings,

$$y_\nu = \frac{m_\nu}{v} \sim 4 \times 10^{-13} \ll y_e = 2.9 \times 10^{-6} \ll y_t \sim \mathcal{O}(1) ,$$

extremely small  $y_\nu$  needs further explanation. Thus, we search other possible ways for neutrinos to obtain mass.

Majorana particles are a class of particles that are their own antiparticles [31]. i.e., a Majorana particle  $\psi$  transforms as

$$\hat{C}\psi = \psi^C = C\bar{\psi}^T \quad (2.4)$$

under charge conjugation operator  $\hat{C}$ . Furthermore, Majorana condition  $\psi = \psi^c$  implies

$$\psi = \psi^c = (\psi_L)^c + (\psi_R)^c = (\psi_L)^c + (\psi^c)_L = \psi_L + (\psi_L)^c . \quad (2.5)$$

i.e., left-chiral and right-chiral components of Majorana fermions are dependent.

All the Standard Model fermions are known to be Dirac fermions except neutrinos, which could be either Dirac or Majorana. Hence, we can write down a new Majorana mass term,

$$\mathcal{L}_M = -\frac{1}{2}m_L \overline{(\nu_L)^c} \nu_L - \frac{1}{2}M_R \overline{(N_R)^c} N_R + \text{h.c.}, \quad (2.6)$$

for neutrinos. This term is allowed by SM gauge symmetry, as both  $\overline{(N_R)^c}$  and  $N_R$  are singlets. However, unlike Dirac mass term, Majorana mass term violates lepton number conservation. Even though we have not observed any processes that violate lepton number conservation, lepton number is not a symmetry in the Standard Model. Hence, there are no mathematical restrictions on this term. The Standard Model allows lepton number violating processes such as double beta decay at non-perturbative level. The majority of BSM models feature Lepton flavour Violating (LFV) processes and consider more general symmetries such as  $U(1)_{B-L}$  or  $U(1)_{L_e-L_\mu-L_\tau}$ . Thus, it is not a big leap to write a Majorana mass term in the Lagrangian.

Now, combining both Dirac and Majorana mass terms for neutrinos,

$$\mathcal{L}_\nu = -m_D \overline{\nu_L} N_R - \frac{1}{2}m_L \overline{(\nu_L)^c} \nu_L - \frac{1}{2}M_R \overline{(N_R)^c} N_R + \text{h.c.}, \quad (2.7)$$

where  $m_L$  is Majorana mass of left-handed neutrinos and  $M_R$  is Majorana mass of right-handed neutrinos.

In matrix form,

$$\mathcal{L}_\nu = -\frac{1}{2} \left( \overline{\nu_L}, \overline{(N_R)^c} \right) \begin{pmatrix} m_L & m_D \\ m_D^T & M_R \end{pmatrix} \begin{pmatrix} (\nu_L)^c \\ N_R \end{pmatrix} + \text{h.c.}, \quad (2.8)$$

where we can define neutrino mass matrix,

$$\mathcal{M} = \begin{pmatrix} m_L & m_D \\ m_D^T & M_R \end{pmatrix}. \quad (2.9)$$

In 3 flavour formalism,  $\mathcal{M}$  is a  $6 \times 6$  matrix.

It is important to note that Majorana masses  $M_R, m_L$  are independent of vacuum expectation value  $v$ . Thus, Majorana masses could be much larger than electroweak scale.

Let's try to block diagonalize the neutrino mass matrix so that we can get separate mass terms for left-handed and right-handed neutrinos.

We define a matrix

$$U = \begin{pmatrix} \mathbf{1} - \frac{1}{2}bb^\dagger & b \\ -b^\dagger & \mathbf{1} - \frac{1}{2}b^\dagger b \end{pmatrix}, \quad (2.10)$$

which is unitary at  $\mathcal{O}(b^4)$ .

$$UU^\dagger = U^\dagger U = \begin{pmatrix} 1 + \frac{1}{4}bb^\dagger bb^\dagger & 0 \\ 0 & 1 + \frac{1}{4}b^\dagger bb^\dagger b \end{pmatrix} = 1 + \mathcal{O}(b^4) \simeq 1. \quad (2.11)$$

Now, in order to compute the diagonalized matrix  $\tilde{M} = U^T M U$ ,

$$\begin{aligned} U^T M &= \begin{pmatrix} \mathbf{1} - \frac{1}{2} b b^\dagger & -b^\dagger \\ b & \mathbf{1} - \frac{1}{2} b^\dagger b \end{pmatrix} \begin{pmatrix} m_L & m_D \\ m_D^T & M_R \end{pmatrix} \\ &= \begin{pmatrix} m_L - \frac{1}{2} b^* b^\dagger m_L - b^* m_D^T & m_D - \frac{1}{2} b^* b^T m_D - b^* M_R \\ b^T m_L + m_D^T - \frac{1}{2} b^T b^* m_D^T & b^T m_D + M_R - \frac{1}{2} b^T b^* M_R \end{pmatrix} \end{aligned} \quad (2.12)$$

$$\tilde{M} = U^T M U \simeq \begin{pmatrix} m_L - b^* m_D^T & m_D - b^* M_R \\ m_D^T & b^T m_D + M_R - \frac{1}{2} b^T b^* M_R \end{pmatrix} \begin{pmatrix} \mathbf{1} - \frac{1}{2} b b^\dagger & b \\ -b^\dagger & \mathbf{1} - \frac{1}{2} b^\dagger b \end{pmatrix} \quad (2.13)$$

where we have kept only relevant terms up to  $\mathcal{O}(b^2)$ .

For  $\tilde{M}$  to be diagonal,  $\tilde{M}_{12} = \tilde{M}_{21} = 0$ . Then we can obtain relations,

$$\tilde{M}_{12} \simeq m_L b - b^* m_D^T b + m_D - b^* M_R \simeq m_D - b^* M_R \stackrel{!}{=} 0 \Rightarrow b^* = m_D M_R^{-1}. \quad (2.14)$$

Substituting  $b$  gives us the final diagonalized neutrino mass matrix,

$$\tilde{M} \equiv U^T M U \simeq \begin{pmatrix} m_L - m_D M_R^{-1} m_D^T & 0 \\ 0 & M_R \end{pmatrix} \equiv \begin{pmatrix} m_\nu & 0 \\ 0 & m_s \end{pmatrix}, \quad (2.15)$$

where  $m_\nu, m_s$  represent active, sterile neutrino masses respectively.

Assuming there is no Majorana mass for active neutrinos, i.e.,  $m_L = 0$ , we get

$$m_\nu = -m_D M_R^{-1} m_D^T = -\frac{m_D^2}{M_R}, \quad m_s = M_R. \quad (2.16)$$

this is the famous *type-I see-saw mechanism*.

Assuming Dirac mass of neutrinos arising from Yukawa coupling in the same order of other fermion masses, active neutrino mass  $m_\nu$  can be made small by having a much larger sterile neutrino mass. If a sterile neutrino has GUT scale ( $\sim 10^{14}$  GeV) mass,

$$m_D \sim 100 \text{ GeV} \Rightarrow m_\nu \simeq \frac{(100 \text{ GeV})^2}{10^{14} \text{ GeV}} = 0.1 \text{ eV}. \quad (2.17)$$

These neutrinos with mass several TeV are called *right-handed neutrinos* and are of cosmological significance. However, it is also possible to have smaller sterile masses. Different sterile neutrinos are studied to solve different aspects of neutrino puzzle:

- *eV sterile neutrinos* can explain anomalies in laboratory oscillation experiments [32].
- *keV sterile neutrinos* can act as Dark Matter candidates [33].
- *GeV to TeV scale neutrinos* can explain matter-antimatter asymmetry via Leptogenesis [34, 35].

There are other more complicated models such as *supersymmetry breaking, extra dimensions* to explain neutrino masses. Those are beyond the scope of this overview and reader can refer to detailed reviews [15, 11] for more detailed picture.

## 2.2 Neutrino oscillations

One of the main consequences of neutrino mass is neutrino oscillations. All fermions propagate as a combination of mass eigenstates but we can only observe them as flavour (weak interaction) eigenstates. Similar to quark sector and CKM matrix, neutrino flavour eigenstates are connected to mass eigenstates by neutrino mixing matrix often called *Pontecorvo-Maki-Nakagawa-Sakata matrix (PMNS matrix)*.

$$\begin{pmatrix} \nu_e \\ \nu_\mu \\ \nu_\tau \end{pmatrix} = U_{\text{PMNS}}(\theta_{12}, \theta_{13}, \theta_{23}; \delta_{CP}) \begin{pmatrix} \nu_1 \\ \nu_2 \\ \nu_3 \end{pmatrix}, \quad (2.18)$$

where  $\theta_{ij}$  is the mixing angle between mass eigenstates  $i, j$  and  $\delta_{CP}$  is the CP-violating phase.

Global fit from various neutrino experiments NuSTAR [28] gives

$$|U|_{3\sigma}^{\text{PMNS}} = \begin{pmatrix} 0.801 \rightarrow 0.845 & 0.513 \rightarrow 0.579 & 0.143 \rightarrow 0.155 \\ 0.234 \rightarrow 0.500 & 0.471 \rightarrow 0.689 & 0.637 \rightarrow 0.776 \\ 0.271 \rightarrow 0.525 & 0.477 \rightarrow 0.694 & 0.613 \rightarrow 0.756 \end{pmatrix}, \quad (2.19)$$

with corresponding mixing angles ( $\theta_{ij}$ ) and CP-violating phase  $\delta_{CP}$  given in Fig. 2.1.

Mixing phenomena can be extended for additional flavours. Hence, the following

		NuFIT 5.0 (2020)			
without SK atmospheric data		Normal Ordering (best fit)		Inverted Ordering ( $\Delta\chi^2 = 2.7$ )	
		bfp $\pm 1\sigma$	3 $\sigma$ range	bfp $\pm 1\sigma$	3 $\sigma$ range
$\sin^2 \theta_{12}$		$0.304^{+0.013}_{-0.012}$	$0.269 \rightarrow 0.343$	$0.304^{+0.013}_{-0.012}$	$0.269 \rightarrow 0.343$
$\theta_{12}/^\circ$		$33.44^{+0.78}_{-0.75}$	$31.27 \rightarrow 35.86$	$33.45^{+0.78}_{-0.75}$	$31.27 \rightarrow 35.87$
$\sin^2 \theta_{23}$		$0.570^{+0.018}_{-0.024}$	$0.407 \rightarrow 0.618$	$0.575^{+0.017}_{-0.021}$	$0.411 \rightarrow 0.621$
$\theta_{23}/^\circ$		$49.0^{+1.1}_{-1.4}$	$39.6 \rightarrow 51.8$	$49.3^{+1.0}_{-1.2}$	$39.9 \rightarrow 52.0$
$\sin^2 \theta_{13}$		$0.02221^{+0.00068}_{-0.00062}$	$0.02034 \rightarrow 0.02430$	$0.02240^{+0.00062}_{-0.00062}$	$0.02053 \rightarrow 0.02436$
$\theta_{13}/^\circ$		$8.57^{+0.13}_{-0.12}$	$8.20 \rightarrow 8.97$	$8.61^{+0.12}_{-0.12}$	$8.24 \rightarrow 8.98$
$\delta_{CP}/^\circ$		$195^{+51}_{-25}$	$107 \rightarrow 403$	$286^{+27}_{-32}$	$192 \rightarrow 360$
$\frac{\Delta m_{21}^2}{10^{-5} \text{ eV}^2}$		$7.42^{+0.21}_{-0.20}$	$6.82 \rightarrow 8.04$	$7.42^{+0.21}_{-0.20}$	$6.82 \rightarrow 8.04$
$\frac{\Delta m_{3\ell}^2}{10^{-3} \text{ eV}^2}$		$+2.514^{+0.028}_{-0.027}$	$+2.431 \rightarrow +2.598$	$-2.497^{+0.028}_{-0.028}$	$-2.583 \rightarrow -2.412$
with SK atmospheric data		Normal Ordering (best fit)		Inverted Ordering ( $\Delta\chi^2 = 7.1$ )	
		bfp $\pm 1\sigma$	3 $\sigma$ range	bfp $\pm 1\sigma$	3 $\sigma$ range
$\sin^2 \theta_{12}$		$0.304^{+0.012}_{-0.012}$	$0.269 \rightarrow 0.343$	$0.304^{+0.013}_{-0.012}$	$0.269 \rightarrow 0.343$
$\theta_{12}/^\circ$		$33.44^{+0.77}_{-0.74}$	$31.27 \rightarrow 35.86$	$33.45^{+0.78}_{-0.75}$	$31.27 \rightarrow 35.87$
$\sin^2 \theta_{23}$		$0.573^{+0.016}_{-0.020}$	$0.415 \rightarrow 0.616$	$0.575^{+0.016}_{-0.019}$	$0.419 \rightarrow 0.617$
$\theta_{23}/^\circ$		$49.2^{+0.9}_{-1.2}$	$40.1 \rightarrow 51.7$	$49.3^{+0.9}_{-1.1}$	$40.3 \rightarrow 51.8$
$\sin^2 \theta_{13}$		$0.02219^{+0.00062}_{-0.00063}$	$0.02032 \rightarrow 0.02410$	$0.02238^{+0.00063}_{-0.00062}$	$0.02052 \rightarrow 0.02428$
$\theta_{13}/^\circ$		$8.57^{+0.12}_{-0.12}$	$8.20 \rightarrow 8.93$	$8.60^{+0.12}_{-0.12}$	$8.24 \rightarrow 8.96$
$\delta_{CP}/^\circ$		$197^{+27}_{-24}$	$120 \rightarrow 369$	$282^{+26}_{-30}$	$193 \rightarrow 352$
$\frac{\Delta m_{21}^2}{10^{-5} \text{ eV}^2}$		$7.42^{+0.21}_{-0.20}$	$6.82 \rightarrow 8.04$	$7.42^{+0.21}_{-0.20}$	$6.82 \rightarrow 8.04$
$\frac{\Delta m_{3\ell}^2}{10^{-3} \text{ eV}^2}$		$+2.517^{+0.026}_{-0.028}$	$+2.435 \rightarrow +2.598$	$-2.498^{+0.028}_{-0.028}$	$-2.581 \rightarrow -2.414$

FIGURE 2.1: Three-flavour oscillation parameters from global fit as of July 2020 [28].

treatment is also valid for active-sterile neutrino mixing.

Starting with

$$|\nu_\alpha\rangle = U \cdot |\nu_i\rangle = \sum_{i=1}^n U_{\alpha i} |\nu_i\rangle , \quad (2.20)$$

where  $\nu_\alpha$  are the flavour eigenstates and  $\nu_i$  are mass eigenstates with  $i = 1, 2, 3, \dots$ . In the Standard Model context, there are three neutrino flavours,  $\alpha = \{e, \mu, \tau\}$  and three mass eigenstates,  $i = \{1, 2, 3\}$ .

We assume mass eigenstates are orthonormal. Then, unitarity of mixing matrix  $U$  implies flavour eigenstates are also orthonormal. i.e.,

$$\langle \nu_i | \nu_j \rangle = \delta_{ij} , \langle \nu_\alpha | \nu_\beta \rangle = \delta_{\alpha\beta} . \quad (2.21)$$

Massive eigenstates that propagate through space-time are eigenstates of Hamiltonian,

$$\mathcal{H} |\nu_i\rangle = E_i |\nu_i\rangle \quad (2.22)$$

with energy eigenvalues

$$E_i = \sqrt{\vec{p}^2 + m_i^2} . \quad (2.23)$$

Then, Schrödinger equation for mass eigenstates,

$$i \frac{d}{dt} |\nu_i(t)\rangle = \mathcal{H} |\nu_i(t)\rangle , \quad (2.24)$$

implies that the massive neutrino states evolve as plane waves:

$$|\nu_i(t)\rangle = e^{-iE_i t} |\nu_i\rangle . \quad (2.25)$$

Substituting mass eigenstate in Eq. (2.25) to Eq. (2.20),

$$|\nu_\alpha(t)\rangle = \sum_i U_{\alpha i} e^{-iE_i t} |\nu_i\rangle , \quad (2.26)$$

where  $|\nu_\alpha(t)\rangle$  now describes the evolution of flavour eigenstate created at  $t = 0$  with  $|\nu_\alpha(t=0)\rangle = |\nu_\alpha\rangle$ .

Expressing massive eigenstates states in terms of flavour states by inverting mixing matrix

$$|\nu_i\rangle = \sum_\alpha U_{\alpha i}^* |\nu_\alpha\rangle , \quad (2.27)$$

and substituting into Eq. (2.26), we obtain a relation connecting different flavour eigenstates:

$$|\nu_\alpha(t)\rangle = \sum_{\beta=e,\mu,\tau} \left( \sum_i U_{\alpha i} e^{-iE_i t} U_{\beta i}^* \right) |\nu_\beta\rangle . \quad (2.28)$$

Eq. (2.28) describes the evolution of flavour eigenstate with time  $t$ . Amplitude of flavour  $\nu_\beta$  in  $\nu_\alpha$  after time  $t$  is given by,

$$\psi_{\nu_\alpha \rightarrow \nu_\beta}(t) \equiv \langle \nu_\beta | \nu_\alpha(t) \rangle = \sum_i U_{\alpha i}^* U_{\beta i} e^{-i E_i t}. \quad (2.29)$$

Transition probability can be calculated as

$$P_{\nu_\alpha \rightarrow \nu_\beta}(t) = |A_{\nu_\alpha \rightarrow \nu_\beta}(t)|^2 = \sum_{i,j} U_{\alpha i}^* U_{\beta i} U_{\alpha j} U_{\beta j}^* e^{-i(E_i - E_j)t}. \quad (2.30)$$

Assuming neutrinos are ultra-relativistic, the dispersion relation in Eq. (2.23) can be approximated by

$$E_i \simeq E + \frac{m_i^2}{2E}, \text{ where } E = |\vec{p}|. \quad (2.31)$$

Now energy difference  $\Delta E$  can be approximated as

$$\Delta E = E_i - E_j \simeq \frac{\Delta m_{ij}^2}{2E}, \quad \Delta m_{ij}^2 \equiv m_i^2 - m_j^2, \quad (2.32)$$

where  $\Delta m_{ij}^2$  is the squared-mass difference.

Then, transition probability Eq. (2.30) can be rewritten as

$$P_{\nu_\alpha \rightarrow \nu_\beta}(t) = \sum_{i,j} U_{\alpha i}^* U_{\beta i} U_{\alpha j} U_{\beta j}^* \exp\left(-i \frac{\Delta m_{ij}^2 t}{2E}\right). \quad (2.33)$$

Propagation length  $L$  is often the measurable quantity in neutrino experiments instead of propagation time  $t$ . As we already made the assumption that neutrinos are ultra-relativistic, we have  $t \approx L$ , gives us final form of neutrino transition probability,

$$P_{\nu_\alpha \rightarrow \nu_\beta}(L, E) = \sum_{i,j} U_{\alpha i}^* U_{\beta i} U_{\alpha j}^* U_{\beta j} \exp\left(-i \frac{\Delta m_{ij}^2 L}{2E}\right). \quad (2.34)$$

Restructuring Eq. (2.34),

$$P_{\nu_\alpha \rightarrow \nu_\beta}(L, E) = \sum_k |U_{\alpha i}|^2 |U_{\beta i}|^2 + 2\Re \sum_{i>j} U_{\alpha i} U_{\beta i}^* U_{\alpha j}^* U_{\beta j} \exp\left(-i \frac{\Delta m_{ij}^2 L}{2E}\right) \quad (2.35)$$

separates transition probability to incoherent transition probability and oscillation probability.

It is important to note that neutrino oscillations can only tell us difference of squared masses, not absolute masses of neutrinos. It is still not clear whether neutrino mass eigenstates are arranged as  $m_1 < m_2 < m_3$  (*Normal Ordering*) or  $m_3 < m_1 < m_2$  (*Inverted Ordering*) (Fig. 2.2). Cosmological observations and experiments that consider single  $\beta$ -decay such as KATRIN [16] can tell us more about absolute mass of neutrinos. Another process that can shed light on absolute mass on neutrinos is neutrinoless double beta( $0\nu\beta\beta$ ) decay [36] which have never been observed in nature. Existence of neutrinoless double beta decay will also confirm Majorana nature of neutrinos.

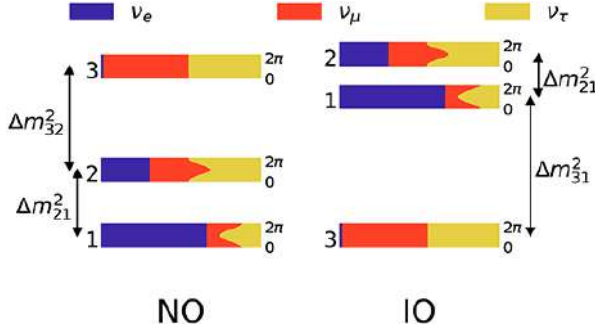


FIGURE 2.2: Normal and Inverted mass hierarchy of active neutrinos.  
0 –  $2\pi$  represents CP-violating phase,  $\delta_{CP}$  (Taken from [37]).

### 2.2.1 Neutrino oscillations in vacuum

Two-flavour neutrino mixing is of high practical importance. Electron neutrino disappearance experiments often use 2-flavour approximation, where  $\nu_\alpha = \nu_e$ , and  $\nu_\beta = c_\mu\nu_\mu + c_\tau\nu_\tau$ , with  $c_\mu^2 + c_\tau^2 = 1$ , as they do not need to distinguish between  $\mu, \tau$  flavours. Sterile neutrino calculations also usually consider one of the active species or a superposition of three flavours as one  $\nu_a$  flavour to mix with sterile state  $\nu_S$  for simplicity.

Let  $\nu_1, \nu_2$ , be the mass eigenstates for flavours  $\nu_\alpha, \nu_\beta$ .

$$\begin{pmatrix} \nu_\alpha \\ \nu_\beta \end{pmatrix} = \begin{pmatrix} \cos(\theta) & \sin(\theta) \\ -\sin(\theta) & \cos(\theta) \end{pmatrix} \begin{pmatrix} \nu_1 \\ \nu_2 \end{pmatrix}, \quad (2.36)$$

where  $\theta$  is the mixing angle.

$$\begin{aligned} |\nu_\alpha\rangle &= \cos(\theta)|\nu_1\rangle + \sin(\theta)|\nu_2\rangle, \\ |\nu_\beta\rangle &= -\sin(\theta)|\nu_1\rangle + \cos(\theta)|\nu_2\rangle. \end{aligned} \quad (2.37)$$

From Eq. (2.34), transition probability in vacuum is given by,

$$P_{\nu_\alpha \rightarrow \nu_\beta}(L, E) = \frac{1}{2} \sin^2 2\theta \left[ 1 - \cos \left( \frac{\Delta m_{12}^2 L}{2E} \right) \right] \quad (2.38)$$

or equivalently,

$$P_{\nu_\alpha \rightarrow \nu_\beta}(L, E) = \sin^2 2\theta \sin^2 \left( \frac{\Delta m_{12}^2 L}{4E} \right). \quad (2.39)$$

Taking time average of Eq. (2.39),

$$\langle P_{\nu_\alpha \rightarrow \nu_\beta} \rangle = \frac{1}{2} \sin^2 2\theta \quad (\alpha \neq \beta). \quad (2.40)$$

We observe that time averaged transition probability in vacuum only depends on the active-sterile mixing angle  $\theta$ .

If we define two flavour states as active,  $\nu_\alpha = \nu_a$ , and sterile,  $\nu_\beta = \nu_s$ :

$$|\nu_a\rangle = \cos(\theta_{as})|\nu\rangle + \sin(\theta_{as})|N\rangle, \quad (2.41)$$

$$|\nu_s\rangle = -\sin(\theta_{as})|\nu\rangle + \cos(\theta_{as})|N\rangle, \quad (2.42)$$

where  $|\nu\rangle, |N\rangle$  are mass eigenstates with eigenvalues  $m_\nu, m_s$  respectively from the neutrino mass matrix from the Eq. (2.15).

We can see that sterile neutrino  $\nu_s$  is an admixture of mass eigenstates of both left- and right-handed neutrinos.

Active-sterile transition probability in vacuum is then given by Eq. (2.40),

$$\langle P_{\nu_a \rightarrow \nu_s} \rangle = \frac{1}{2} \sin^2 2\theta_{as} . \quad (2.43)$$

### 2.2.2 Neutrino oscillations in a medium

When neutrino travels through a medium, it can interact with particles in the background and change the dispersion relation. We can use an effective potential to quantify this effect. Neutrino oscillations in matter were first studied by Lincoln Wolfenstein [38]. He found that neutrino propagation can be changed by coherent forward scattering with the particles in the medium (electrons and nucleons). Extending Wolfenstein's work, Stanislav Mikheyev and Alexei Smirnov predicted resonant enhancement of oscillations [39]. Thus, this matter effect is also known as *Mikheyev-Smirnov-Wolfenstein effect (MSW effect)*. The vacuum mixing angle is then replaced by an effective mixing angle in matter, which can become large for suitable matter densities even if the vacuum mixing angle is very small. This effect has become popular as it successfully explained solar neutrino problem [40]. A similar effect can be expected for active-sterile conversion, as neutrinos are propagating through highly dense primordial plasma. Hence, understanding matter effect is essential to understand sterile neutrino production mechanisms.

Starting with Eq. (2.20), the total Hamiltonian in matter can be written as

$$\mathcal{H} = \mathcal{H}_0 + \mathcal{H}_\alpha , \quad (2.44)$$

where  $\mathcal{H}_0$  is vacuum Hamiltonian and  $\mathcal{H}_\alpha$  is the extra term contributed by medium.

$$\mathcal{H}_0 |\nu_i\rangle = E_i |\nu_i\rangle , \quad \mathcal{H}_\alpha |\nu_\alpha\rangle = V_\alpha |\nu_\alpha\rangle . \quad (2.45)$$

$V_\alpha$  is the effective potential on neutrino flavour  $\alpha$  when it propagates through the medium. For the Standard Model interactions, we can separate  $V_\alpha$  into

$$V_\alpha = V_{CC} + V_{NC} , \quad (2.46)$$

as active neutrinos interact to the medium via charged current (CC) and neutral current (NC) interactions. If we have some additional new non-standard interactions,

$$V_\alpha = V_{CC} + V_{NC} + V_{NSI} . \quad (2.47)$$

Detailed derivation of thermal potential is given in Appendix C. For now, let's consider it as  $V_\alpha$ .

Evolution of neutrino flavour eigenstate  $|\nu_\alpha(t)\rangle$  is given similar to Eq. (2.24) as

$$i \frac{d}{dt} |\nu_\alpha(t)\rangle = \mathcal{H} |\nu_\alpha(t)\rangle , \quad \text{with} \quad |\nu_\alpha(0)\rangle = |\nu_\alpha\rangle . \quad (2.48)$$

Transition probability for  $\nu_\alpha \rightarrow \nu_\beta$  after time  $t$  is given similar to Eq. (2.30) by squared amplitude  $\psi_{\alpha\beta}(t) = \langle \nu_\beta | \nu_\alpha(t) \rangle$ ,

$$P_{\nu_\alpha \rightarrow \nu_\beta}(t) = |\psi_{\alpha\beta}(t)|^2 . \quad (2.49)$$

We can write the time evolution equation of the flavour transition amplitudes as

$$i \frac{d}{dt} \psi_{\alpha\beta}(t) = \sum_{\eta} \left( \sum_k U_{\beta k}^* E_k U_{\eta k} + \delta_{\beta\eta} V_{\beta} \right) \psi_{\alpha\eta}(t) , \quad (2.50)$$

where  $U_{\beta i}$  are elements of PMNS matrix. Using ultra-relativistic approximation

$$E_k \simeq E + \frac{m_k^2}{2E}, \quad p \simeq E, \quad t \simeq x , \quad (2.51)$$

and omitting terms irrelevant for flavour transition, we get

$$i \frac{d}{dx} \psi_{\alpha\beta}(x) = \sum_{\eta} \left( \sum_i U_{\beta i}^* \frac{\Delta m_{k1}^2}{2E} U_{\eta i} + \delta_{\beta\eta} V_{\beta} \right) \psi_{\alpha\eta}(x) , \quad (2.52)$$

which can be written in matrix form as

$$i \frac{d}{dx} \Psi_{\alpha} = \mathcal{H}_M \Psi_{\alpha} , \quad (2.53)$$

where

$$\Psi_{\alpha} = \begin{pmatrix} \psi_{\alpha\alpha} \\ \psi_{\alpha\beta} \\ \vdots \end{pmatrix} , \quad \mathcal{H}_M = U \text{diag} \left( 0, \frac{\Delta m_{k1}^2}{2E}, \dots \right) U^{\dagger} + \text{diag} (V_{\alpha}, V_{\beta}, \dots) . \quad (2.54)$$

Let us consider two flavour case where  $\alpha = a$ , active neutrinos with mass  $m_{\nu}$  and  $\beta = s$ , sterile neutrinos with mass  $m_s$  mix with vacuum mixing angle  $\theta_{as}$ .

Here,

$$U = \begin{pmatrix} \cos(\theta_{as}) & \sin(\theta_{as}) \\ -\sin(\theta_{as}) & \cos(\theta_{as}) \end{pmatrix} , \quad \mathbb{M}^2 = \begin{pmatrix} 0 & 0 \\ 0 & \frac{\Delta m_{as}^2}{2E} \end{pmatrix} , \quad \mathbb{V} = \begin{pmatrix} V_a & 0 \\ 0 & 0 \end{pmatrix} , \quad (2.55)$$

with the assumption that sterile neutrinos do not have any interactions with the primordial plasma. If there are any new sterile neutrino interactions,  $\mathbb{V}_{22} \neq 0$ .

Now we can write Schrödinger-like equation Eq. (2.53) for active-sterile conversion,

$$i \frac{d}{dx} \begin{pmatrix} \psi_{aa} \\ \psi_{as} \end{pmatrix} = \frac{1}{2} \begin{pmatrix} V_a - \Delta(p) \cos 2\theta_{as} & \Delta(p) \sin 2\theta_{as} \\ \Delta(p) \sin 2\theta_{as} & \Delta(p) \cos 2\theta_{as} - V_a \end{pmatrix} \begin{pmatrix} \psi_{aa} \\ \psi_{as} \end{pmatrix} , \quad (2.56)$$

where  $\Delta(p) = \Delta m_{as}^2 / 2E \approx m_s^2 / 2p$ . We can diagonalize the effective Hamiltonian matrix,

$$\mathcal{H}_M = \frac{1}{2} \begin{pmatrix} V_a - \Delta(p) \cos 2\theta_{as} & \Delta(p) \sin 2\theta_{as} \\ \Delta(p) \sin 2\theta_{as} & \Delta(p) \cos 2\theta_{as} - V_a \end{pmatrix} \quad (2.57)$$

by an orthogonal transformation

$$\tilde{\mathcal{H}}_M = U_M^T \mathcal{H}_M U_M , \quad (2.58)$$

where  $U_M$  is effective mixing matrix for the medium with mixing angle given by

$$\tan 2\theta_M = \frac{\tan 2\theta_{as}}{1 - \frac{V_a}{\Delta \cos 2\theta_{as}}} . \quad (2.59)$$

Then, diagonalized effective Hamiltonian matrix

$$\tilde{\mathcal{H}}_M = \text{diag}(-\Delta_M, \Delta_M) , \text{ where } \Delta_M = \sqrt{\Delta^2 \sin^2 2\theta_{as} + (\Delta^2 \cos 2\theta_{as} - V_a)^2} \quad (2.60)$$

Then Eq. (2.56) can be written as

$$i \frac{d}{dx} \begin{pmatrix} \psi_{aa} \\ \psi_{as} \end{pmatrix} = \begin{pmatrix} -\Delta_M \cos 2\theta_M & \Delta_M \sin 2\theta_M \\ \Delta_M \sin 2\theta_M & \Delta_M \cos 2\theta_M \end{pmatrix} \begin{pmatrix} \psi_{aa} \\ \psi_{as} \end{pmatrix} \quad (2.61)$$

with

$$\cos 2\theta_M = \frac{\Delta \cos 2\theta_{as} - V_a}{\Delta_M}, \quad \sin 2\theta_M = \frac{\Delta \sin 2\theta_{as}}{\Delta_M} . \quad (2.62)$$

Then we get active-sterile transition probability as

$$P_{\nu_a \rightarrow \nu_s}(t) = \sin^2 2\theta_M \sin^2 \left( \frac{\Delta_M t}{2} \right) \quad (2.63)$$

and time averaged transition probability as

$$\langle P_{\nu_a \rightarrow \nu_s}(p, t) \rangle = \frac{1}{2} \sin^2 2\theta_M = \frac{1}{2} \frac{\Delta^2 \sin 2\theta_{as}}{\Delta^2 \sin^2 2\theta_{as} + (\Delta^2 \cos 2\theta_{as} - V_a)^2} \quad (2.64)$$

where  $\theta_{as}$  is the active-sterile mixing angle in vacuum.

We can also see from Eq. (2.59) that resonance condition requires

$$V_a \stackrel{!}{=} \Delta \cos 2\theta_{vac} . \quad (2.65)$$

Effective mixing angle is  $\frac{\pi}{4}$  at resonance. If the resonance region is wide enough, maximal mixing leads to total transition between two flavours. This mechanism is known as the *MSW effect*.

In the context of sterile neutrino dark matter, this resonance can be achieved by assuming finite Lepton asymmetry in the early universe. Resonant and non-resonant production of sterile neutrinos are discussed in the next section.

## 2.3 Sterile neutrino dark matter production mechanisms

Dark matter production in early universe can be mathematically treated by solving the Boltzmann equation to find distribution function of the particle [41].

General form of the Boltzmann equation is given by,

$$\hat{L}[f] = \hat{C}[f] , \quad (2.66)$$

where  $\hat{L}$  is the Liouville operator, describing evolution of a phase space volume and  $\hat{C}$  is the collision operator describing interaction of particle species with the medium. Assuming the dark matter particle interact with the Standard Model particles, we

can write integrated Boltzmann equation as,

$$\frac{dn_{\text{DM}}}{dt} + 3Hn_{\text{DM}} = \underbrace{-\langle\sigma_{\text{ann}}v\rangle n_{\text{DM}}^2}_{\text{decreases } n_{\text{DM}}} + \underbrace{\langle\sigma_{\text{prod}}v\rangle n_{\text{SM}}^2}_{\text{increases } n_{\text{DM}}}, \quad (2.67)$$

where  $\langle\sigma v\rangle$  is the thermally averaged cross section.

Using the fact that two terms on the right hand side of Eq. (2.67) cancel each other at equilibrium:

$$\langle\sigma_{\text{ann}}v\rangle (n_{\text{DM}}^{\text{eq}})^2 = \langle\sigma_{\text{prod}}v\rangle (n_{\text{SM}}^{\text{eq}})^2 \Rightarrow \langle\sigma_{\text{prod}}v\rangle = \langle\sigma_{\text{ann}}v\rangle \left(\frac{n_{\text{DM}}^{\text{eq}}}{n_{\text{SM}}^{\text{eq}}}\right)^2. \quad (2.68)$$

As the standard model particle always stays in equilibrium,  $n_{\text{SM}} = n_{\text{SM}}^{\text{eq}}$ . Then, we can rewrite the integrated Boltzmann equation purely in terms of dark matter number density,  $n_{\text{DM}}$ :

$$\frac{dn_{\text{DM}}}{dt} + 3Hn_{\text{DM}} = -\langle\sigma_{\text{ann}}v\rangle [n_{\text{DM}}^2 - (n_{\text{DM}}^{\text{eq}})^2]. \quad (2.69)$$

It is often useful to define the dark matter yield  $Y_{\text{DM}} = n_{\text{DM}}/s$ , with  $s$  being the entropy density. Dark matter yield stays constant in the absence of number changing processes. In terms of dark matter yield, Eq. (2.69) can be written as

$$\frac{x}{Y_{\text{DM}}^{\text{eq}}} \frac{dY_{\text{DM}}}{dx} = -\frac{\Gamma_{\text{ann}}}{H} \left[ \left(\frac{Y_{\text{DM}}}{Y_{\text{DM}}^{\text{eq}}}\right)^2 - 1 \right], \quad (2.70)$$

where we changed the time variable  $t$  to an equivalent inverse temperature,  $x = m_{\text{DM}}/T$ .

At high temperatures ( $x \ll 1$ ), when  $\Gamma_{\text{ann}} \gg H$ , dark matter yield tries to reach equilibrium. But once the universe starts to cool down, dark matter particles become non-relativistic ( $x > 1$ ) and  $Y_{\text{DM}}^{\text{eq}}$  and  $\Gamma_{\text{ann}}$  are exponentially suppressed.

Depending on the initial yield  $Y_{\text{DM}}(x_0)$ , this leads to two scenarios: *freeze-in* and *freeze-out*.

### Freeze-out

If we assume dark matter particles are already present in the early Universe, initial yield,

$$Y_{\text{DM}}(x_0) \approx Y_{\text{DM}}^{\text{eq}}. \quad (2.71)$$

Once the particles become non-relativistic ( $x > 1$ ), interaction rates are exponentially suppressed.

$$\Gamma_{\text{ann}} \ll H \Rightarrow \frac{dY_{\text{DM}}}{dx} \approx 0 \Rightarrow \text{dark matter yield stays constant.}$$

Thus, dark matter relic abundance freezes out to a value  $Y_{\text{DM}}(x_f)$  from the equilibrium yield at freeze-out temperature  $T_f$  and stays constant from then on.

In the freeze-out scenario, relic abundance can be calculated to

$$\Omega_{\text{DM}} h^2 \propto m_{\text{DM}} \quad (2.72)$$

for hot thermal relics. For a light neutrino that decouples around few MeV,  $\Omega_{\text{DM}} h^2 < 1$  translates to  $m_\nu < \mathcal{O}(10)$  eV. This is known as *Cowsik-McClelland bound* [42]. For cold dark matter,

$$\Omega_{\text{DM}} h^2 \propto \frac{1}{\langle \sigma v \rangle} \propto \frac{1}{m_{\text{DM}}^2}, \quad (2.73)$$

and for a heavy neutrino,  $\Omega_{\text{DM}} h^2 < 1$  translates to  $m_\nu \gtrsim 2$  GeV. This is often known as *Lee-Weinberg bound* [42].

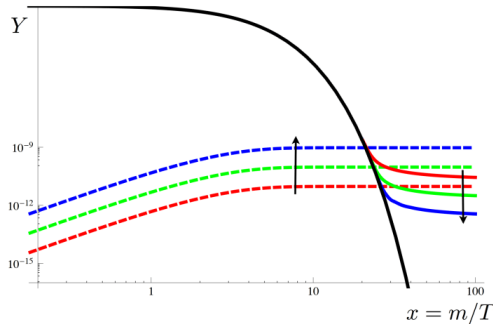


FIGURE 2.3: Evolution of dark matter yield with inverse temperature  $x$ . The thick black line indicates the equilibrium yield  $Y_{\text{DM}}^{\text{eq}}$ . Dashed coloured lines represent the freeze-in scenario and solid coloured lines represents the freeze-out scenario, where arrows point in the increasing coupling strength for the two processes (Taken from [43]).

### Freeze-in

If the dark matter particle has a feeble coupling with the Standard Model particles, it can never reach the equilibrium yield, and we can assume  $Y_{\text{DM}}(x \approx x_0) \ll Y_{\text{DM}}^{\text{eq}}$ . Then,

$$\Gamma_{\text{ann}} < H \Rightarrow \frac{dY_{\text{DM}}}{dx} > 0 \Rightarrow \text{dark matter yield slowly increases.}$$

When  $\Gamma_{\text{ann}} \ll H$ , dark matter yield freezes in to a constant value  $Y_{\text{DM}}(x_f)$  at freeze-in temperature  $T_f$  similar to freeze-out case. We can see from Fig. 2.3 that as opposed to the freeze-out mechanism, freeze-in relic abundance is proportional to dark matter coupling to the Standard Model particles. Freeze-in mechanisms often produce a non-thermal momentum distribution and are interesting from a phenomenological perspective.

In the case of sterile neutrinos, freeze-in mechanism is driven by active-sterile mixing explained in Sec. 2.2.2.

#### 2.3.1 Non-resonant production

Non-resonant production or *Dodelson-Widrow mechanism* is the most generic mechanism for sterile neutrino production. Assuming there is a sterile neutrino species that has non-zero mixing angle with active neutrinos, this mechanism is unavoidable. The idea that sterile neutrinos can be produced from active-sterile transition was first proposed by Paul Langacker in 1989 [44]. However, its application in dark matter sector was discussed by Scott Dodelson and Lawrence Widrow in 1994 [45]. Hence, the name Dodelson-Widrow mechanism. They found out that sterile neutrinos with  $m_s \sim 0.1 - 1$  keV would make excellent warm dark matter candidates.

Producing full relic abundance by DW mechanism is ruled out by astrophysical experiments [46, 47]. However this is a great starting point to build new production scenarios. DW mechanism can also act as a secondary mechanism with non-trivial initial abundances [48].

Boltzmann-like equation governing sterile neutrino evolution is given by

$$\frac{\partial}{\partial t} f_s(p, t) - H p \frac{\partial}{\partial p} f_s(p, t) \approx \frac{1}{4} h(p, T) [f_a(p, t) - f_s(p, t)] , \quad (2.74)$$

where

$$h(p, T) = \frac{\Gamma_a(p, T) \Delta^2(p) \sin^2 2\theta}{\Delta^2(p) \sin^2 2\theta + \left(\frac{\Gamma_a(p, T)}{2}\right)^2 + [\Delta(p) \cos 2\theta - \mathcal{V}_a(p, T)]^2} \quad (2.75)$$

includes the contribution from active-sterile transition probability. We assume mixing angles to be much smaller than 1.

Effective potential  $\mathcal{V}_a(p, T)$  can be separated into finite density potential  $V_D$  and thermal potential  $V_T$  given as

$$V_D = \frac{2\sqrt{2}\zeta(3)}{\pi^2} G_F T^3 \left( \mathcal{L}^a \pm \frac{\eta}{4} \right) , \quad (2.76)$$

$$V_T = -\frac{8\sqrt{2}G_F p}{3m_W^2} [n_a \langle E_a \rangle + n_{\bar{a}} \langle E_{\bar{a}} \rangle] - \frac{8\sqrt{2}G_F p}{3m_Z^2} [n_{\nu_a} \langle E_{\nu_a} \rangle + n_{\bar{\nu}_e} \langle E_{\bar{\nu}_e} \rangle] . \quad (2.77)$$

We assume a lepton symmetric universe ( $\mathcal{L} = 0$ ), hence finite density potential becomes negligible with only contribution from baryon asymmetry  $\eta \sim 10^{-10}$ .

When  $T > 1$  GeV,

$$\Gamma_a \gg \Delta \gg V_T \Rightarrow h(p, T) \sim \frac{\Delta^2(p) \sin^2 2\theta}{\Gamma_a(p, T)} \approx 0 . \quad (2.78)$$

i.e., sterile neutrino production is negligible above  $T > 1$  GeV. A lower limit can be taken as  $T \sim 1$  MeV where neutrinos decouple from the plasma.

Since  $V_T(p, T)$  is always much less than  $\Delta(p) \cos 2\theta$ , production never pass through resonance. Non-resonant production slowly start at  $T \sim 1$  GeV and peaks around QCD phase transition temperature  $T \sim 150$  MeV.

We will discuss this mechanism in detail in Chapter 3.

### 2.3.2 Resonant production

Matter-antimatter asymmetry implies that early universe does not need to be lepton symmetric. Including non-zero lepton asymmetry in the picture can drastically change active-sterile transitions. This possibility and its connection to MSW resonance was first studied by Enqvist et al. [49, 50]. In 1999, Shi and Fuller proposed this mechanism can be used to produce sterile neutrino dark matter [51]. Hence it is also known as *Shi-Fuller mechanism*. Resonance condition strongly favors low-energy neutrinos and can lead to a colder spectrum than other light neutrino dark matter candidates.

If  $\mathcal{L}^a \neq 0$  in Eq. (2.76) and sufficiently large, effective potential can be comparable to  $\Delta(p)$ . At the resonance condition

$$\Delta(p) \cos 2\theta \stackrel{!}{=} V_a(p, T) , \quad (2.79)$$

$$h(p_{\text{res}}, T_{\text{res}}) \simeq \frac{\Gamma_a(p_{\text{res}}, T_{\text{res}})\Delta^2(p_{\text{res}})\sin^2 2\theta}{\Delta^2(p_{\text{res}})\sin^2 2\theta + 0 + 0} \approx \Gamma_a(p_{\text{res}}, T_{\text{res}}), \quad (2.80)$$

that can be substantially large and generate an MSW-like effect.

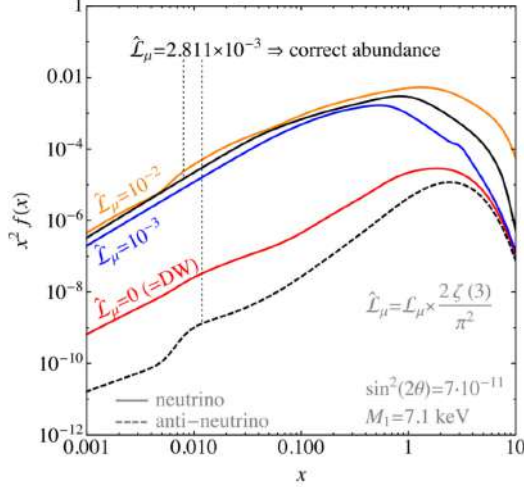


FIGURE 2.4: Sterile neutrino distribution functions: Resonant and non-resonant production (Taken from [11]).

This mechanism requires fairly large lepton asymmetry. Sterile neutrinos of  $M \sim \mathcal{O}(10)$  keV requires a lepton asymmetry of  $\mathcal{L} \sim 10^{-3}$  [51], which is much larger compared to baryon asymmetry  $\eta_B \sim 10^{-10}$ . But if it is possible to create such large asymmetry by some leptogenesis mechanisms [52, 53] in the early universe, Shi-Fuller mechanism provides an interesting way to produce sterile neutrino dark matter.

### 2.3.3 Production from scalar decays

There can be other portals for sterile neutrino production if we assume sterile neutrinos can couple to other particles. One such method is production via decay of heavy scalar particles. If we assume a scalar dark matter particle  $S$  is present in the early universe, it would be possible for this particle to decay into sterile neutrinos. Sterile neutrinos produced by this mechanism can also explain observed pulsar velocities [54].

Assume a scalar  $S$  that interacts to SM via Higgs coupling and interacts to sterile neutrinos  $N$  via Yukawa-like coupling.

$$\mathcal{L}_{\text{int}} \supset - \left[ \frac{y}{2} S \bar{N}^c N + \text{h.c.} \right] - 2\lambda S^2 \Phi^\dagger \Phi. \quad (2.81)$$

If  $S$  is heavier than the sterile neutrino, there is possibility of decay  $S \rightarrow NN$ . If we know the thermal history of the scalar particle, we can calculate the sterile neutrino distribution function  $f_N$ . Depending on whether scalar freezes in or out, sterile neutrino production would look different, nonetheless it is always some form of freeze-in mechanism (Fig. 2.5).

Sterile neutrino relic abundance [55],

$$\Omega_s h^2 \propto \frac{M_{\text{Pl}} m_N}{m_S^2}, \quad (2.82)$$

where  $m_N, m_S$  are sterile neutrino and scalar masses respectively and  $M_{\text{Pl}}$  is the Planck mass. For an *inflaton* with mass  $\sim 100$  GeV,  $m_N \sim \mathcal{O}(10)$  MeV can give the

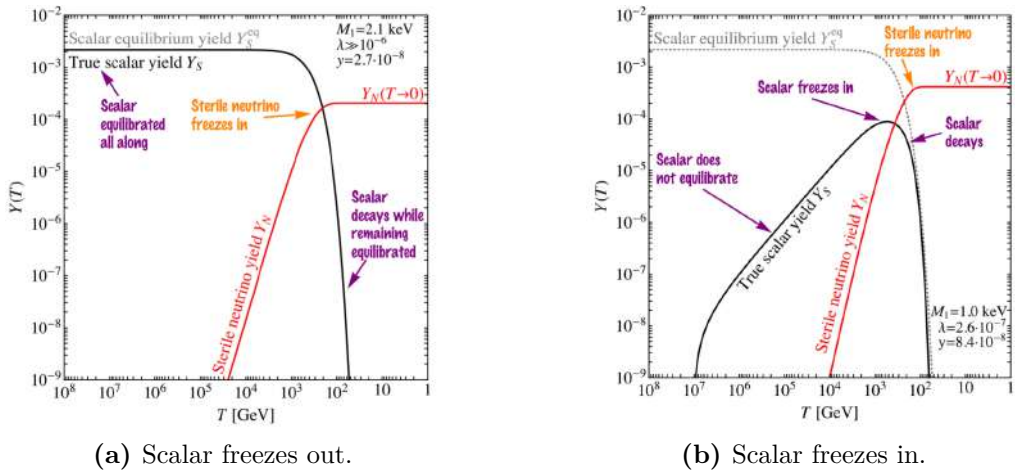


FIGURE 2.5: Sterile neutrino production via scalar decay (Taken from [11]).

correct relic abundance [55]. Several modifications to parent scalar such as charged scalars [56], vectors [57] or fermions [58] exist and given the right conditions, not only they produce keV sterile neutrinos with correct abundance but also solve some interesting problems in the particle physics.

## 2.4 Experimental searches for sterile neutrino dark matter

Laboratory based experimental searches for sterile neutrino dark matter is an extremely difficult task since it has to rely on tiny active-sterile mixing angles. However, direct neutrino mass experiments like KATRIN [16], TRISTAN [17], PTOLEMY [59], ECHo [59], HUNTER [19], BeEST [60], HOLMES [61], Project 8 [62] could potentially detect a sterile mass eigenstate. These experiments mainly utilize two different processes to determine neutrino mass: beta decay and electron capture.

### 2.4.1 Single beta decay

Ordinary beta decay,

$$(Z, A) \rightarrow (Z + 1, A) + e^- + \bar{\nu}_e ,$$

emits a highly relativistic electron from the nuclei accompanied by an electron antineutrino. Antineutrino, by being massive, slightly changes the electron energy spectrum. By measuring this deviation, we can calculate the mass of emitted antineutrino. However, as mentioned before, a flavour eigenstate is a superposition of mass eigenstates. That means, if the  $Q$ -value is high enough, there is a non-zero probability to produce a sterile mass eigenstate. As shown in Fig. 2.6, sterile neutrinos can change electron energy spectrum in two ways: an overall reduction in the decay rate and a kink near the sterile neutrino mass in the electron spectrum.

*Karlsruhe Tritium Neutrino Experiment (KATRIN)* use tritium beta decay with a  $Q$ -value of 18.6 keV to measure neutrino masses. This implies it can potentially detect sterile neutrino masses up to  $\sim 18.6$  keV. However, KATRIN experiment, to be more efficient to detect active neutrino masses, discards low energy electrons that are away from kinematic endpoint. Upgrading KATRIN by modifying the MAC-E filter that only selects high energy electrons and using silicon detectors with better

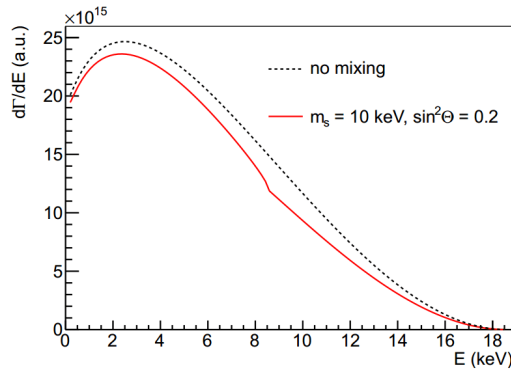


FIGURE 2.6: Possible effect of sterile neutrino on beta decay spectrum. Dotted line represent the standard beta decay spectrum and red line represents the effect of a sterile neutrino with a mass,  $m_s = 10$  keV and mixing angle  $\sin^2 \theta = 0.2$  (Taken from [63]).

energy resolution, we will be able to look for a wider range of energies and possibly detect sterile neutrinos. This upgrade is known as *Tritium Beta Decay to Search for Sterile Neutrinos (TRISTAN)*.

#### 2.4.2 Electron capture decay

Electron capture decay is a type of beta decay where a bound electron (usually from either K or L shells) is captured by unstable nuclei, resulting in an electron neutrino emission:

$$p + e^- \rightarrow n + \nu_e .$$

Similar to the ordinary beta decay, if the process has enough  $Q$ -value, it is possible to measure a sterile mass eigenstate in principle. However, as neutrinos carry away the entire decay energy, we measure discrete neutrino spectrum unlike electron energy spectrum in beta decay. Electron capture of  $^{163}\text{Ho}$  nuclei is being studied in experi-

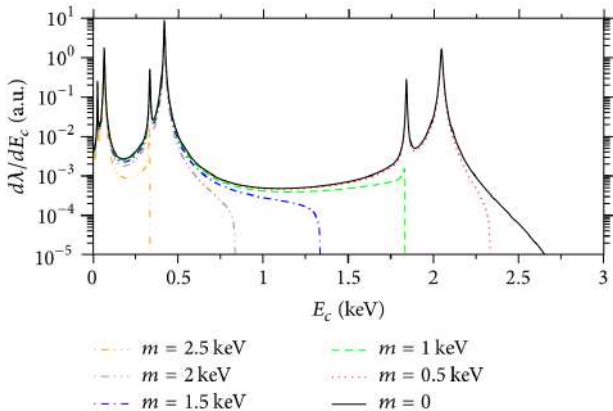


FIGURE 2.7: Effect of sterile neutrinos on electron capture in  $^{163}\text{Ho}$ . Black line represent the standard case without sterile neutrinos and coloured line represents the various cases of non-zero sterile neutrino masses (Taken from [64]).

ments such as *ECHO* [18] and *HOLMES* [61]. However, this process has a  $Q$ -value of 2.8 keV, which makes it less interesting for keV sterile neutrino dark matter. Another

upcoming experiment, *Heavy Unseen Neutrinos from Total Energy-Momentum Reconstruction (HUNTER)* [19], studies higher  $Q$ -value electron capture in  $^{131}\text{Cs}$ . This experiment can detect sterile neutrinos with a mass range  $7 - 300$  keV. However, this experiment is still in its development stage, and it would take years to reach the desired sensitivity.

## 2.5 Non-standard neutrino interactions

Non-standard neutrino interactions or NSIs in short refer to any neutrino interactions exist beyond the Standard Model. We often treat NSIs from an effective field theory perspective, as we can see NSI as a low-energy limit of the Standard Model Effective Field Theory (SMEFT) below electroweak scale. A review and status of NSI can be found in Refs. [65] and constraints on NSI parameters from neutrino oscillation experiments can be found in Refs. [66, 67].

If we introduce right-handed neutrino fields and extend NSI, we have General Neutrino Interactions(GNI). Most generalized GNI Lagrangian can be written as [68],

$$\mathcal{L}^{\text{NC}} = -\frac{G_F}{\sqrt{2}} \sum_{j=1}^{10} (\epsilon_{j,f})^{\alpha\beta\gamma\delta} (\bar{\nu}_\alpha \mathcal{O}_j \nu_\beta) (\bar{f}_\gamma \mathcal{O}'_j f_\delta), \quad (2.83)$$

$$\mathcal{L}^{\text{CC}} = -\frac{G_F V_{\gamma\delta}}{\sqrt{2}} \sum_{j=1}^{10} (\epsilon_{j,ud})^{\alpha\beta\gamma\delta} (\bar{e}_\alpha \mathcal{O}_j \nu_\beta) (\bar{u}_\gamma \mathcal{O}'_j d_\delta) + \text{h.c.}, \quad (2.84)$$

where  $f = \nu, e, u, d$  are fermions and  $\mathcal{O}_j, \mathcal{O}'_j$  are GNI operators given in Table 2.2.

$j$	$\epsilon_j$	$\mathcal{O}_j$	$\mathcal{O}'_j$
1	$\epsilon_L$	$\gamma_\mu (\mathbb{I} - \gamma^5)$	$\gamma^\mu (\mathbb{I} - \gamma^5)$
2	$\tilde{\epsilon}_L$	$\gamma_\mu (\mathbb{I} + \gamma^5)$	$\gamma^\mu (\mathbb{I} - \gamma^5)$
3	$\epsilon_R$	$\gamma_\mu (\mathbb{I} - \gamma^5)$	$\gamma^\mu (\mathbb{I} + \gamma^5)$
4	$\tilde{\epsilon}_R$	$\gamma_\mu (\mathbb{I} + \gamma^5)$	$\gamma^\mu (\mathbb{I} + \gamma^5)$
5	$\epsilon_S$	$(\mathbb{I} - \gamma^5)$	$\mathbb{I}$
6	$\tilde{\epsilon}_S$	$(\mathbb{I} + \gamma^5)$	$\mathbb{I}$
7	$-\epsilon_P$	$(\mathbb{I} - \gamma^5)$	$\gamma^5$
8	$-\tilde{\epsilon}_P$	$(\mathbb{I} + \gamma^5)$	$\gamma^5$
9	$\epsilon_T$	$\sigma_{\mu\nu} (\mathbb{I} - \gamma^5)$	$\sigma^{\mu\nu} (\mathbb{I} - \gamma^5)$
10	$\tilde{\epsilon}_T$	$\sigma_{\mu\nu} (\mathbb{I} + \gamma^5)$	$\sigma^{\mu\nu} (\mathbb{I} + \gamma^5)$

TABLE 2.2: Operator basis of General Neutrino Interactions [68].

There are strict constraints on non-standard neutrino interactions with leptons and quarks from beta decays and coherent elastic neutrino-nucleus scattering [66]. However, neutrino self-interaction NSIs are loosely constrained due to the very hard detectability. Thus, we will use non-standard neutrino self-interactions (NSSIs) to modify sterile neutrino production in this work.

### 2.5.1 Non-Standard neutrino Self-Interactions (NSSIs)

We will use a slightly different NSSI Lagrangian from the NSI Lagrangian Eq. (2.83), as we will be working in the context of the Dodelson-Widrow mechanism, which requires higher order terms in the Lagrangian.

Assuming only one active neutrino flavour for simplicity and starting with a Yukawa-like interaction between active neutrinos  $\nu$  and complex scalar  $\phi$ ,

$$\mathcal{L}_{\text{int}} \supset \lambda_\phi \bar{\nu} \mathcal{O} \nu \phi + \text{h.c.} , \quad (2.85)$$

where  $\mathcal{O}$ , an element of a complete set of bilinear covariants  $\{\mathbb{I}, \gamma^\mu, i\gamma^5, \sigma^{\mu\nu}\}$ , indicates the nature of the interaction.

The full Lagrangian with the complex scalar  $\phi$  can be written as

$$\mathcal{L}_{\text{full}} = \partial_\mu \phi^\dagger \partial^\mu \phi - m^2 \phi^\dagger \phi + \lambda_\phi \bar{\nu} \mathcal{O} \nu \phi + \lambda_\phi^* \phi^\dagger \bar{\nu} \bar{\mathcal{O}} \nu , \quad \text{where } \bar{\mathcal{O}} = \gamma^0 \mathcal{O}^\dagger \gamma^0 . \quad (2.86)$$

However, if the mediator is much heavier than the temperature range we are interested in ( $m_\phi \gg T$ ), we can employ effective field theory framework and integrate out heavy degrees of freedom in the full Lagrangian. The Dodelson-Widrow production mainly occurs around  $T \sim 1 - 0.1$  GeV. That means, if the mediator  $\phi$  is heavier than  $\sim \mathcal{O}(10)$  GeV, we can use effective approach. To find EFT Lagrangian, we first solve equation of motion for the heavy degree of freedom  $\phi$ ,

$$\frac{\partial \mathcal{L}_{\text{full}}}{\partial \phi} - \partial_\mu \frac{\partial \mathcal{L}_{\text{full}}}{\partial (\partial_\mu \phi)} = 0 . \quad (2.87)$$

Solving equation of motion

$$-m^2 \phi^\dagger + \lambda_\phi \bar{\nu} \mathcal{O} \nu - \partial_\mu \partial^\mu \phi^\dagger = 0 \Rightarrow (\square + m^2) \phi^\dagger = \lambda_\phi \bar{\nu} \mathcal{O} \nu , \quad (2.88)$$

and we obtain an expression for  $\phi^\dagger$ ,

$$\phi^\dagger = \frac{\lambda_\phi \bar{\nu} \mathcal{O} \nu}{(\square + m^2)} . \quad (2.89)$$

A similar expression,

$$\phi = \frac{\lambda_\phi^* \bar{\nu} \bar{\mathcal{O}} \nu}{(\square + m^2)} , \quad (2.90)$$

can be obtained by solving equation of motion for  $\phi$ . Substituting these in the full Lagrangian Eq. (2.86) to integrate out the heavy complex scalar  $\phi$ , we obtain

$$\mathcal{L}_{\text{NSSI}} = \lambda_\phi^2 \frac{(\bar{\nu} \mathcal{O} \nu)(\bar{\nu} \bar{\mathcal{O}} \nu)}{(\square + m_\phi^2)} . \quad (2.91)$$

Keeping terms up to first order in  $\square$  to retain momentum dependence, we have

$$\mathcal{L}_{\text{NSSI}} = \frac{G_\phi}{\sqrt{2}} \left( (\bar{\nu} \mathcal{O} \nu)(\bar{\nu} \bar{\mathcal{O}} \nu) - (\bar{\nu} \mathcal{O} \nu) \frac{\square}{m_\phi^2} (\bar{\nu} \bar{\mathcal{O}} \nu) \right) , \quad \text{where } G_\phi = \frac{\sqrt{2} \lambda_\phi^2}{m_\phi^2} \quad (2.92)$$

is the strength of NSSI defined similar to the Fermi constant  $G_F$ .

Using  $G_\phi = G_F \epsilon$ , where  $\epsilon$  indicates the NSSI strength compared to the standard weak interactions, we get final form of NSSI Lagrangian:

$$\mathcal{L}_{\text{NSSI}} = \frac{G_F \epsilon}{\sqrt{2}} (\bar{\nu} \mathcal{O} \nu) (\bar{\nu} \bar{\mathcal{O}} \nu) - \frac{G_F \epsilon}{\sqrt{2}} (\bar{\nu} \mathcal{O} \nu) \frac{\square}{m_\phi^2} (\bar{\nu} \bar{\mathcal{O}} \nu) , \quad (2.93)$$

where different types of interactions and corresponding  $\epsilon, \mathcal{O}$  are given in Table 2.3.

	$\epsilon_j$	$\mathcal{O}$	$\bar{\mathcal{O}} = \gamma^0 \mathcal{O}^\dagger \gamma^0$
Scalar	$\epsilon_S$	$\mathbb{I}$	$\mathbb{I}$
Vector	$\epsilon_V$	$\gamma_\mu$	$\gamma_\mu$
Tensor	$\epsilon_T$	$\sigma_{\mu\nu}$	$\sigma_{\mu\nu}$
Axialvector	$\epsilon_A$	$\gamma_\mu \gamma^5$	$\gamma_\mu \gamma^5$
Pseudoscalar	$\epsilon_P$	$i\gamma^5$	$i\gamma^5$

TABLE 2.3: Operators for non-standard neutrino self-interactions.

Second term in the Lagrangian Eq. (2.93) gives momentum dependent Feynman rules and will be important for effective potential calculations in the early universe.

Interaction strength of  $G_\phi \sim 10^7 - 10^9 G_F$  [69],

$$G_\phi = \begin{cases} (4.7^{+0.4}_{-0.6} \text{MeV})^{-2} & (\text{SI}\nu) \\ (89^{+171}_{-61} \text{MeV})^{-2} & (\text{MI}\nu) \end{cases} , \quad (2.94)$$

has been shown to solve Hubble tension.

Four neutrino interactions are loosely constrained compare to other NSIs. CMB measurements allows large values of  $G_\phi$  mentioned above. But, strong bounds from invisible  $Z$ -decay [70] sets

$$G_\phi \leq (1 - 10) \cdot G_F . \quad (2.95)$$

We will use  $G_\phi = (0.1 - 100) \cdot G_F$  in this work.

We have done a brief review of important tools required to study sterile neutrino production in the early universe. Now we are equipped to deal with the Dodelson-Widrow mechanism in the presence of non-standard neutrino self-interactions, and we will take a detailed look at it in the next chapter.

## Chapter 3

# Dodelson-Widrow mechanism in presence of NSSIs

The Dodelson-Widrow mechanism is the most generic sterile neutrino production mechanism. Expanding the brief introduction in Sec. 2.3.1, we will work out the mechanism in detail. The first section of this chapter focuses on the basic Dodelson-Widrow mechanism with active-sterile mixing as the only BSM interaction. In the next section, we include non-standard neutrino self-interactions introduced in Sec 2.5.1 and study how it can affect non-resonant production. We use publications by Abazajian et al. [71], Venumadhav et al. [72] and Merle [48] as starting point. We will assume electron neutrinos as our active neutrinos, so that this study would be interesting for experiments such as KATRIN [16], ECHo [18], HUNTER [19] discussed in Sec. 2.4. However, the following treatment can be generalized to any other flavour as long as we consider single active neutrino flavour.

### 3.1 Basic Dodelson-Widrow mechanism

Assuming an active neutrino flavour  $\nu_a$  and sterile flavour  $\nu_s$  mix with each other as explained in Sec. 2.2.2,

$$|\nu_a\rangle = \cos(\theta)|\nu\rangle + \sin(\theta)|N\rangle , \quad (3.1)$$

$$|\nu_s\rangle = -\sin(\theta)|\nu\rangle + \cos(\theta)|N\rangle , \quad (3.2)$$

where  $\theta = \theta_{as}$  is the vacuum mixing angle and  $\nu, N$  are active and sterile mass eigenstates respectively.

Time averaged active-sterile transition probability from Eq. (2.64),

$$\langle P_m (\nu_a \rightarrow \nu_s; p, t) \rangle = \frac{1}{2} \sin^2 2\theta_M = \frac{1}{2} \frac{\Delta^2(p) \sin 2\theta}{\Delta^2(p) \sin^2 2\theta + (\Delta^2(p) \cos 2\theta - V_a(p, T))^2} . \quad (3.3)$$

We will derive the evolution of sterile neutrino distribution in the early Universe using Boltzmann equation with certain assumptions explained in the next section.

#### 3.1.1 The sterile neutrino Boltzmann equation

Statistical description of the evolution of a particle in the phase space is given by the Boltzmann equation [73],

$$\hat{L}[f] = \hat{C}[f] , \quad (3.4)$$

where  $\hat{L}$  is the Liouville operator, describing evolution of a phase space volume and  $\hat{C}$  is the collision operator describing interaction of particle species with the medium.

In a homogeneous and isotropic universe, the momentum distribution function  $f(\vec{p}, t)$  does not depend on the direction of momentum. It only depends on the modulus of the momentum  $p$  and time  $t$  (or equivalently on the temperature of the universe  $T$ ).

Hence,

$$f(\vec{p}, t) \equiv f(p, t) \equiv f(p, T) .$$

In a flat-FLRW metric, the Liouville operator  $\hat{L}[f]$  can be written as,

$$\hat{L}[f] = \frac{\partial f}{\partial t} - \frac{\dot{a}}{a} p^i \frac{\partial f}{\partial p^i} , \quad (3.5)$$

where  $p_i$  is the local momentum. Substituting Hubble constant  $H = \frac{\dot{a}}{a}$ , the Liouville operator is written as,

$$\hat{L}(f) = \frac{\partial f}{\partial t} - H p \frac{\partial f}{\partial p} . \quad (3.6)$$

A complete solution of collisional operator  $\hat{C}[f]$  for active-sterile mixing requires density matrix formalism presented in Ref [74, 75]. A recent presentation can be found in [76]. However, this is beyond the scope of this thesis. Thus, we start with the collision operator derived from semiclassical approximation of the quantum kinetic equations (QKE) [71, 72, 76],

$$\begin{aligned} \hat{C}[f] = \sum_i \int \Gamma_i(p'_a, p) f_a(p'_a, t) [1 - f_s(p, t)] d^3 p'_a \\ - \int \Gamma_i(p'_a, p) f_s(p, t) [1 - f_a(p'_a, t)] d^3 p'_a , \end{aligned} \quad (3.7)$$

$$\hat{C}[f] \approx \Gamma(\nu_a \rightarrow \nu_s; p, t) [f_a(p, t) - f_s(p, t)] , \quad (3.8)$$

where  $\Gamma(\nu_a \rightarrow \nu_s; p, t)$  is the damped conversion rate for active-sterile transition. Damped conversion rate is the product of total interaction rate of the neutrinos with the plasma,  $\Gamma = \Gamma_a + \Gamma_s$ , and the time averaged probability for active-sterile transition,  $\langle P_m \rangle$ .

$$\Gamma(\nu_a \rightarrow \nu_s; p, t) \approx \Gamma(p, t) \cdot \langle P_m(\nu_a \rightarrow \nu_s; p, t) \rangle . \quad (3.9)$$

However, sterile neutrinos do not interact with the background. i.e.,  $\Gamma_s = 0$ . An extra correction factor  $\frac{1}{2}$  also comes from this fact that only one particle ( $\nu_a$ ) in the two-state system ( $\nu_\alpha, \nu_s$ ) interacts with the plasma.

Another correction comes from the quantum Zeno effect that damps the transition probability [77],

$$\langle P_m(\nu_a \rightarrow \nu_s; p, t) \rangle = \underbrace{\frac{1}{2} \sin^2 2\theta_M \left[ 1 + \left( \frac{\Gamma_a(p, t) l_m}{2} \right)^2 \right]^{-1}}_{\text{damping factor}} , \quad (3.10)$$

where  $l_m$  is the oscillation length of active neutrino in the background plasma,

$$l_m = \left[ \Delta^2(p) \sin^2 2\theta + (\Delta(p) \cos 2\theta - V_a(p, T))^2 \right]^{-1/2}. \quad (3.11)$$

Then,

$$\langle P_m (\nu_a \rightarrow \nu_s; p, t) \rangle = \frac{1}{2} \frac{\Delta^2(p) \sin 2\theta}{\Delta^2(p) \sin^2 2\theta + \left( \frac{\Gamma_a(p,t)}{2} \right)^2 + (\Delta^2(p) \cos 2\theta - V_a(p, T))^2}. \quad (3.12)$$

Including all the corrections mentioned above, we can write a more accurate expression for damped conversion rate Eq. (3.9),

$$\Gamma (\nu_a \rightarrow \nu_s; p, t) = \frac{1}{4} \frac{\Gamma_a(p, t) \Delta^2(p) \sin 2\theta}{\Delta^2(p) \sin^2 2\theta + \left( \frac{\Gamma_a(p,t)}{2} \right)^2 + (\Delta^2(p) \cos 2\theta - V_a(p, T))^2}. \quad (3.13)$$

Boltzmann equation Eq. (3.4) then becomes

$$\frac{\partial}{\partial t} f_s(p, t) - H p \frac{\partial}{\partial p} f_s(p, t) = \frac{1}{4} \frac{\Gamma_a(p, t) \Delta^2(p) \sin 2\theta}{\Delta^2(p) \sin^2 2\theta + \left( \frac{\Gamma_a(p,t)}{2} \right)^2 + (\Delta^2(p) \cos 2\theta - V_a(p, T))^2} [f_a(p, t) - f_s(p, t)]. \quad (3.14)$$

We make one last simplification that there are no sterile neutrinos present in the Universe before the production. This make sure that  $\nu_s \rightarrow \nu_a$  transition is negligible, and we can ignore the  $-f_s(p, t)$  in the RHS. However, if we have any other sterile neutrino production mechanisms such as scalar decays present in the early universe, this term becomes significant [48].

Then We can write the Boltzmann equation for the Dodelson-Widrow mechanism,

$$\frac{\partial}{\partial t} f_s(p, t) - H p \frac{\partial}{\partial p} f_s(p, t) = \frac{1}{4} \frac{\Gamma_a(p, t) \Delta^2(p) \sin 2\theta}{\Delta^2(p) \sin^2 2\theta + \left( \frac{\Gamma_a(p,t)}{2} \right)^2 + (\Delta^2(p) \cos 2\theta - V_a(p, T))^2} f_a(p, t), \quad (3.15)$$

where

$f_a(p, t)$  = active neutrino momentum distribution,

$f_s(p, t)$  = sterile neutrino momentum distribution,

$H(t)$  = Hubble constant,

$\theta$  = active-sterile mixing angle in vacuum,

$\Gamma_a$  = active neutrino interaction rate,

$V_a$  = active neutrino effective potential,

$$\Delta(p) = \frac{\Delta m_{as}^2}{2p} \approx \frac{m_s^2}{2p}$$

Now let's take a look at two important quantities in Eq. (3.15), Active neutrino interaction rate and effective potential.

### 3.1.2 Active neutrino interaction rate in the Standard Model

Active neutrinos interact with particles in the primordial plasma through electroweak interactions. Total interaction rate depends on the number and types of particles in the plasma. As we see in Fig. 3.1, effective degrees of freedom changes with temperature of the early universe. Thus, total interaction rate is a complicated function of temperature.

Considering a general reaction  $\nu_a(p) + A(p_A) \rightarrow B(p_B) + C(p_C)$ , total cross-section

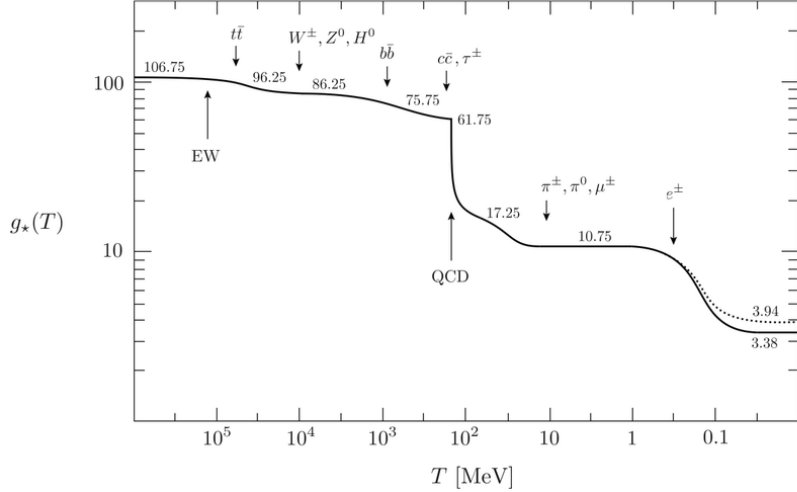


FIGURE 3.1: Effective number of relativistic degrees of freedom in the early Universe as a function of temperature. The dotted line indicate the entropic degrees of freedom. Decoupling of particles from the plasma at different temperatures are also shown (Taken from [78]).

is approximately [29],

$$\sigma \propto G_F^2 s, \text{ where } s = (p + p_A)^2 . \quad (3.16)$$

Total interaction rate can be then found out using [79],

$$\Gamma_a(p, T) \propto \int \frac{d^3 \vec{p}_A}{(2\pi)^3} f(E_A, T) \sigma(\vec{p}, \vec{p}_A) v_{\text{M}\ddot{\text{o}}\text{l}\text{l}\text{er}} , \quad (3.17)$$

where  $f(E', T) = 1 / (1 + \exp [E'/T])$  is the Fermi-Dirac distribution function for the particle  $A$ . Møller velocity can be approximated to  $(1 - \cos \theta)$  for ultra-relativistic particles [80].

$$\Gamma_a(p, T) \propto \int \frac{4\pi p_A^2 dp_A}{(2\pi)^3} \frac{1}{1 + \exp(E_A/T)} G_F^2 (p + p_A)^2 \cdot (1 - \cos \theta) \quad (3.18)$$

gives

$$\Gamma_a(p, T) \propto G_F^2 p T^4 . \quad (3.19)$$

A more detailed calculation of interaction rate in the context of non-standard interactions presented in Appendix B.

The exact expression of  $\Gamma_a(p, T)$  depends on the dynamics of the early universe. As we see from Fig. 3.1, QCD phase transition drastically changes the available number of particles in the plasma around 150 MeV. A detailed 2-loop calculation including

all the QCD contribution was done by Asaka, Laine and Shaposhnikov [81, 55] and we make use of the machine-readable numerical data files<sup>1</sup> available from this work. Then we can write the total interaction rate as,

$$\Gamma_a(p, T) = C_a(T) G_F^2 p T^4 , \quad (3.20)$$

where  $C_a(T)$  is a temperature and flavour dependent function shown in Fig. 3.2.

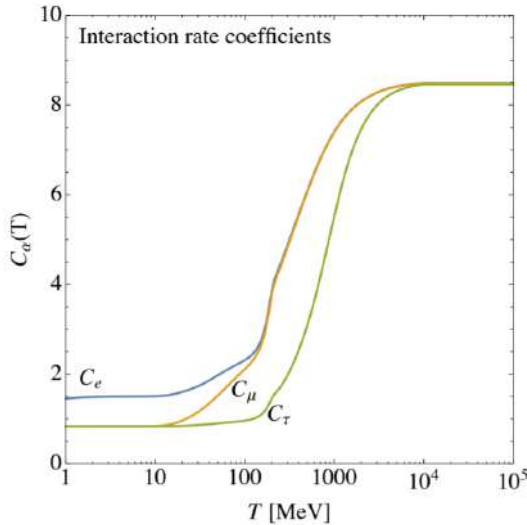


FIGURE 3.2:  $T$  Vs  $C_a(T)$  for  $a = e, \mu, \tau$  (Taken from [48]).

### 3.1.3 The Standard Model effective potential

Effective potential or equivalently thermal potential experienced by active neutrinos in the early universe can be derived from dispersion relation of neutrinos [82]. One of the first calculations using Finite Temperature formalism can be found in [83]. However, we follow a more detailed and student-friendly derivation presented by D’Olivo et al. [84].

The Dirac equation for neutrinos propagating through a medium with charged leptons and nucleons in the background is given by

$$(\not{k} - \Sigma_{\text{eff}}) \psi = 0 , \quad (3.21)$$

where  $\Sigma_{\text{eff}}$  is the effective Self-energy. There are two diagrams contributing to Self-energy: Tadpole diagram mediated by  $Z$ - boson(left panel) and Sunset diagram mediated by  $W$ - boson (right panel), as shown in Fig. 3.3.

Chiral nature of the active neutrinos implies  $\Sigma_{\text{eff}} = P_R(a_0 \not{k} + b_0 \not{\psi}) P_L$ , and dispersion relation can be written as

$$\omega_\kappa = \kappa - b_0 (\omega_\kappa = -\kappa) \quad (3.22)$$

for neutrinos, and

$$\bar{\omega}_\kappa = \kappa - b_0 (\omega_\kappa = -\kappa) \quad (3.23)$$

---

<sup>1</sup>See <http://www.laine.itp.unibe.ch/neutrino-rate/>

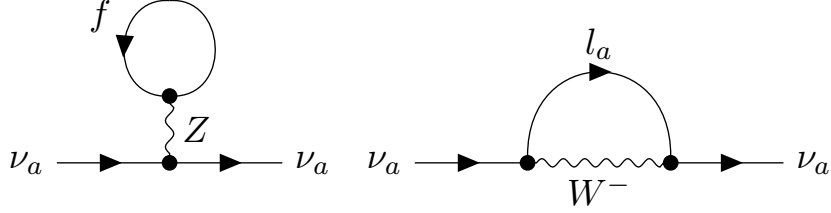


FIGURE 3.3: Self-energy contributions to effective potential.  $f$  represents any fermion species in the background.

for anti neutrinos at the first order.

We can visualize the effective potential as a contribution to the energy of the particle by background medium. That means,

$$\begin{aligned} \text{Energy of Neutrino propagating through a medium} = \\ \text{Energy of neutrino in vacuum} + \text{Effective potential in the medium ,} \end{aligned}$$

$$\omega_\kappa = \kappa + V_a \quad (3.24)$$

Thus, to calculate effective potential, we essentially have to find  $b_0$  from the effective Self-energy.

A detailed calculation in the context of non-standard interactions is presented in Appendix C. We find that for an electron neutrino,

$$\begin{aligned} V_e = \pm \sqrt{2} G_F \left( n_e - n_{\bar{e}} + n_{\nu_e} - n_{\bar{\nu}_e} + 2 \sum_f \frac{X_f}{g_f} (n_f - n_{\bar{f}}) \right) \\ - \frac{8\sqrt{2}G_F\kappa}{3m_W^2} (n_e \langle E_e \rangle + n_{\bar{e}} \langle E_{\bar{e}} \rangle) - \frac{8\sqrt{2}G_F\kappa}{3m_Z^2} (n_{\nu_e} \langle E_{\nu_e} \rangle + n_{\bar{\nu}_e} \langle E_{\bar{\nu}_e} \rangle) . \quad (3.25) \end{aligned}$$

In a lepton symmetric universe, leptonic number densities in the first term cancels out and only baryonic asymmetry  $\eta_B$  remains.

Thus, final equation for effective potential to use in Boltzmann equation Eq. (3.15),

$$V_e(p, T) = \pm \sqrt{2} G_F \frac{2\zeta(3)T^3}{\pi^2} \frac{\eta_B}{4} - \frac{8\sqrt{2}G_F}{3m_W^2} \cdot \frac{11.36}{\pi^2} p T^4 - \frac{8\sqrt{2}G_F}{3m_Z^2} \cdot \frac{7\pi^2}{120} p T^4 , \quad (3.26)$$

where we numerically calculated electron and electron neutrino number density and average energy to be

$$(n_e \langle E_e \rangle + n_{\bar{e}} \langle E_{\bar{e}} \rangle) = \frac{11.36 T^4}{\pi^2} , \quad (3.27)$$

$$(n_{\nu_e} \langle E_{\nu_e} \rangle + n_{\bar{\nu}_e} \langle E_{\bar{\nu}_e} \rangle) = \frac{7\pi^2 T^4}{120} . \quad (3.28)$$

### 3.1.4 Numerical implementation of the Boltzmann equation

Numerical implementation of Boltzmann equation in full generality is a complicated task. There are Boltzmann solvers such as **CLASS** [85] and **CAMB** [86] in the context of cosmic microwave background (CMB) calculations. Publicly available codes such

as `sterile-dm` [72] and `LASAGNA` [87] can solve sterile neutrino production with non-zero lepton asymmetry. However, they are difficult to modify and repurpose for non-standard interactions. Thus, we will use `MATHEMATICA` to numerically solve the Boltzmann equation after analytically simplifying Eq. (3.15). Our code is publicly available on GitHub<sup>2</sup>.

Analytical solution of the Boltzmann equation derived in Appendix A gives sterile neutrino distribution function

$$f_s(r) = \int_{T_i}^{T_f} \sqrt{\frac{90 M_{\text{Pl}}^2}{8\pi^3 g_{*s}(T)}} \frac{1}{T^3} \left( 1 + \frac{Tg'_{*s}(T)}{3g_{*s}(T)} \right) \cdot h(p_{\text{redshift}}, T) \frac{1}{\exp\left(\frac{p_{\text{redshift}}}{T}\right) + 1} dT , \quad (3.29)$$

where  $p_{\text{redshift}} = r \cdot T \left( \frac{g_{*s}(T)}{g_{*s}(T_f)} \right)^{1/3}$  is the redshifted momentum. The Planck mass is denoted by  $M_{\text{Pl}}$ , and  $g_{*s}(T)$  represent effective entropic degrees of freedom in the universe at temperature  $T$ .

This expression is numerically evaluated to obtain the sterile neutrino distribution function  $f_s(r) \equiv f_s(p, T)$ . We set initial and final temperature to be  $T_i = 1$  GeV and  $T_f = 1$  MeV as the main production window lies in this regime as explained in Sec 2.3.1. Fig 3.4 gives momentum distribution function for a sterile neutrino with  $m_s = 10$  keV and an active-sterile mixing angle of  $\sin^2 2\theta = 1.1 \times 10^{-9}$ , that gives sterile neutrino relic abundance  $\Omega_{sh}h^2 = 0.12$ . We can see from the brown dashed line in the figure that sterile neutrino distribution function differs from pure Fermi-Dirac thermal distribution.

Once we have the distribution functions, we can find relic abundance by integrating

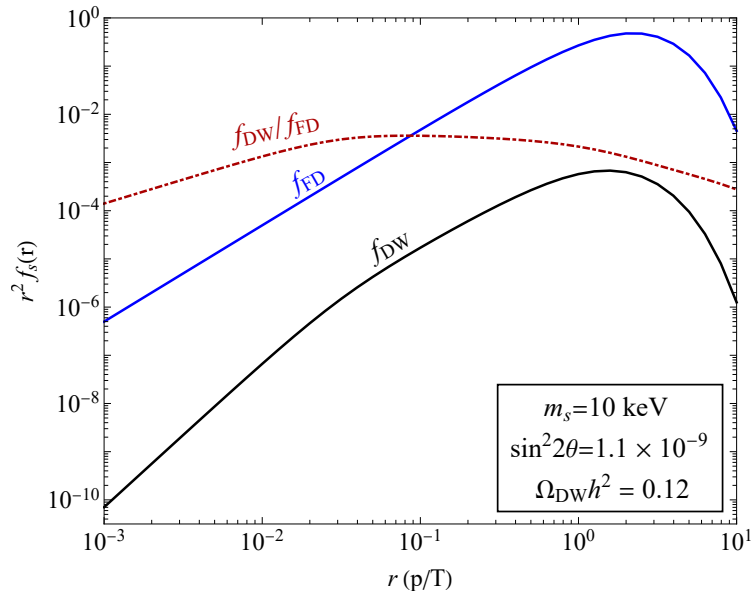


FIGURE 3.4: Sterile neutrino distribution function for the basic Dodelson-Widrow mechanism as a function of rescaled momentum  $r$ . The Fermi-Dirac distribution is indicated as a blue line for comparison. The brown dotted line represents the ratio  $f_{DW}/f_{FD}$ .

<sup>2</sup>See <https://github.com/cristinabenso92/Sterile-neutrino-production-via-Dodelson-Widrow-with-NSSI>

them over the momentum. Derived in Appendix A.2,

$$\Omega_s h^2 = 2.74 \times 10^2 \left( \frac{m_s}{\text{keV}} \right) \frac{45}{4\pi^4} \frac{g_s}{g_{*s}(T_f)} \int_0^\infty r^2 f_s(r) dr , \quad (3.30)$$

where  $g_s$  is the degrees of freedom for sterile neutrinos and  $g_{*s}(T)$  is the effective entropic degrees of freedom in the early Universe at temperature  $T$ .

Parameter space presented in Fig. 3.5 features experimental sensitivities<sup>3</sup> from KATRIN [16], TRISTAN [17] (an upgrade of KATRIN), ECHO [18] and HUNTER [19]. X-ray bound from NuSTAR [28] gives an indication that sterile neutrinos produced by the basic Dodelson-Widrow mechanism cannot account for 100% of dark matter. However, “cocktail DM” scenario where sterile neutrinos make up only a fraction of

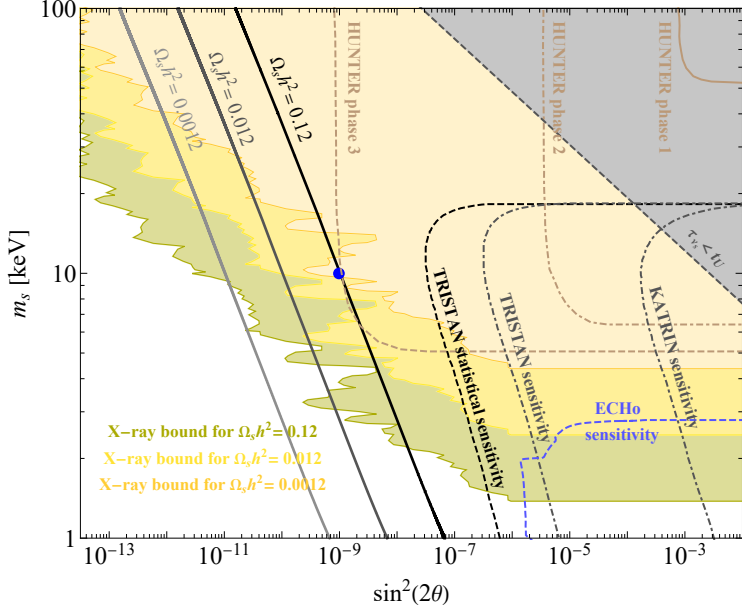


FIGURE 3.5: Sterile neutrino parameter space for the basic Dodelson-Widrow mechanism. Blue dot represent the benchmark point taken for Fig. 3.4. The black line corresponds to full dark matter abundance provided by the basic DW scenario. The grey lines represent the cocktail DM scenario, where only a fraction of the dark matter is produced by the basic DW mechanism. Experimental bounds featured in the plot are explained in Sec. 3.1.4.

the dark matter might be possible with this production mechanism due to relaxation of X-ray constraints with decreasing sterile neutrino abundance. But this scenario is out of reach for terrestrial neutrino experiments. Best sensitivity among the experiments comes from phase 3 of HUNTER [19] experiment, which is set in the near future.

Non-resonant production of sterile neutrinos is an unavoidable mechanism, even if it is ruled out to produce the full dark matter abundance. Thus, shortcomings of the basic Dodelson-Widrow mechanism motivate us to introduce new interactions and study whether it can be enhanced to reach current experimental sensitivities or evade astrophysical constraints.

<sup>3</sup>Taken from <https://github.com/cristinabenso92/sterile-neutrino-in-non-standard-cosmology>

## 3.2 Dodelson-Widrow mechanism in presence of NSSIs

As we saw in the previous section, the Dodelson-Widrow mechanism cannot be the sole source of sterile neutrinos as the only dark matter particle. Thus, we try to introduce secret neutrino interactions in addition to active-sterile mixing and see how it can modify DW production. There have been some attempts with sterile neutrino self-interactions with heavy scalar mediator [88], active neutrino self-interactions with scalar [89] and vector [79] mediators. While sterile self-interactions lead to resonances and overabundance, active neutrino self-interactions give promising results that can be probed in experiments such as DUNE [89]. We will thus take a look at active neutrino self-interactions but from an EFT perspective, which has never been attempted before. The obvious assumption of EFT treatment is that the mediators are heavy. However, NSSI treatment can work out different kinds of mediators without at the same time, which gives a more broad result than other approaches.

### 3.2.1 Non-standard neutrino self-interactions

Non-standard neutrino self-interaction Lagrangian defined in Eq. (2.93),

$$\mathcal{L}_{\text{NSSI}} = \frac{G_F \epsilon}{\sqrt{2}} (\bar{\nu} \mathcal{O} \nu) (\bar{\nu} \bar{\mathcal{O}} \nu) - \frac{G_F \epsilon}{\sqrt{2} m_\phi^2} (\bar{\nu} \mathcal{O} \nu) \square (\bar{\nu} \bar{\mathcal{O}} \nu) , \quad (3.31)$$

where  $\mathcal{O}$  being element of complete set of fermionic bilinears.

We will consider Majorana neutrinos as previous works considered active Dirac neutrinos [89, 79]. The choice of Majorana neutrinos could also be interesting for phenomenology, since the nature of neutrinos is still an open question. As a consequence of this choice of Majorana neutrinos, vector and tensor non-standard interactions become zero.

$$\bar{\psi} \gamma^\mu \psi = \overline{\psi^C} \gamma^\mu \psi^C = -\psi^T \mathcal{C}^\dagger \gamma^\mu \mathcal{C} \bar{\psi}^T = \bar{\psi} \mathcal{C} \gamma^{\mu T} \mathcal{C}^\dagger \psi = -\bar{\psi} \gamma^\mu \psi = 0 , \quad (3.32)$$

$$\bar{\psi} \sigma^{\mu\nu} \psi = \overline{\psi^C} \sigma^{\mu\nu} \psi^C = -\psi^T \mathcal{C}^\dagger \sigma^{\mu\nu} \mathcal{C} \bar{\psi}^T = \bar{\psi} \mathcal{C} (\sigma^{\mu\nu})^T \mathcal{C}^\dagger \psi = -\bar{\psi} \sigma^{\mu\nu} \psi = 0 . \quad (3.33)$$

Thus, we are left with scalar, pseudoscalar and axial vector NSSI operators.

	$\epsilon_j$	$\mathcal{O}$	$\bar{\mathcal{O}} = \gamma^0 \mathcal{O}^\dagger \gamma^0$
Scalar	$\epsilon_S$	$\mathbb{I}$	$\mathbb{I}$
Axialvector	$\epsilon_A$	$\gamma_\mu \gamma^5$	$\gamma_\mu \gamma^5$
Pseudoscalar	$\epsilon_P$	$i\gamma^5$	$i\gamma^5$

TABLE 3.1: NSSI operators considered in this work.

### 3.2.2 Non-standard self-interaction rate

Secret self-interactions open up new channels for neutrino scattering in addition to the Standard Model interactions discussed in Sec. 3.1.2. There will be an extra channel for neutrino-neutrino scattering, as given in Fig. 3.6.

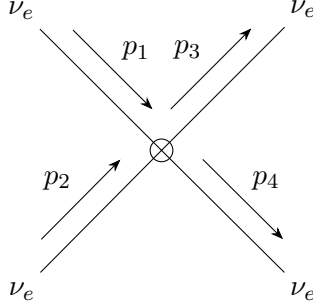


FIGURE 3.6: NSSI contribution to the interaction rate

However, we can ignore the second term in Eq. (3.31) as it will only contribute at the order  $\frac{G_F^2}{m_\phi^4} \sim \mathcal{O}\left(\frac{1}{m_\phi^8}\right)$  compared to  $\mathcal{O}\left(\frac{1}{m_\phi^4}\right)$  contribution by the first term.

Using Majorana Feynman rules presented in Refs. [31, 90], amplitudes are calculated with FEYNCALC [91]. Non-standard self-interaction rates can then be obtained from total cross section  $\sigma_{\text{NSSI}}$  using Eq. (3.17),

$$\Gamma_{\text{NSSI}}(E, T) = \int \frac{d^3 \vec{p}_\nu}{(2\pi)^3} f(E_\nu, T) \sigma_{\text{NSSI}}(\vec{p}, \vec{p}_\nu) v_{\text{M\o ller}} , \quad (3.34)$$

where  $f(E_\nu, T) = 1/(1 + \exp[E_\nu/T])$  is the Fermi-Dirac distribution function for an active neutrino. From the detailed calculation presented in Appendix B, we get the following results,

$$\textbf{Scalar NSSI: } \Gamma_S(p, T) = \frac{7\pi G_F^2 \epsilon_S^2}{180} p T^4 , \quad (3.35)$$

$$\textbf{Axial vector NSSI: } \Gamma_A(p, T) = \frac{7\pi G_F^2 \epsilon_A^2}{135} p T^4 , \quad (3.36)$$

$$\textbf{Pseudoscalar NSSI: } \Gamma_P(p, T) = \frac{7\pi G_F^2 \epsilon_P^2}{180} p T^4 . \quad (3.37)$$

### 3.2.3 Non-standard self-interaction effective potential

As explained in Sec. 3.1.3, effective potential on active neutrinos can be calculated from the dispersion relations and Self-energy. We can follow the same treatment provided in the context of the Standard Model [84] for non-standard interactions. In fact, effective field theory treatment makes Self-energy calculations easier. But, if we only consider the first term in the NSSI Lagrangian as it is done often, we end up getting only temperature independent lepton asymmetric potential. But these terms are not relevant for the Dodelson-Widrow mechanism with zero lepton asymmetry. Thus, it is essential to go higher order in effective field theory and include momentum dependent terms in the Lagrangian.

Effective potential calculated from the non-standard contribution to active neutrino Self-energy shown in Fig. 3.7 is calculated in Appendix C. We get the following results,

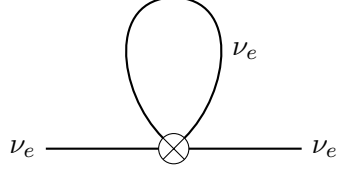


FIGURE 3.7: NSSI contribution to the active neutrino self-energy.

**Scalar NSSI:**

$$V_S = -\frac{8\sqrt{2}G_F \epsilon_S}{3m_\phi^2} \cdot \omega \cdot (n_\nu \langle E_\nu \rangle + n_{\bar{\nu}} \langle E_{\bar{\nu}} \rangle) = -\frac{7\sqrt{2}\pi^2 G_F \epsilon_S}{45m_\phi^2} \epsilon_S \cdot p T^4 , \quad (3.38)$$

**Axial vector NSSI:**

$$V_A = -\frac{16\sqrt{2}G_F \epsilon_A}{3m_\phi^2} \cdot \omega \cdot (n_\nu \langle E_\nu \rangle + n_{\bar{\nu}} \langle E_{\bar{\nu}} \rangle) = -\frac{14\sqrt{2}\pi^2 G_F \epsilon_A}{45m_\phi^2} \cdot p T^4 , \quad (3.39)$$

**Pseudoscalar NSSI:**

$$V_P = -\frac{8\sqrt{2}G_F \epsilon_P}{3m_\phi^2} \cdot \omega \cdot (n_\nu \langle E_\nu \rangle + n_{\bar{\nu}} \langle E_{\bar{\nu}} \rangle) = -\frac{7\sqrt{2}\pi^2 G_F \epsilon_P}{45m_\phi^2} \cdot p T^4 . \quad (3.40)$$

**3.2.4 Numerical implementation**

Now that we have all the necessary ingredients, we can numerically solve the Boltzmann equation similar to Sec. 3.1.4.

The Boltzmann equation for sterile neutrino evolution in presence of non-standard self-interaction is given by,

$$\frac{\partial}{\partial t} f_s(p, t) - H p \frac{\partial}{\partial p} f_s(p, t) = \frac{1}{4} \frac{\Gamma_{\text{total}}(p, t) \Delta^2(p) \sin 2\theta}{\Delta^2(p) \sin^2 2\theta + \left(\frac{\Gamma_{\text{total}}(p, t)}{2}\right)^2 + (\Delta^2(p) \cos 2\theta - V_{\text{total}}(p, T))^2} f_a(p, t) , \quad (3.41)$$

where total interaction rate and effective potential modified from the standard case to

$$\begin{aligned} \Gamma_{\text{total}} &= \Gamma_{\text{SM}} + \Gamma_{\text{NSSI}} , \\ V_{\text{total}} &= V_{\text{SM}} + V_{\text{NSSI}} . \end{aligned}$$

Non-standard interaction rates calculated in Sec. 3.2.2 have the same sign as the standard model interaction rates presented in Sec. 3.1.2. As a result, unlike in the case of sterile neutrino self-interactions [88], there is no possibility of resonance. It is also important to note that both scalar and pseudoscalar interactions give the same results for both interaction rate and effective potential, hence we expect they give the same momentum distribution for sterile neutrinos. This implies it is not possible to distinguish between two interactions from the perspective of sterile neutrino production. Numerically implementing the Dodelson-Widrow mechanism in presence of NSSIs similar to Sec. 3.1.4, we present the results in the next section.

### 3.2.5 Results and discussion

As mentioned in the Sec. 2.5.1, the strongest constraint on NSSI parameter  $\epsilon$  comes from invisible  $Z$ -decay [70] that sets  $|\epsilon| = 0 - 10$ . We report results for  $\epsilon$  ranging from 0.1 to 100. We can safely neglect negative values of  $\epsilon$  as we only have active neutrino self-interaction with single flavour. Since it would be complicated to plot for all mediator masses, we take three benchmark masses:

- $m_\phi = 10$  GeV, lower mass limit of effective field theory treatment,
- $m_\phi = 100$  GeV, mediator mass comparable to electroweak mediators,
- $m_\phi = 50$  GeV, midpoint between lower and upper limits.

We observed that mediator masses much higher than electroweak scale have no considerable impact in the sterile neutrino production. We will not get any interesting results as thermal potential contribution would have less impact if  $m_\phi \gg M_{W,Z}$ .

#### Differential sterile neutrino production rate

Differential sterile neutrino production rate,  $\frac{df}{dT}$  gives us an idea about how sterile neutrino production evolves with temperature. For resonant production mechanisms, this plot will feature a sharp peak around the resonance temperature [51]. But that is not the case in this work. We present the differential rate for one set of sterile neutrino mass, mixing angle and rescaled momentum values:

$$m_s = 10 \text{ keV}, \sin^2 2\theta = 1.1 \times 10^{-9}, r = 1 ,$$

for pseudoscalar NSSI in Fig. 3.8. Other NSSIs feature almost identical spectra. From the figure, we can infer:

- active neutrino NSSIs cannot induce any resonance.
- Sterile neutrino production slowly starts at  $T = 1$  GeV and peaks around  $\mathcal{O}(100)$  MeV and then decreases.
- The basic Dodelson-Widrow production has a peak temperature  $T \sim 133$  keV ·  $(m_s/\text{keV})^{\frac{1}{3}}$ . Non-standard interactions can shift this peak production temperature.
- Temperature dependence of sterile neutrino production implies it is important to include momentum dependent terms in the EFT Lagrangian and use finite temperature field theory (FTFT) formalism. However, the peak temperature is around  $T \sim 0.1$  GeV, our choice of mediator masses are always much higher than the relevant production temperatures. Thus, we can truncate the momentum dependence at the  $\mathcal{O}(p^2)$  and EFT framework with mediator masses  $m_\phi \geq 10$  GeV is justified.
- Dashed lines in the figure represents the NSSI interactions that give correct abundance with the given parameters. As the mediator mass increases, we can see that this dashed lines get closer to the standard Dodelson-Widrow line and at for  $m_\phi \gg 100$  GeV, this line coincide with standard DW scenario.

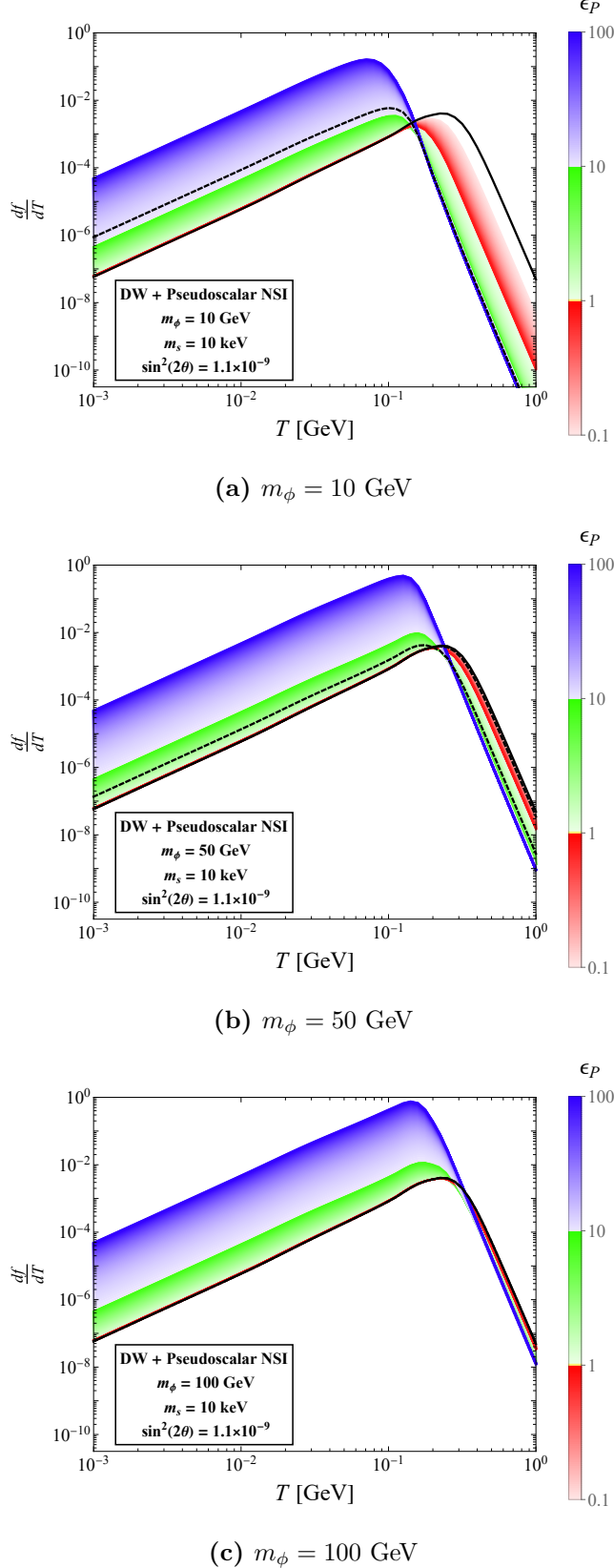


FIGURE 3.8: Sterile neutrino production rate as a function of temperature  $T$  for the Dodelson-Widrow mechanism in presence of a pseudoscalar NSSI. The thick black line corresponds to the basic DW scenario. The dashed black line corresponds to the NSSI strength that gives the correct abundance in the new production mechanism. NSSI strength  $\epsilon$  is colour coded in the bar legend and  $r = 1$ .

### Sterile neutrino distribution function

We plot sterile neutrino distribution function for all three types of interactions as a function of rescaled momentum  $r$ . We take the same combination of sterile neutrino mass and mixing angle in the previous section,

$$m_s = 10 \text{ keV}, \sin^2 2\theta = 1.1 \times 10^{-9},$$

that gives correct relic abundance ( $\Omega_{\text{DWh}} h^2 = 0.12$ ) in the standard Dodelson-Widrow mechanism. Distribution functions are shown in Fig. 3.9 for scalar NSSI, Fig. 3.11 for axial vector NSSI and Fig. 3.10 for pseudoscalar NSSI. We can clearly see that non-standard self-interactions shift the sterile neutrino momentum distribution function. There are few comments in order:

- Scalar and pseudoscalar NSSIs give the same distribution. Axialvector NSSIs give a slightly different distribution function as its interaction rate and effective potential differs from the other two NSSIs.
- It is possible to have distribution momentum suppression compared to basic DW scenario for lower mediator masses. As mediator mass increases, suppression reduces and sterile neutrino distribution function is enhanced for  $\epsilon > 1$ . There is still a small suppression for  $\epsilon < 1$ .
- There is a reversal in trend around  $\epsilon = 1$  as we increase  $\epsilon$  from 0.1 to 100. Increasing  $\epsilon$  from 0.1 to 1 suppresses the sterile neutrino momentum distribution. From  $\epsilon = 1 - 100$ , sterile neutrino distribution function increases with increasing NSSI strength  $\epsilon$ .
- Average momentum  $\langle p/T \rangle$  stays more or less the same throughout the  $\epsilon$  values. However, there is a slight shift to the right, which will be clear from the free streaming length plots presented in the last subsection.

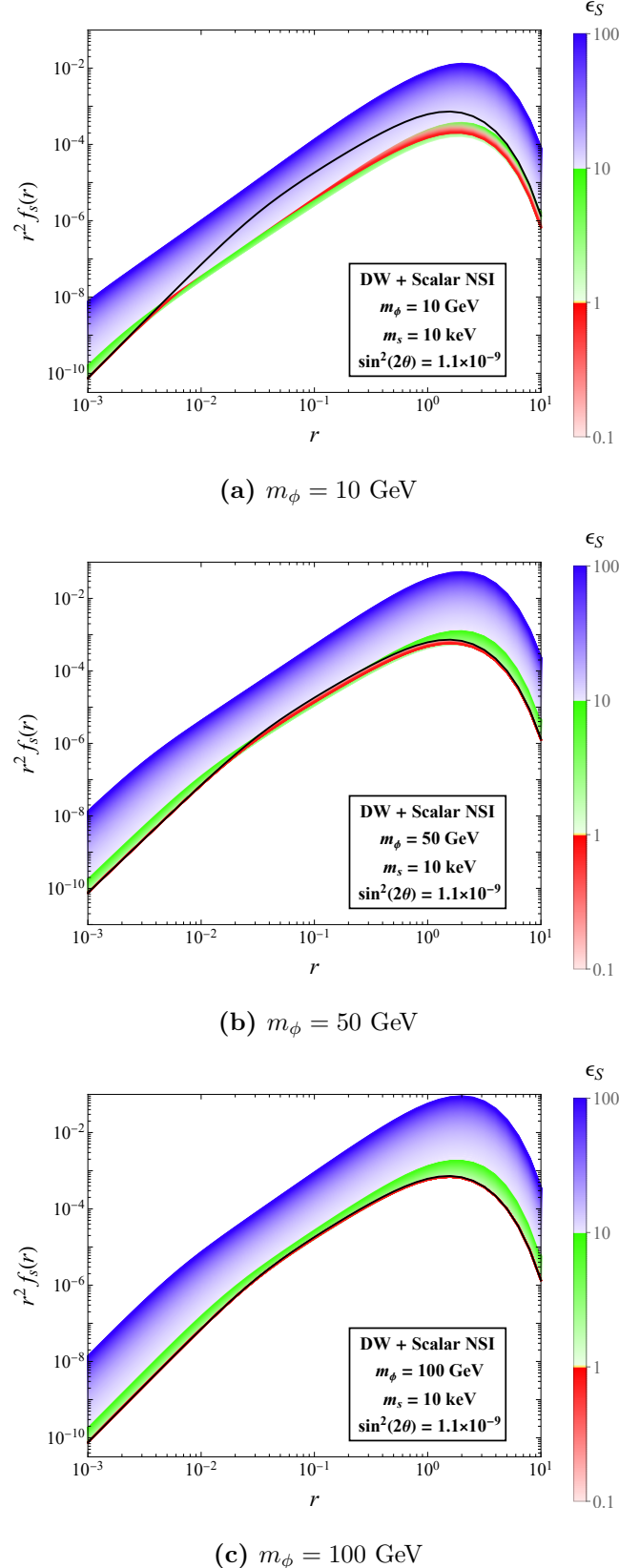


FIGURE 3.9: Sterile neutrino distribution function for the Dodelson-Widrow mechanism in presence of a scalar NSSI as a function of rescaled momentum  $r = p/T$ . The black line corresponds to the basic DW scenario. NSSI strength  $\epsilon$  is colour coded in the bar legend.

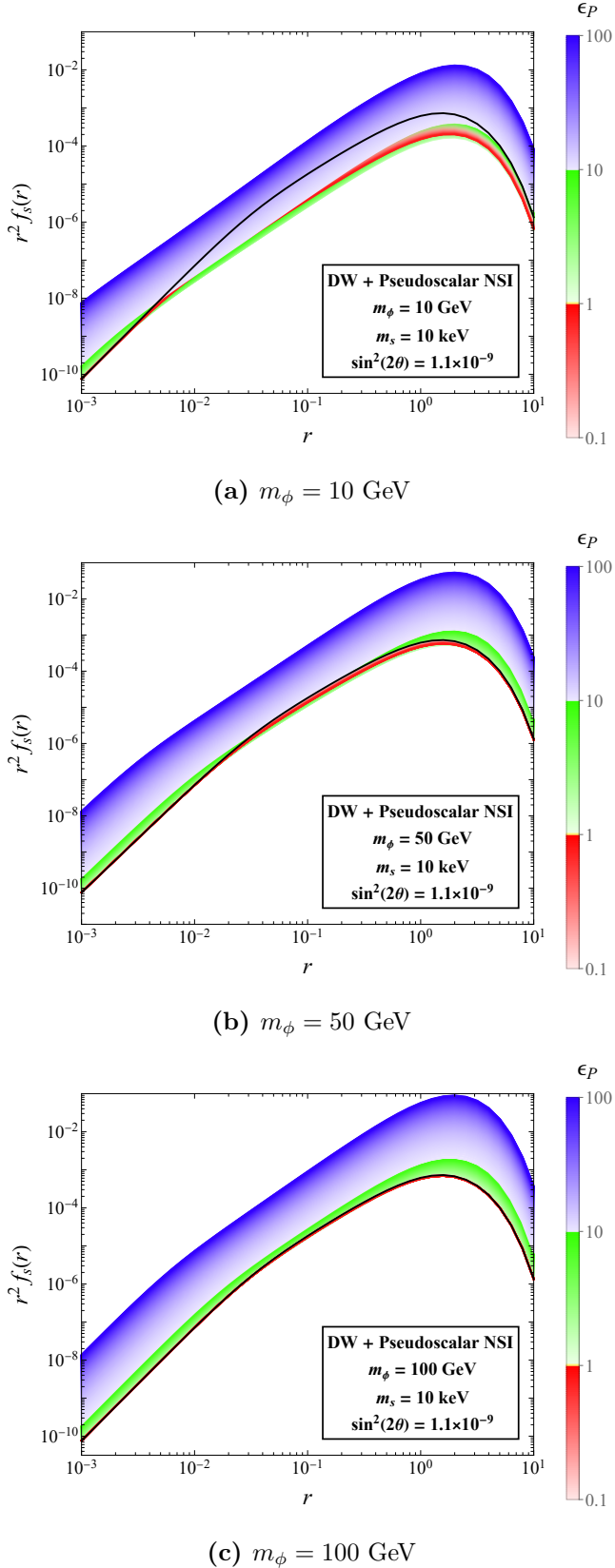


FIGURE 3.10: Sterile neutrino distribution function for the Dodelson-Widrow mechanism in presence of a pseudoscalar NSSI as a function of rescaled momentum  $r = p/T$ . The black line corresponds to the basic DW scenario. NSSI strength  $\epsilon$  is colour coded in the bar legend.

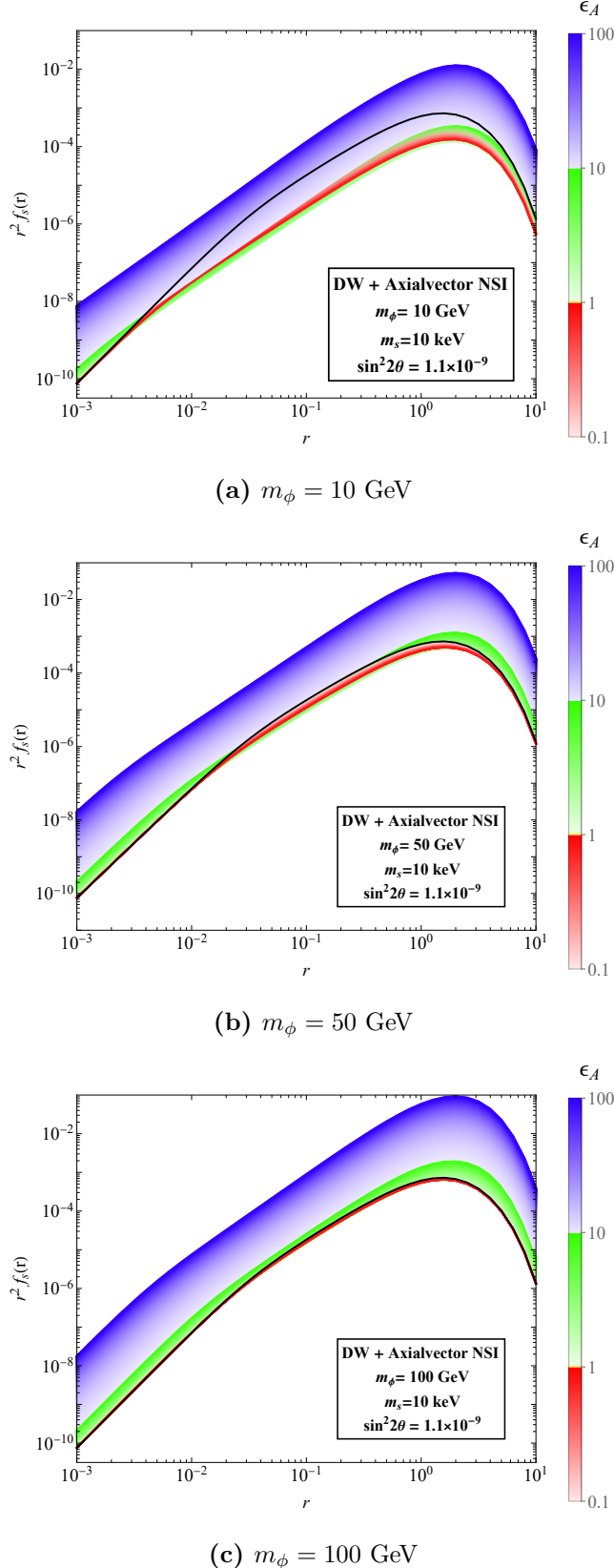


FIGURE 3.11: Sterile neutrino distribution function for the Dodelson-Widrow mechanism in presence of an axial vector NSSI as a function of rescaled momentum  $r = p/T$ . The black line corresponds to the basic DW scenario. NSSI strength  $\epsilon$  is colour coded in the bar legend.

### Sterile neutrino relic abundance

Integrating the sterile neutrino distribution functions to obtain relic abundance, we plot parameter space with sterile neutrinos making up 100% of the dark matter ( $\Omega_{sh}^2 = 0.12$ ), and a “cocktail DM” scenario where sterile neutrinos making up 10% of the total dark matter present in the Universe ( $\Omega_s h^2 = 0.012$ ). We include sensitivities of the following neutrino mass experiments in the plot:

- KATRIN [16],
- TRISTAN [17], TRISTAN statistical sensitivity,
- phase 1,2,3 of HUNTER [19],
- ECHo [18],
- X-ray bounds from not observing decay of sterile neutrinos [28],
- Bound from stability of dark matter ( $\tau_{\nu_s} < t_{\text{Universe}}$ ).

Sterile neutrino parameter spaces are shown in Fig. 3.12 for scalar NSSI, Fig. 3.12 for pseudoscalar NSSI, and Fig. 3.12 for axial vector NSSI.

We make the following observations from the plots:

- Scalar and pseudoscalar NSSIs give identical parameter spaces.
- Similar to the trend in distribution functions, relic abundance decreases as we increase  $\epsilon$  from 0.1 to 1, and then it increases with  $\epsilon$ . This also implies that the same relic abundance can be obtained for two different values of NSSI strength  $\epsilon$ .
- Increase in mediator mass shifts the parameter space to the left. But when mediators are heavier than electroweak mediator, the effect of NSSI diminished and the parameter space resembles standard Dodelson-Widrow scenario with a multiplication factor.
- Similar to the basic Dodelson-Widrow mechanism, astrophysical constraints almost rule out the parameter space for  $\Omega_s h^2 = 0.12$ . However, “cocktail DM” scenario changed parameter space two-fold: X-ray constraints will be relaxed for lower sterile neutrino abundances and sterile neutrino relic abundance lines shift to the lower values of mixing angle. This enhancement is however unreachable to experimental sensitivities.
- Experimental sensitivities of KATRIN, TRISTAN and ECHo cannot reach allowed mixing angles for Dodelson-Widrow production even when NSSIs are present. However, phase 3 sensitivities of HUNTER can reach the mass and mixing angle values required to produce 100% dark matter abundance, with  $\epsilon = 0 - 10$  values for mediator with the lowest mass. If we further reduced the mediator mass, it would not be possible to use the EFT framework. However, we expect non-trivial changes for light mediators and there can be resonances which could change the parameter space.

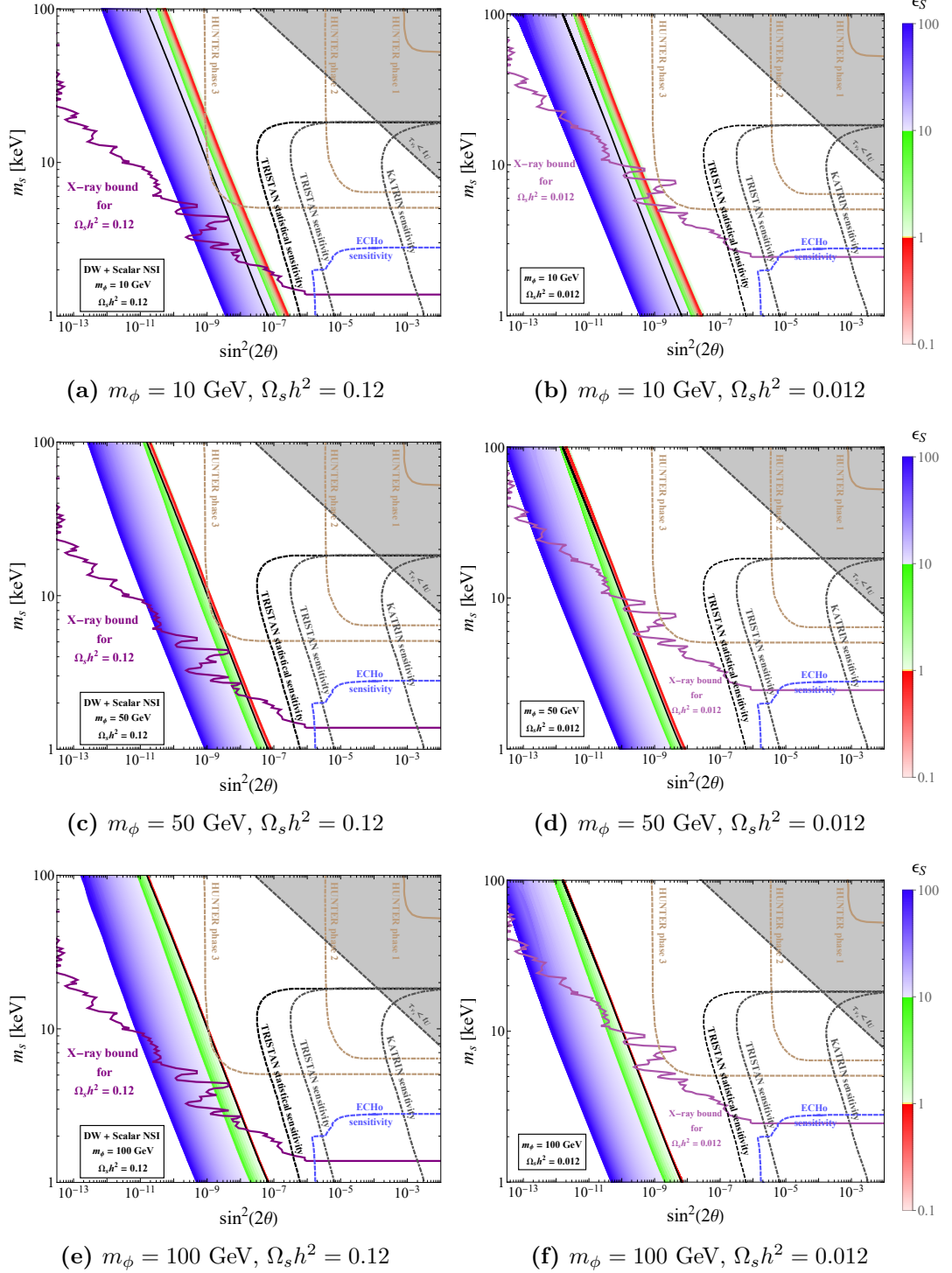


FIGURE 3.12: Relic abundance parameter space for DW mechanism with the scalar NSSI. Figures in the right represent cocktail DM scenario with 10% relic abundance. NSSI strength  $\epsilon_S$  is colour coded from 0.1 to 100 in the bar legend. The black line corresponds to the standard DW scenario. Beige (HUNTER), black (KATRIN/TRISTAN), and blue (ECHO) dashed lines represent experimental sensitivities. X-ray constraints for corresponding relic abundance shown in purple.

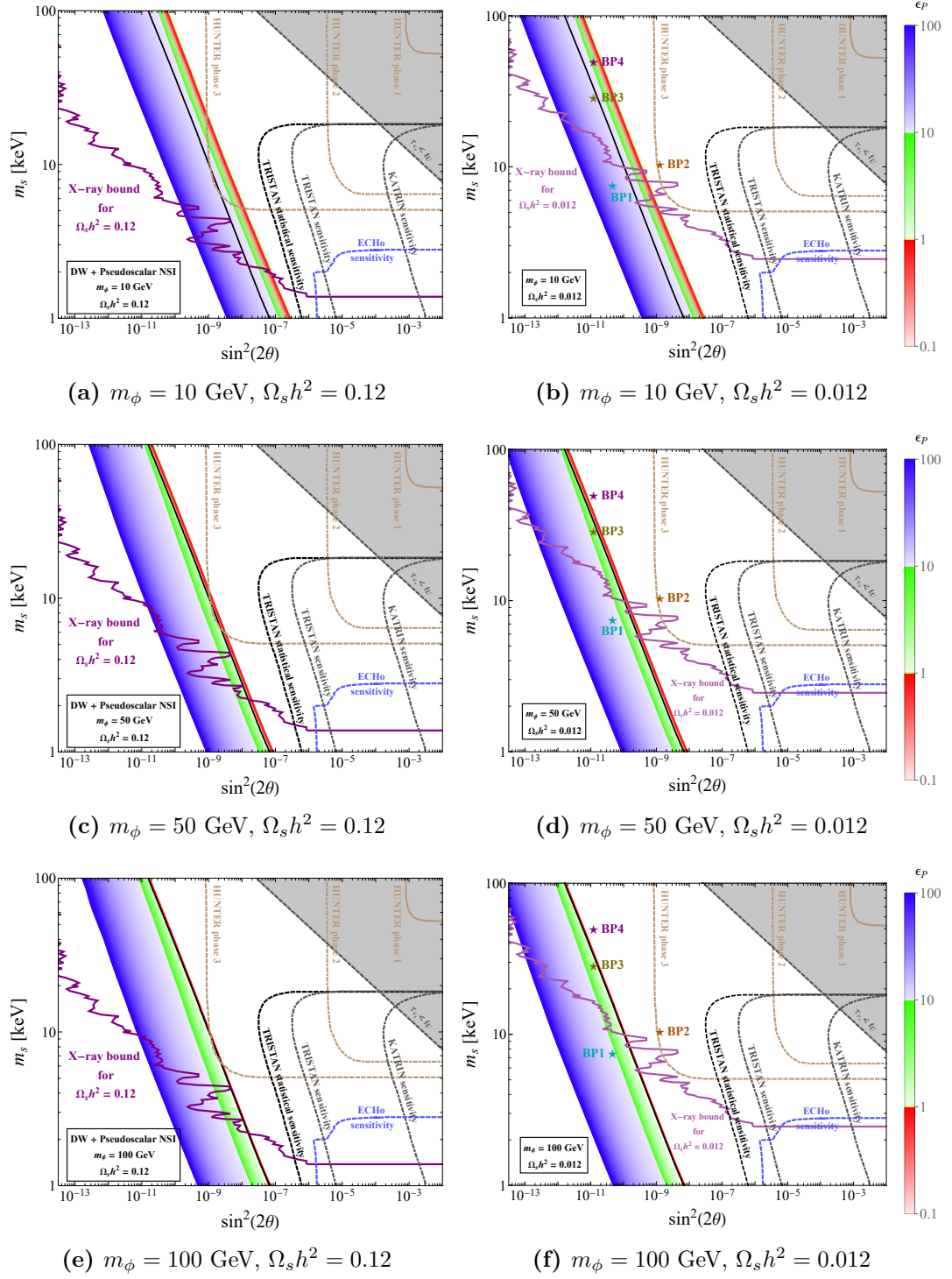


FIGURE 3.13: Relic abundance parameter space for DW mechanism with the pseudoscalar NSSI. Figures in the right represent cocktail DM scenario with 10% relic abundance. NSSI strength  $\epsilon_P$  is colour coded from 0.1 to 100 in the bar legend. The black line corresponds to the standard DW scenario. Beige (HUNTER), black (KATRIN/TRISTAN), and blue (ECHO) dashed lines represent experimental sensitivities. X-ray constraints for corresponding relic abundance shown in purple.

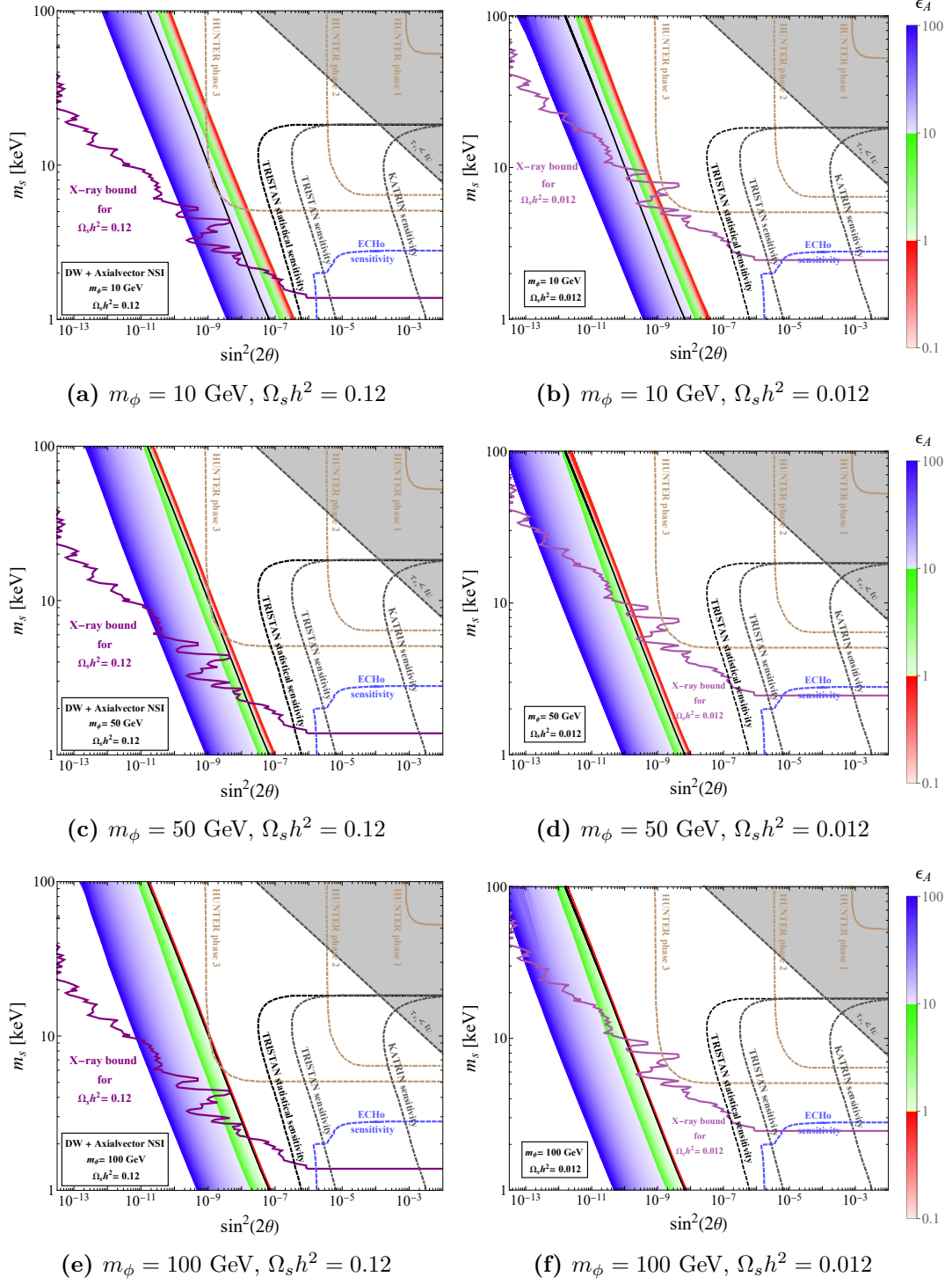


FIGURE 3.14: Relic abundance parameter space for DW mechanism with the axial vector NSSI. Figures in the right represent cocktail DM scenario with 10% relic abundance. NSSI strength  $\epsilon_A$  is colour coded from 0.1 to 100 in the bar legend. The black line corresponds to the standard DW scenario. Beige (HUNTER), black (KATRIN/TRISTAN), and blue (ECHO) dashed lines represent experimental sensitivities. X-ray constraints for corresponding relic abundance shown in purple.

### Free streaming length

Free streaming length or free streaming horizon,  $\lambda_{\text{FS}}$ , is the distance a dark matter particle would travel if they were not gravitationally trapped [41]. Free streaming length gives a measure on how large-scale structure are formed from the given particle species. It can be calculated as

$$\lambda_{\text{FS}} = \int_{t=t_{\text{in}}}^{t_0} dt \frac{\langle v(t) \rangle}{a(t)}, \quad (3.42)$$

where  $t_0$  is the present time and  $t_{\text{in}}$  is the time when dark matter production happened. Average velocity  $\langle v(t) \rangle$  is given by

$$\langle v(t) \rangle = \frac{\int d^3 \mathbf{p} \left( \frac{p}{E} \right) f(\mathbf{p}, T)}{\int d^3 \mathbf{p} f(\mathbf{p}, T)} = \frac{\int_{p=0}^{\infty} \frac{p}{\sqrt{p^2 + m_{DM}^2}} p^2 dp f(p, t)}{\int_{p=0}^{\infty} p^2 dp f(p, t)}. \quad (3.43)$$

We will use an approximated equation for sterile neutrinos [71],

$$\lambda_{\text{FS}} \approx 40 \text{Mpc} \left( \frac{30 \text{eV}}{m_s} \right) \left( \frac{\langle p/T \rangle}{3.15} \right), \quad (3.44)$$

where average rescaled momentum,  $\langle r \rangle = \langle p/T \rangle$ , can be calculated as

$$\langle r \rangle = \frac{\int d^3 \mathbf{p} \left( \frac{p}{T} \right) f(\mathbf{p}, T)}{\int d^3 \mathbf{p} f(\mathbf{p}, T)} = \frac{\int_{r=0}^{\infty} r^3 dr f(r)}{\int_{r=0}^{\infty} r^2 dr f(r)}. \quad (3.45)$$

Dark matter can be classified according to free streaming length as:

- Hot Dark Matter  $\Leftrightarrow \lambda_{\text{FS}} > 0.1 \text{ Mpc}$ ,
- Warm Dark Matter  $\Leftrightarrow 0.01 \text{ Mpc} < \lambda_{\text{FS}} < 0.1 \text{ Mpc}$ ,
- Cold Dark Matter  $\Leftrightarrow \lambda_{\text{FS}} < 0.01 \text{ Mpc}$ .

Hot dark matter scenario with large free streaming length is ruled out by structure formation bounds to be a major source of dark matter in the universe [92]. We expect our keV sterile neutrinos to be warm dark matter candidates.

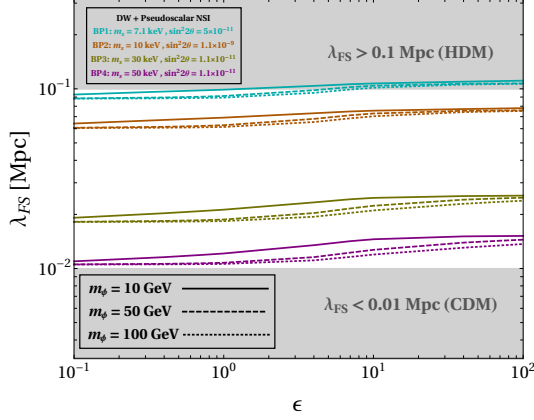
We select four benchmark points:

- BP1:  $m_s = 7.1 \text{ keV}$ ,  $\sin^2 2\theta = 5 \cdot 10^{-11}$ , point that corresponds to the unidentified X-ray line at 3.55 keV [93],
- BP2:  $m_s = 10 \text{ keV}$ ,  $\sin^2 2\theta = 1.1 \cdot 10^{-9}$ , point that is reachable by phase 3 of HUNTER,
- BP3:  $m_s = 30 \text{ keV}$ ,  $\sin^2 2\theta = 1.1 \cdot 10^{-10}$ ,
- BP4:  $m_s = 50 \text{ keV}$ ,  $\sin^2 2\theta = 1.1 \cdot 10^{-11}$ ,

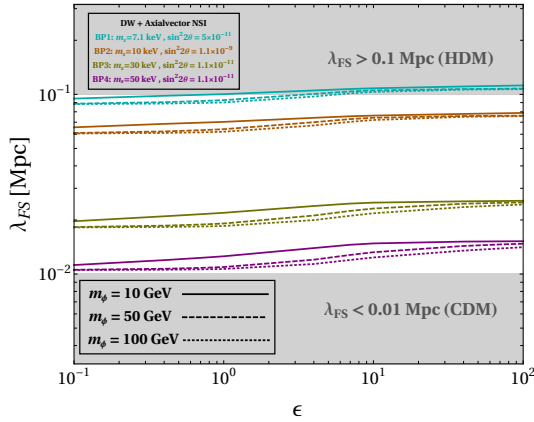
and plot free streaming length as a function of NSSI strength  $\epsilon$  to see whether our production mechanisms are compatible with the structure formation. We find the following results from Fig. 3.15:

- Sterile neutrinos produced by the Dodelson-Widrow mechanism in presence of NSSIs can be considered as warm dark matter candidates if they have a mass between 7 – 50 keV.

- Sterile neutrinos of mass less than few keV are ruled out by structure formation bounds.
- Active-sterile mixing angle has little to no influence on the free streaming lengths.
- Free streaming length decrease as we increase the mediator mass for lower range of  $\epsilon$ . However, as we increase  $\epsilon$ , free streaming length converges for a specific type of NSSI. This is what we expect from the results of distribution function.



(a) Dodelson-Widrow mechanism with the pseudoscalar NSSI



(b) Dodelson-Widrow mechanism with the axial vector NSSI

FIGURE 3.15: Free streaming length as a function of  $\epsilon$ . Grey areas in the plot represent regions excluded for warm dark matter. Scalar NSSI gives the same results as pseudoscalar NSSI and hence not included here.



## Chapter 4

# Conclusion and outlook

In this thesis, we have taken a close look at keV sterile neutrino dark matter production in the early Universe. Studying the standard Dodelson-Widrow mechanism in detail, we recalculated the sterile neutrino distribution function and relic abundance in full generality. We see that the basic mechanism is disfavoured by astrophysical observations and unreachable to neutrino experiments. Thus, we need to go beyond active-sterile mixing and modify the Dodelson-Widrow mechanism.

We introduced non-standard neutrino interactions to modify the sterile neutrino production. Inspired by previous works [89, 79], we have introduced active neutrino self-interactions. However, we made an assumption that mediators are much heavier than the production temperature, which allowed us to use an effective field theory framework. Usual NSI as EFT treatments [68] does not incorporate momentum dependence in the Lagrangian. Hence, we modified the NSI Lagrangian and included a higher order term of the  $\mathcal{O}(p^2)$ , which is essential for the effective potential calculations. The choice of Majorana active neutrinos forbids vector and tensor self-interaction and further reduces the possible interactions to three types: scalar, pseudoscalar, and axial vector. Nonetheless, Majorana neutrinos are an interesting choice since the previous works considered Dirac neutrinos.

From the results presented in the previous chapter, we find that sterile neutrino production can be enhanced for larger values of  $\epsilon$  and suppressed for smaller values of  $\epsilon$ , where  $\epsilon$  gives the strength of NSSI compared to the standard electroweak interactions. Enhancement in production helps to evade the astrophysical constraints, while suppression of production becomes interesting in the context of reaching neutrino experimental sensitivities. “Cocktail DM” scenario, where sterile neutrinos constitute only a fraction of the dark matter in the Universe, is also presented as a possible alternative. Finally, we have also checked the free streaming length of the sterile neutrinos produced by these new mechanisms to check whether they are compatible with the structure formation. We find that sterile neutrinos of mass around 7 keV to 50 keV can be considered warm dark matter, which is expected. Our results also show that sterile neutrinos produced through these mechanisms become slightly colder with heavier mediator masses. Another important inference is that even though we have three different non-standard interactions, they are not radically different from each other. This can be attributed to the EFT treatment, where it is not important how mediators behave at high energies.

We saw that it is not possible for laboratory neutrino experiments to convincingly cover the parameter space for the Dodelson-Widrow scenario, even in the presence of non-standard interactions. The best sensitivity out of the experiments we considered comes from phase 3 of HUNTER [19], an experiment that is still in its starting stage. Experiments like TRISTAN [17], KATRIN [16], and ECHo [18] fall short to reach desired sensitivities. However, it is also worth noting that all these experimental sensitivities are almost covered by astrophysical observations [28].

Future extensions of this thesis would be interesting from a phenomenological perspective. We can include Dirac active neutrinos in this study to present a complete picture of non-resonant sterile neutrino production with active neutrino self-interactions. Inclusion of non-standard neutrino interactions involving charged leptons would mean an even richer phenomenology with stronger constraints from the various reactor and atmospheric neutrino experiments.

Sterile neutrinos of keV range are a well-motivated dark matter candidate, even if it is not detectable by current experiments. As we improve our understanding of neutrinos, we will get new insights and new ideas to solve the neutrino puzzle. The Dodelson-Widrow mechanism studied in this work is surely not the full picture, but will always be a great starting point to get into the world of massive neutrinos. Hopefully, future experiments and upgrades make sterile neutrino dark matter relevant and exciting in the next decades.

## Appendix A

# Analytical solution of the Boltzmann equation

Following Ref. [48], we present the analytical solution of sterile neutrino Boltzmann equation.

### A.1 Formal solution

The Boltzmann equation for non-resonant production with zero initial abundance is given by Eq. (3.15),

$$\frac{\partial}{\partial t} f_s(p, t) - H p \frac{\partial}{\partial p} f_s(p, t) = h(p, t) f_a(p, t) \quad (\text{A.1})$$

where  $p$  is local momentum and  $t$  is cosmic time and  $h(p, t)$  is given by

$$h(p, t) = \frac{1}{4} \frac{\Gamma_a(p, t) \Delta^2(p) \sin 2\theta}{\Delta^2(p) \sin^2 2\theta + \left(\frac{\Gamma_a(p, t)}{2}\right)^2 + (\Delta^2(p) \cos 2\theta - V_a(p, T))^2} \quad (\text{A.2})$$

changing variable  $t \rightarrow T$ , temperature of the photons that stay in equilibrium until CMB decoupling, we can rewrite the equation as

$$\frac{dT}{dt} \frac{\partial}{\partial T} f_s(p, T) - H p \frac{\partial}{\partial p} f_s(p, T) = h(p, T) f_a(p, T) , \quad (\text{A.3})$$

$$\frac{\partial}{\partial T} f_s(p, T) - \kappa(T) p \frac{\partial}{\partial p} f_s(p, T) = \frac{dt}{dT} h(p, T) f_a(p, T) , \quad (\text{A.4})$$

where we define

$$\kappa(T) = \frac{dt}{dT} H(T) = \frac{dt}{dT} \frac{1}{a} \frac{da}{dt} = \frac{1}{a} \frac{da}{dT} . \quad (\text{A.5})$$

Conservation of the comoving entropy density,  $g_{*s}(T) T^3 a^3(T) = \text{const.}$ , implies

$$\frac{dg_{*s}}{dT} T^3 a^3 + 3g_{*s} T^2 a^3 + 3g_{*s} T^3 a^2 \frac{da}{dT} = 0 , \quad (\text{A.6})$$

where  $g_{*s}(T)$  is the entropic number of freedom in the early universe as a function of temperature given in Fig. 3.1.

Then,

$$\begin{aligned}\frac{1}{a} \frac{da}{dT} &= \frac{-1}{3g_{*s}T^3a^3} \left( 3g_{*s}T^2a^3 + T^3a^3 \frac{dg_{*s}}{dT} \right) , \\ \kappa(T) &= \frac{-1}{T} \left( 1 + \frac{Tg'_{*s}(T)}{3g_{*s}(T)} \right) .\end{aligned}\quad (\text{A.7})$$

Now Eq. (A.4),

$$\frac{\partial}{\partial T} f_s(p, T) + \left( \frac{1}{T} + \frac{g'_{*s}(T)}{3g_{*s}(T)} \right) p \frac{\partial}{\partial p} f_s(p, T) = \frac{dt}{dT} h(p, T) f_a(p, T) , \quad (\text{A.8})$$

can be compared to a first order semilinear partial differential equation of the form

$$a(x, y)u_x + b(x, y)u_y = c(x, y, u) ,$$

which satisfies

$$\frac{dx}{a(x, y)} = \frac{dy}{b(x, y)} = \frac{du}{c(x, y, u)} .$$

We can write similar equalities from Eq. (A.8):

$$\frac{dT}{1} = \frac{dp}{\left( \frac{1}{T} + \frac{g'_{*s}(T)}{3g_{*s}(T)} \right) p} = \frac{df_s}{\frac{dt}{dT} h(p, T) f_a(p, T)} . \quad (\text{A.9})$$

Using the first pair of equality

$$\frac{dT}{1} = \frac{dp}{\left( \frac{1}{T} + \frac{g'_{*s}(T)}{3g_{*s}(T)} \right) p} \Rightarrow \left( \frac{1}{T} + \frac{g'_{*s}(T)}{3g_{*s}(T)} \right) dT - \frac{dp}{p} = 0 , \quad (\text{A.10})$$

and integrating between two arbitrary values of temperature  $T$ ,

$$\begin{aligned}\int_{T_1}^{T_2} \left( \frac{1}{T} + \frac{1}{3g_{*s}(T)} \frac{dg_{*s}}{dT} \right) dT - \int_{p(T_1)}^{p(T_2)} \frac{dp}{p} &= 0 , \\ \ln \frac{T_2}{T_1} + \frac{1}{3} \ln \frac{g_{*s}(T_2)}{g_{*s}(T_1)} + \ln \frac{p(T_1)}{p(T_2)} &= 0 ,\end{aligned}\quad (\text{A.11})$$

we get a characteristic curve for momentum,  $p(T)$  as

$$p(T) = p(T_i) \frac{T}{T_i} \left( \frac{g_{*s}(T)}{g_{*s}(T_i)} \right)^{1/3} . \quad (\text{A.12})$$

We can also get a relation

$$\frac{p(T_f)}{p(T_i)} = \frac{T_f}{T_i} \left( \frac{g_{*s}(T_f)}{g_{*s}(T_i)} \right)^{1/3} , \quad (\text{A.13})$$

which will be useful later.

Substituting the characteristics curve  $p(T)$  in the second pair of equality,

$$\frac{dT}{1} = \frac{df_s(p, T)}{\frac{dt}{dT} h(p, T) f_a(p, T)} , \quad (\text{A.14})$$

we get an ordinary differential equation for  $f_s$  in terms of variable  $T$ :

$$df_s(p, T) = \frac{dt}{dT} h(p(T), T) f_a(p(T), T) dT . \quad (\text{A.15})$$

Integrating from the initial production temperature  $T_i$  to the final temperature  $T_f$  where production stops,

$$\int_{f_s(p(T_i), T_i)}^{f_s(p(T_f), T_f)} df_s = \int_{T_i}^{T_f} \frac{dt}{dT} h(p(T), T) f_a(p(T), T) dT , \quad (\text{A.16})$$

$$\begin{aligned} f_s(p(T_f), T_f) - f_s(p(T_i), T_i) &= \int_{T_i}^{T_f} \frac{dt}{dT} h\left(p(T_i) \frac{T}{T_i} \left(\frac{g_{*s}(T)}{g_{*s}(T_i)}\right)^{1/3}, T\right) \\ &\quad \cdot f_a\left(p(T_i) \frac{T}{T_i} \left(\frac{g_{*s}(T)}{g_{*s}(T_i)}\right)^{1/3}, T\right) dT . \end{aligned} \quad (\text{A.17})$$

Initial condition  $f_s(p(T_i), T_i) = 0$  implies

$$f_s(p(T_f), T_f) = \int_{T_i}^{T_f} \frac{dt}{dT} h\left(p(T_i) \frac{T}{T_i} \left(\frac{g_{*s}(T)}{g_{*s}(T_i)}\right)^{1/3}, T\right) f_a\left(p(T_i) \frac{T}{T_i} \left(\frac{g_{*s}(T)}{g_{*s}(T_i)}\right)^{1/3}, T\right) dT . \quad (\text{A.18})$$

Since we are finding sterile neutrino distribution at the final temperature  $f(p(T_f), T_f)$ , it is better to remove  $T_i$ s from the expression. Using the relation Eq. (A.13), we get

$$\begin{aligned} f_s(p_f, T_f) &= \int_{T_i}^{T_f} \frac{-1}{HT} \left(1 + \frac{Tg'_{*s}(T)}{3g_{*s}(T)}\right) \cdot h\left(p(T_f) \frac{T}{T_f} \left(\frac{g_{*s}(T)}{g_{*s}(T_f)}\right)^{1/3}, T\right) \\ &\quad \cdot f_a\left(p(T_f) \frac{T}{T_f} \left(\frac{g_{*s}(T)}{g_{*s}(T_f)}\right)^{1/3}, T\right) dT . \end{aligned} \quad (\text{A.19})$$

Rescaled momentum  $r = \frac{p}{T}$  is often used to simplify the solution. Changing variables from  $(p, T) \rightarrow (r)$ , sterile neutrino distribution function at final temperature  $T_f$  is written as

$$f_s(r_f) = \int_{T_i}^{T_f} \frac{-1}{HT} \left(1 + \frac{Tg'_{*s}(T)}{3g_{*s}(T)}\right) h\left(r \cdot T_f \frac{T}{T_f} \left(\frac{g_{*s}(T)}{g_{*s}(T_f)}\right)^{1/3}, T\right) f_a\left(r \cdot T_f \frac{T}{T_f} \left(\frac{g_{*s}(T)}{g_{*s}(T_f)}\right)^{1/3}, T\right) dT , \quad (\text{A.20})$$

$$f_s(r_f) = \int_{T_i}^{T_f} \frac{-1}{HT} \left(1 + \frac{Tg'_{*s}(T)}{3g_{*s}(T)}\right) \cdot h\left(r \cdot T \left(\frac{g_{*s}(T)}{g_{*s}(T_f)}\right)^{1/3}, T\right) \cdot f_a\left(r \cdot T \left(\frac{g_{*s}(T)}{g_{*s}(T_f)}\right)^{1/3}, T\right) dT . \quad (\text{A.21})$$

We can further simplify the solution using Hubble expansion rate for a radiation dominated universe

$$H(T) = \sqrt{\frac{8\pi^3 g_{*s}}{90} \frac{T^2}{M_{\text{Pl}}}} , \quad (\text{A.22})$$

and substituting Fermi-Dirac distribution for active neutrinos,

$$f_a(p, T) = \frac{1}{\exp(p/T) + 1} .$$

We have the final expression of for sterile neutrino distribution function that is numerically solvable,

$$f_s(r) = \int_{T_i}^{T_f} \sqrt{\frac{90}{8\pi^3}} \frac{M_{\text{Pl}}}{\sqrt{g_{*s}(T)} T^3} \left(1 + \frac{Tg'_{*s}(T)}{3g_{*s}(T)}\right) \cdot h(p_{\text{redshift}}, T) \frac{1}{\exp\left(\frac{p_{\text{redshift}}}{T}\right) + 1} dT , \quad (\text{A.23})$$

where  $p_{\text{redshift}} = r \cdot T \left(\frac{g_{*s}(T)}{g_{*s}(T_f)}\right)^{1/3}$  is the redshifted momentum.

In the next section, we briefly explain the derivation of expression for relic abundance.

## A.2 Calculation of relic abundance

Relic abundance  $\Omega_x$  of a particle species  $x$  is

$$\Omega_x = \frac{\rho_x}{\rho_c} , \quad (\text{A.24})$$

where  $\rho_x$  is the energy density of the particle  $x$  and  $\rho_c$ , the critical energy density given by

$$\rho_c = \frac{3H^2 M_{\text{Pl}}^2}{8\pi} .$$

Assuming a flat universe, we have the sum of abundances,  $\sum \Omega_x = 1$ . Yield  $Y_x$  of a given particle species  $x$  is defined as

$$Y_x(T) = \frac{n_x(T)}{s(T)} , \quad (\text{A.25})$$

where  $n_x$  is the number density and  $s$  is the entropy at the temperature  $T$ . The particle yield stays constant after production stops at freeze-in/out temperature  $T_f$  and we can get present day yield

$$Y_{x0} = \frac{n_{x0}}{s_0} = \frac{n_x(T_f)}{s(T_f)} . \quad (\text{A.26})$$

Then, present day number density

$$n_{x0} = \frac{n_x(T_f)}{s(T_f)} \cdot s_0 , \quad (\text{A.27})$$

where  $s_0$  can be measured experimentally and found to be  $s_0 = 2.8912 \times 10^9 / m^3$ .

For a non-relativistic particle, we can approximate energy density as  $\rho \approx m \cdot n$ .

Then, present day relic density for a non-relativistic species  $x$ ,

$$\Omega_{x0} = \frac{m_x \cdot n_{x0}}{\rho_{c,0}} = \frac{m_x}{\rho_{c,0}} \frac{n_x(T_f)}{s(T_f)} \cdot s_0 . \quad (\text{A.28})$$

We often multiply abundance with  $h^2$  as  $\Omega_0 h^2$  is independent of Hubble constant  $H_0$ . Dropping the subscript 0 as it is implied we are reporting the present day relic abundance,

$$\Omega_x h^2 = \frac{m_x \cdot n_{x0}}{\rho_{c,0}/h^2} = \frac{m_x}{\rho_{c,0}/h^2} \frac{n(T_f)}{s(T_f)} \cdot s_0 . \quad (\text{A.29})$$

The number density  $n_x(T)$  at a temperature  $T$ ,

$$n_x(T) = \frac{g_x}{(2\pi)^3} \int d^3\mathbf{p} f_x(\mathbf{p}, T) = \frac{g_x}{(2\pi)^3} \int_0^\infty 4\pi p^2 dp f_x(p, T) , \quad (\text{A.30})$$

where  $g_x$  is the number of relativistic degrees of freedom for the particle  $x$ . Changing momentum variable  $p$  to rescaled momentum  $r = \frac{p}{T}$ ,

$$n_x(T) = \frac{g_x T^3}{2\pi^2} \int_0^\infty r^2 dr f_x(r) . \quad (\text{A.31})$$

Entropy density  $s$  is given as a function of time,

$$s(T) = \frac{2\pi^2}{45} g_{*s}(T) \cdot T^3 , \quad (\text{A.32})$$

where  $g_{*s}(T)$  is the effective number of degrees of freedom in the universe at temperature  $T$ . Now substituting

$$\frac{n(T_f)}{s(T_f)} = \frac{45}{4\pi^4} \frac{g_x}{g_{*s}(T_f)} \int_0^\infty r^2 dr f_x(r) \quad (\text{A.33})$$

to Eq. (A.29), and plugging in  $\rho_{c,0}/h^2 = 10.537 \text{ GeV}/m^3$  and  $s_0 = 2.8912 \times 10^9/m^3$ ,

$$\Omega_x h^2 = \frac{m_x s_0}{\rho_{c,0}/h^2} \frac{45}{4\pi^4} \cdot \frac{g_x}{g_{*s}(T_f)} \int_0^\infty r^2 dr f_x(r) \quad (\text{A.34})$$

$$= 2.74 \times 10^8 \left( \frac{m_x}{\text{GeV}} \right) \frac{45}{4\pi^4} \cdot \frac{g_x}{g_{*s}(T_f)} \int_0^\infty r^2 dr f_x(r) \quad (\text{A.35})$$

For a sterile neutrino  $\nu_s$  with  $g_s$  number of relativistic degrees of freedom,

$$\Omega_s h^2 = 2.74 \times 10^2 \left( \frac{m_s}{\text{keV}} \right) \frac{45}{4\pi^4} \frac{g_s}{g_{*s}(T_f)} \int_0^\infty r^2 f_s(r) dr . \quad (\text{A.36})$$



## Appendix B

# Calculation of non-standard neutrino self-interaction rate

The NSSI Lagrangian derived in Sec. 2.5.1,

$$\mathcal{L}_{\text{NSSI}} = \frac{G_F \epsilon}{\sqrt{2} m_\phi^2} (\bar{\nu} \mathcal{O} \nu) (\bar{\nu} \bar{\mathcal{O}} \nu) - \frac{G_F \epsilon}{\sqrt{2}} (\bar{\nu} \mathcal{O} \nu) \square (\bar{\nu} \bar{\mathcal{O}} \nu) \quad (\text{B.1})$$

adds new channels for neutrino scattering in addition to the standard electroweak interactions.

NSSI vertex given in the right panel of Fig. B.1 can be seen as a low-energy limit of the three diagrams in the left panel. An extra topology comes from the fact that our active neutrinos are Majorana [90].

If we only consider one active flavor, there can only be  $\nu_a + \nu_a \rightarrow \nu_a + \nu_a$  scattering

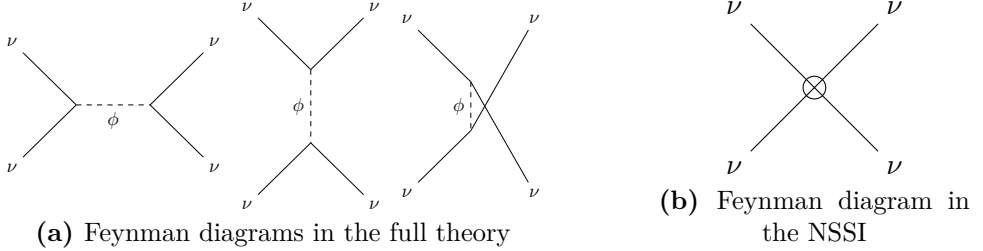
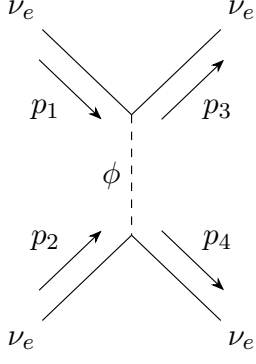


FIGURE B.1: Non-standard contribution to the interaction rate

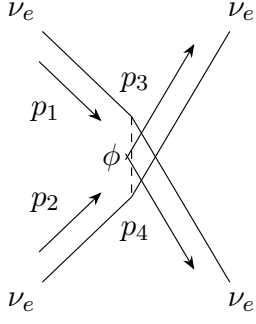
since it is not possible to distinguish Majorana neutrinos and anti-neutrinos [94]. Finding the matrix elements for active neutrino scattering from diagrams in the left panel of Fig. B.1 using Majorana Feynman rules [31] in EFT framework,

$$-i\mathcal{M}_s = -i \frac{G_F \epsilon_j}{\sqrt{2}} [(\bar{v}(p_1) \mathcal{O} u(p_2) - \bar{v}(p_2) \mathcal{O} u(p_1)) \times (\bar{u}(p_3) \mathcal{O} v(p_4) - \bar{u}(p_4) \mathcal{O} v(p_3))] , \quad (\text{B.2})$$

$$-i\mathcal{M}_s = -i \frac{G_F \epsilon_j}{\sqrt{2}} \left[ (\bar{v}(p_1) [\mathcal{O} + \hat{C} \mathcal{O}^T \hat{C}^{-1}] u(p_2)) \times (\bar{u}(p_3) [\mathcal{O} + \hat{C} \mathcal{O}^T \hat{C}^{-1}] v(p_4)) \right] . \quad (\text{B.3})$$



$$-i\mathcal{M}_t = -i \frac{G_F \epsilon_j}{\sqrt{2}} [(\bar{v}(p_1)\mathcal{O}v(p_3) - \bar{u}(p_3)\mathcal{O}u(p_1)) \\ \times (\bar{u}(p_4)\mathcal{O}u(p_2)) - \bar{v}(p_2)\mathcal{O}v(p_4)] , \quad (B.4)$$



$$-i\mathcal{M}_t = -i \frac{G_F \epsilon_j}{\sqrt{2}} [(\bar{v}(p_1)[\mathcal{O} + \hat{C}\mathcal{O}^T \hat{C}^{-1}]v(p_3)) \\ \times (\bar{u}(p_4)[\mathcal{O} + \hat{C}\mathcal{O}^T \hat{C}^{-1}]u(p_2))] . \quad (B.5)$$



$$-i\mathcal{M}_u = -i \frac{G_F \epsilon_j}{\sqrt{2}} [(\bar{v}(p_1)\mathcal{O}v(p_4) - \bar{u}(p_4)\mathcal{O}u(p_1)) \\ \times (\bar{u}(p_3)\mathcal{O}u(p_2)) - \bar{v}(p_2)\mathcal{O}v(p_3)] , \quad (B.6)$$

$$-i\mathcal{M}_u = -i \frac{G_F \epsilon_j}{\sqrt{2}} [(\bar{v}(p_1)[\mathcal{O} + \hat{C}\mathcal{O}^T \hat{C}^{-1}]v(p_4)) \\ \times (\bar{u}(p_3)[\mathcal{O} + \hat{C}\mathcal{O}^T \hat{C}^{-1}]u(p_2))] . \quad (B.7)$$

Where  $\hat{C}$  represents the charge conjugation operator with relation

$$\hat{C}\mathcal{O}^T \hat{C}^{-1} = \mathcal{O} \text{ for } \mathcal{O} = \mathbb{I}, i\gamma^5, \gamma^\mu \gamma^5 . \quad (B.8)$$

Summing the contributions from different topologies including Relative Signs of Interfering Feynman (RSIF) diagrams,

$$-i\mathcal{M}_{\text{total}} = -i(\mathcal{M}_s - \mathcal{M}_t - \mathcal{M}_u) . \quad (B.9)$$

Averaging over initial spin,

$$\overline{|\mathcal{M}_{\text{tot}}|^2} = \frac{1}{4} \sum \mathcal{M}_{\text{tot}}^\dagger \mathcal{M}_{\text{tot}} , \quad (B.10)$$

three possible NSSIs give the following results,

**Scalar NSSI:**

$$\overline{|\mathcal{M}_S|^2} = 4 \epsilon_S^2 G_F^2 (s^2 + 5t^2 + u^2) , \quad (B.11)$$

**Axial vector NSSI:**

$$\overline{|\mathcal{M}_A|^2} = 64 \epsilon_A^2 G_F^2 t^2 , \quad (B.12)$$

**Pseudoscalar NSSI:**

$$\overline{|\mathcal{M}_P|^2} = 4 \epsilon_P^2 G_F^2 (s^2 + 5t^2 + u^2) , \quad (B.13)$$

where  $s, t, u$  are the Mandelstam variables.

We can see matrix elements are of the form,

$$\overline{|\mathcal{M}|^2} = K_s s^2 + K_t t^2 + K_u u^2 . \quad (B.14)$$

## B.1 Total cross section

Differential cross section [95],

$$d\sigma = \frac{\mathcal{S}\hbar^2}{4\sqrt{(p_1 \cdot p_2)^2 - (m_1 m_2 c^2)^2}} |\mathcal{M}|^2 d\Pi_{\text{LIPS}} . \quad (\text{B.15})$$

For a  $2 \rightarrow j$  process, Lorentz Invariant Phase Space can be written as

$$d\Pi_{\text{LIPS}} \equiv \prod_{\text{final states } j} \frac{d^3 p_j}{(2\pi)^3} \frac{1}{2E_{p_j}} (2\pi)^4 \delta^4(\Sigma p) . \quad (\text{B.16})$$

Working in the Center of Mass frame where we define

$$p_1 = (E_1, \mathbf{p}), p_2 = (E_2, -\mathbf{p}), p_3 = (E_3, \mathbf{p}^*), p_4 = (E_4, -\mathbf{p}^*) , \quad (\text{B.17})$$

$$s = (p_1 + p_2)^2, t = (p_1 - p_3)^2, u = (p_1 - p_4)^2 , \quad (\text{B.18})$$

Now, differential cross section for  $1 + 2 \rightarrow 3 + 4$  process with massless particle assumption,

$$\begin{aligned} d\sigma &= \frac{\mathcal{S}}{2s} |\mathcal{M}|^2 \frac{d^3 p_3}{2E_3 (2\pi)^3} \frac{d^3 p_4}{2E_4 (2\pi)^3} (2\pi)^4 \delta^4(p_1 + p_2 - p_3 - p_4) \\ &= \frac{\mathcal{S}}{2s} |\mathcal{M}|^2 \frac{d^3 p_3}{2E_3 (2\pi)^3} \frac{d^3 p_4}{2E_4 (2\pi)^3} (2\pi)^4 \delta(\sqrt{s} - E_3 - E_4) \delta^3(\mathbf{p}_3 + \mathbf{p}_4) \\ &= \frac{\mathcal{S}}{2 \cdot (2\pi)^2 \cdot s} |\mathcal{M}|^2 \frac{d^3 p_3}{2E_3} \frac{d^3 p_4}{2E_4} \delta(\sqrt{s} - E_3 - E_4) \delta^3(\mathbf{p}_3 + \mathbf{p}_4) , \end{aligned} \quad (\text{B.19})$$

where  $\mathcal{S}$  is the symmetry factor, and we took  $\hbar = c = 1$ .

For  $\nu_a + \nu_a \rightarrow \nu_a \nu_a$  scattering,

$$\sigma_{\nu\nu-\nu\nu} = \frac{\frac{1}{2}}{2 \cdot (2\pi)^2 \cdot s} \int \frac{d^3 p_3}{2E_3} \frac{d^3 p_4}{2E_4} \delta(\sqrt{s} - E_3 - E_4) \delta^3(\mathbf{p}_3 + \mathbf{p}_4) \cdot (K_s s^2 + K_t t^2 + K_u u^2) , \quad (\text{B.20})$$

where we can separate the total cross section to three parts,

$$\sigma_{\nu\nu-\nu\nu} = \sigma_s + \sigma_t + \sigma_u , \quad (\text{B.21})$$

with

$$\begin{aligned} \sigma_s &= \frac{1}{4 \cdot (2\pi)^2 \cdot s} \int \frac{d^3 p_3}{2E_3} \frac{d^3 p_4}{2E_4} \delta(\sqrt{s} - E_3 - E_4) \delta^3(\mathbf{p}_3 + \mathbf{p}_4) \cdot K_s s^2 , \\ \sigma_t &= \frac{1}{4 \cdot (2\pi)^2 \cdot s} \int \frac{d^3 p_3}{2E_3} \frac{d^3 p_4}{2E_4} \delta(\sqrt{s} - E_3 - E_4) \delta^3(\mathbf{p}_3 + \mathbf{p}_4) \cdot K_t t^2 , \\ \sigma_u &= \frac{1}{4 \cdot (2\pi)^2 \cdot s} \int \frac{d^3 p_3}{2E_3} \frac{d^3 p_4}{2E_4} \delta(\sqrt{s} - E_3 - E_4) \delta^3(\mathbf{p}_3 + \mathbf{p}_4) \cdot K_u u^2 . \end{aligned} \quad (\text{B.22})$$

Integrating out  $\mathbf{p}_4$  using properties of Dirac delta function,  $\sigma_s$  is calculated to be

$$\sigma_s = \frac{K_s s^2}{4 \cdot (2\pi)^2 \cdot s} \int \frac{d^3 p_3}{(2E_3)^2} \delta(\sqrt{s} - 2E_3) \quad (\text{B.23})$$

$$= \frac{K_s s^2}{4 \cdot (2\pi)^2 \cdot s} \int \frac{p_3^2 dp_3 d\Omega_3}{(2E_3)^2} \delta(2E_3 - \sqrt{s}) \quad (\text{B.24})$$

$$= \frac{K_s s}{4 \cdot (2\pi)^2} \cdot \frac{1}{2} \cdot \frac{1}{4} \cdot 4\pi = \frac{K_s s}{32\pi} . \quad (\text{B.25})$$

Similarly, using

$$t = (p_1 - p_3)^2 = -2p_1 \cdot p_3 = 2(\mathbf{p}_1 \cdot \mathbf{p}_3 - E_1 E_3) = 2|p_1||p_3|(\cos \theta - 1) , \quad (\text{B.26})$$

$$u = (p_1 - p_4)^2 = -2p_1 \cdot p_4 = 2(\mathbf{p}_1 \cdot \mathbf{p}_4 - E_1 E_4) = 2|p_1||p_4|(\cos(\pi - \theta) - 1) , \quad (\text{B.27})$$

$\sigma_t, \sigma_u$  can be calculated.

$$\sigma_t = \frac{K_t s}{3 \cdot 64\pi} , \sigma_u = \frac{K_u s}{3 \cdot 64\pi} . \quad (\text{B.28})$$

Summing all three contributions, total NSSI cross section,

$$\sigma_{\text{NSSI}} = \sigma_{\nu\nu-\nu\nu} = \sigma_s + \sigma_t + \sigma_u = \frac{s}{64\pi} \left( 2K_s + \frac{K_t + K_u}{3} \right) . \quad (\text{B.29})$$

## B.2 Interaction rate

Interaction rate for a neutrino with energy  $E$  is given as [79],

$$\Gamma(E, T) = 2 \int \frac{d^3 \mathbf{p}'}{(2\pi)^3} f_\nu(E', T) \sigma_{\text{total}}(\mathbf{p}, \mathbf{p}') v_{\text{Møller}} \quad (\text{B.30})$$

where  $f_\nu(E', T) = 1/[1 + \exp(E'/T)]$  is the Fermi-Dirac distribution for active neutrino,  $\sigma_{\text{total}}$  is the total cross-section. The Møller velocity can be approximated to  $(1 - \cos \theta)$  for ultra-relativistic neutrinos. The prefactor of 2 captures contributions from both helicity states of Majorana active neutrinos.

Total cross section Eq. (B.31) can be rewritten as

$$\sigma_{\text{total}} = \frac{s}{64\pi} \left( 2K_s + \frac{K_t + K_u}{3} \right) = \frac{6K_s + K_t + K_u}{192\pi} \cdot (2|\mathbf{p}||\mathbf{p}'|(1 - \cos \theta)) , \quad (\text{B.31})$$

where  $\theta$  is the angle between  $\mathbf{p}$  and  $\mathbf{p}'$  and Mandelstam variable,

$$s = 2p_1 \cdot p_2 = 2(EE' - \mathbf{p} \cdot \mathbf{p}') = 2|\mathbf{p}||\mathbf{p}'|(1 - \cos \theta) .$$

$$\begin{aligned} \Gamma_{\text{NSSI}}(p, T) &= 2 \int \frac{d^3 \mathbf{p}'}{(2\pi)^3} f_\nu(E', T) \sigma_{\text{NSSI}}(\mathbf{p}, \mathbf{p}') v_{\text{Møller}} \\ &= \frac{6K_s + K_t + K_u}{48\pi} \int \frac{|p'|^2 dp' d\Omega}{(2\pi)^3} \frac{1}{1 + \exp(E'/T)} \cdot |p||p'|(1 - \cos \theta)^2 \end{aligned} \quad (\text{B.32})$$

$$\Gamma_{\text{NSSI}}(p, T) = \frac{6K_s + K_t + K_u}{48\pi \cdot (2\pi)^3} \int \frac{p|E'|^3 dE'}{1 + \exp(E'/T)} \cdot \int d\Omega (1 - \cos \theta)^2 \quad (\text{B.33})$$

$$= (6K_s + K_t + K_u) \frac{p}{24 \cdot (2\pi)^4} \int \frac{|E'|^3 dE'}{1 + \exp(E'/T)} \cdot \int d\Omega (1 - \cos \theta)^2 \quad (\text{B.34})$$

Numerically integrating, we get

$$\Gamma_{\text{NSSI}}(p, T) = (6K_s + K_t + K_u) \frac{p}{24 \cdot (2\pi)^4} \cdot \frac{7\pi^4 T^4}{120} \cdot \frac{16\pi}{3}. \quad (\text{B.35})$$

Thus, non-standard neutrino self interaction rate

$$\Gamma_{\text{NSSI}}(p, T) = (6K_s + K_t + K_u) \cdot \frac{7\pi}{8640} \cdot p T^4. \quad (\text{B.36})$$

A scalar NSSI with  $K_s = 4\epsilon_S^2 G_F^2$ ,  $K_t = 20\epsilon_S^2 G_F^2$ ,  $K_u = 4\epsilon_S^2 G_F^2$  gives

$$\Gamma_S(p, T) = \frac{7\pi G_F^2 \epsilon_S^2}{180} \cdot p T^4, \quad (\text{B.37})$$

an axial vector NSSI with  $K_s = 0$ ,  $K_t = 64\epsilon_A^2 G_F^2$ ,  $K_u = 0$  gives

$$\Gamma_A(p, T) = \frac{7\pi G_F^2 \epsilon_A^2}{135} \cdot p T^4, \quad (\text{B.38})$$

and a pseudoscalar NSSI with  $K_s = 4\epsilon_P^2 G_F^2$ ,  $K_t = 20\epsilon_P^2 G_F^2$ ,  $K_u = 4\epsilon_P^2 G_F^2$  gives

$$\Gamma_P(p, T) = \frac{7\pi G_F^2 \epsilon_P^2}{180} \cdot p T^4. \quad (\text{B.39})$$



## Appendix C

# Calculation of NSSI thermal potential

Following the method presented by D’Olivo et al. [84] for the Standard Model contribution to neutrino effective potential, we calculate non-standard self-interaction contribution to the active neutrino effective potential.

### C.1 Neutrino dispersion relation

The properties of a neutrino that propagates through a medium is determined by the Dirac equation, which in momentum space is

$$(\not{k} - \Sigma_{\text{eff}}) \psi = 0 , \quad (\text{C.1})$$

where  $k_\mu$  is the neutrino momentum and  $\Sigma_{\text{eff}}$  is the neutrino self-energy, which depends on the medium of propagation. In vacuum, self-energy can only depend on the neutrino four-momentum  $k_\mu$ . i.e.,

$$\Sigma_{\text{eff}} = a\not{k} . \quad (\text{C.2})$$

However, if neutrinos are propagating through a medium with velocity  $u_\mu$ ,

$$\Sigma_{\text{eff}} = a\not{k} + b\not{u} + c[\not{k}, \not{u}] . \quad (\text{C.3})$$

But, if we are only considering one-loop level, as show in [83], we can assume  $c = 0$ . The coefficients  $a, b$  depend on invariant quantities  $\omega = k \cdot u$  and  $\kappa = \sqrt{\omega^2 - k^2}$ .

Now the Dirac Equation can be rewritten as

$$\begin{aligned} & (\not{k} - (a\not{k} + b\not{u})) \psi = 0 \\ & [(1 - a)\not{k} - b\not{u}] \psi = 0 \Rightarrow \not{V}\psi = 0 , \end{aligned} \quad (\text{C.4})$$

where  $V_\mu = (1 - a)k_\mu - bu_\mu$ .

For non-trivial solutions of  $\not{V}\psi = 0$ , we have to solve  $V^2 = 0$ .

$$V^2 = [(1 - a)k_\mu - bu_\mu][(1 - a)k^\mu - bu^\mu] \quad (\text{C.5})$$

$$= (1 - a)^2 k_\mu k^\mu + b^2 u_\mu u^\mu - 2(1 - a)b(k \cdot u) \quad (\text{C.6})$$

$$= (1 - a)^2 k^2 + b^2 u^2 - 2b(1 - a)\omega \quad (\text{C.7})$$

$$= (1 - a)^2 (\omega^2 - \kappa^2) + b^2 - 2b(1 - a)\omega \quad (\text{C.8})$$

$$= [(1 - a)(\omega - \kappa) - b][(1 - a)(\omega + \kappa) - b] \quad (\text{C.9})$$

$$= f(\omega) \times \overline{f}(\omega) \quad (\text{C.10})$$

i.e.,  $V^2 = 0 \Rightarrow f(\omega) \bar{f}(\omega) = 0$  and has the solution:

$$f(\omega_\kappa) = 0 \text{ or } \bar{f}(-\bar{\omega}_\kappa) = 0. \quad (\text{C.11})$$

Since we can separate self-energy into gauge dependent and independent parts, we can write  $f$  as

$$f = f_0 + f_\xi = [(1 - a_0)(\omega - \kappa) - b_0] + [(1 - a_\xi)(\omega - \kappa) - b_\xi]. \quad (\text{C.12})$$

Using the fact that dispersion relation is independent of gauge parameter, we can infer  $f_0$  and  $f_\xi$  must vanish separately at  $\omega = \omega_\kappa$ . Thus, gauge independent

$$f_0(\omega_\kappa) \equiv (1 - a_0)(\omega_\kappa - \kappa) - b_0 = 0 \quad (\text{C.13})$$

implies

$$b_0 = (1 - a_0)(\omega_\kappa - \kappa) \Rightarrow \omega_\kappa - \kappa = b_0 + a_0(\omega_\kappa - \kappa) \quad (\text{C.14})$$

and we can write  $\omega_\kappa = \kappa + b_0 + a_0(\omega_\kappa - \kappa)$ .

In zeroth order,  $\omega_\kappa = \kappa$ . Then, we can find

$$\omega_\kappa = \kappa + b_0 (\omega_\kappa = \kappa) \quad (\text{C.15})$$

at first order.

Thus, we can write the dispersion relation as

$$\omega_\kappa = \kappa + b_0(\kappa) + \text{h.o.} \quad (\text{C.16})$$

for neutrinos.

Similarly, we find

$$\bar{\omega}_\kappa = \kappa - b_0(-\kappa) + \text{h.o.} \quad (\text{C.17})$$

for anti-neutrinos.

## C.2 Effective potential

We can see the effective potential as a contribution to energy of the particle by the background medium. That is,

Energy of Neutrino propagating through a medium =

Energy of neutrino in vacuum + Effective potential in the medium

$$\omega_\kappa = \kappa + V_a \quad (\text{C.18})$$

Comparing with Eq. (C.16) and Eq. (C.17), we can see that effective potential  $V_a$  coincide with  $b_0$  in the lowest order. Now, by calculating self-energy,  $\Sigma_{\text{eff}} = (a_0 + a_\xi)\not{k} + (b_0 + b_\xi)\not{y}$ , we can find the effective thermal potential.

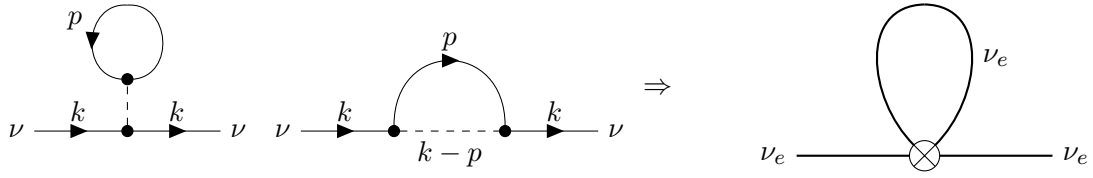


FIGURE C.1: NSSI contribution to the self-energy

### C.3 Calculation of self-energy

The NSSI contribution to the self-energy (Fig. C.1) can be written as

$$-i\Sigma_{\text{eff}} = \frac{i^4 G_F \epsilon_j}{\sqrt{2}} \int \frac{d^4 p}{(2\pi)^4} (\mathcal{O}_j + C \mathcal{O}_j^T C^{-1}) S_F(p) (\bar{\mathcal{O}}_j + C \bar{\mathcal{O}}_j^T C^{-1}) \left( 1 + \frac{q_\mu q^\mu}{m_\phi^2} \right), \text{ where } q_\mu = k_\mu - p_\mu \quad (\text{C.19})$$

denotes the difference between the neutrino momentum  $k$  and four-velocity of the medium  $u$ . The extra factors with charge conjugation matrix comes from the Majorana Feynman rules [31].

In finite-temperature field theory (FTFT) formalism, fermion propagator

$$S_F(p) = (\not{p} + m_l) \left[ \frac{1}{p^2 - m_l^2} + 2\pi i \delta(p^2 - m_l^2) \eta(p \cdot u) \right], \quad (\text{C.20})$$

where

$$\eta(p \cdot u) = \frac{\theta(p \cdot u)}{e^x + 1} + \frac{\theta(-p \cdot u)}{e^{-x} + 1}, \quad x = \frac{(p \cdot u - \mu)}{T}; \quad (\text{C.21})$$

$\theta(x)$  is the unit step function and  $n_\pm = (e^{\pm x} + 1)^{-1}$  is the occupation number for the background fermions ( $n_+$ ) and anti-fermions ( $n_-$ ) with chemical potential  $\mu$ .

The background-independent part of the fermion propagator only renormalizes the wave function and does not contribute to the dispersion relation in the lowest order [84]. To simplify the calculations, we will only consider background-dependent term,

$$S_F^T(p) = 2\pi i \delta(p^2 - m_l^2) \eta(p \cdot u) (\not{p} + m_l). \quad (\text{C.22})$$

Using  $q_\mu q^\mu = (p - k)^2 \approx -2 p \cdot k$ ,

$$i\Sigma_{\text{eff}}^{(T)} = -\frac{G_F \epsilon_j}{\sqrt{2}} \int \frac{d^4 p}{(2\pi)^4} (\mathcal{O}_j + C \mathcal{O}_j^T C^{-1}) S_F^T(p) (\bar{\mathcal{O}}_j + C \bar{\mathcal{O}}_j^T C^{-1}) \left( 1 - \frac{2p \cdot k}{m_\phi^2} \right). \quad (\text{C.23})$$

There will be an extra minus sign for scalar and pseudoscalar NSSIs which comes from the fact that scalar propagator  $\Delta_\phi = \frac{i}{q^2 - m_\phi^2}$  have an extra minus sign compared to the vector propagator  $\Delta_V = \frac{-ig^{\mu\nu}}{q^2 - m_V^2}$ .

For scalar NSSI with  $\mathcal{O}_S = \mathbb{I}$ ,

$$\begin{aligned}
i\Sigma_{\text{eff}}^{(T)} &= \frac{G_F \epsilon_S}{\sqrt{2}} \int \frac{d^4 p}{(2\pi)^4} (\mathcal{O}_S + C \mathcal{O}_S^\text{T} C^{-1}) S_F^T(p) (\bar{\mathcal{O}}_S + C \bar{\mathcal{O}}_S^\text{T} C^{-1}) \left( 1 - \frac{2p \cdot k}{m_\phi^2} \right) \\
&= \frac{4G_F \epsilon_S}{\sqrt{2}} \int \frac{d^4 p}{(2\pi)^4} S_F^T(p) \left( 1 - \frac{2p \cdot k}{m_\phi^2} \right) \\
&= \frac{4G_F \epsilon_S}{\sqrt{2}} \int \frac{d^4 p}{(2\pi)^4} \cdot 2\pi i \delta(p^2 - m_\nu^2) \eta(p \cdot u) \gamma_\mu p^\mu \cdot \left( 1 - \frac{2p \cdot k}{m_\phi^2} \right) \\
&= \frac{4iG_F \epsilon_S}{\sqrt{2}} \int \frac{d^4 p}{(2\pi)^3} \delta(p^2 - m_\nu^2) \eta(p \cdot u) \gamma_\mu p^\mu \left( 1 - \frac{2p \cdot k}{m_\phi^2} \right). 
\end{aligned} \tag{C.24}$$

Defining two momentum dependent integrals

$$I_\mu = \int \frac{d^4 p}{(2\pi)^3} \delta(p^2 - m_\nu^2) \eta(p \cdot u) p_\mu, \tag{C.25}$$

$$I_{\mu\nu} = \int \frac{d^4 p}{(2\pi)^3} \delta(p^2 - m_\nu^2) \eta(p \cdot u) p_\mu p_\nu, \tag{C.26}$$

we can rewrite Eq. (C.24) as

$$i\Sigma_{\text{eff}}^{(T)} = \frac{4iG_F \epsilon_S}{\sqrt{2}} \gamma^\mu \left[ I_\mu - \frac{2k^\nu}{m_\phi^2} I_{\mu\nu} \right] \tag{C.27}$$

We can calculate integral  $I_\mu = Au_\mu$ , which is manifestly covariant and has only  $u_\mu$  dependence, by contracting with  $u^\mu$ .

$$I_\mu u^\mu = Au_\mu u^\mu = A = \int \frac{d^4 p}{(2\pi)^3} \delta(p^2 - m_\nu^2) \eta(p \cdot u) p_\mu u^\mu = J_1^{(\nu)}. \tag{C.28}$$

Where  $J_n^{(f)}$  is defined as  $J_n^{(f)} = \int \frac{d^4 p}{(2\pi)^3} \delta(p^2 - m_f^2) \eta(p \cdot u) (p \cdot u)^n$  and calculated in the last section.

Now we have

$$I_\mu = J_1^{(\nu)} u_\mu. \tag{C.29}$$

Similarly,  $I_{\mu\nu}$ , can be obtained by contracting  $I_{\mu\nu} = Ag_{\mu\nu} + Bu_\mu u_\nu$  with  $u_\mu u_\nu$  and  $g_{\mu\nu}$ .

$$g^{\mu\nu} I_{\mu\nu} = \int \frac{d^4 p}{(2\pi)^3} \delta(p^2 - m_\nu^2) \eta(p \cdot u) p_\mu g^{\mu\nu} p_\nu = m_\nu^2 J_0^{(\nu)} = 4A + B \tag{C.30}$$

$$u^\mu u^\nu I_{\mu\nu} = \int \frac{d^4 p}{(2\pi)^3} \delta(p^2 - m_\nu^2) \eta(p \cdot u) p_\mu u^\mu u^\nu p_\nu = J_2^{(\nu)} = A + B \tag{C.31}$$

Solving for  $A$  and  $B$ , we get

$$A = \frac{1}{3} (m_\nu^2 J_0^{(\nu)} - J_2^{(\nu)}) , \tag{C.32}$$

$$B = \frac{1}{3} (4J_2^{(\nu)} - m_\nu^2 J_0^{(\nu)}) . \tag{C.33}$$

Substituting these expressions for  $I_\mu$  and  $I_{\mu\nu}$  into Eq. (C.27),

$$i\Sigma_{\text{eff}}^{(T)} = \frac{4iG_F\epsilon_S}{\sqrt{2}} \left[ J_1^{(\nu)} \not{u} - \frac{2\gamma^\mu k^\nu}{3m_\phi^2} (m_\nu^2 J_0^{(\nu)} - J_2^{(\nu)}) g_{\mu\nu} - \frac{2\gamma^\mu k^\nu}{3m_\phi^2} (4J_2^{(\nu)} - m_\nu^2 J_0^{(\nu)}) u_\mu u_\nu \right] \quad (\text{C.34})$$

$$= \frac{4iG_F\epsilon_S}{\sqrt{2}} \left[ J_1^{(\nu)} \not{u} - \frac{2}{3m_\phi^2} (m_\nu^2 J_0^{(\nu)} - J_2^{(\nu)}) \not{k} - \frac{2\omega}{3m_\phi^2} (4J_2^{(\nu)} - m_\nu^2 J_0^{(\nu)}) \not{u} \right] \quad (\text{C.35})$$

Taking neutrino mass  $m_\nu \approx 0$ ,

$$i\Sigma_{\text{eff}}^{(T)} = \frac{4iG_F\epsilon_S}{\sqrt{2}} \left[ -\frac{2J_2^{(\nu)}}{3m_\phi^2} \not{k} + \left( J_1^{(\nu)} - \frac{8\omega}{3m_\phi^2} J_2^{(\nu)} \right) \not{u} \right]. \quad (\text{C.36})$$

Now comparing Eq. (C.36) with  $\Sigma_{\text{eff}}^{(T)} = a_0 \not{k} + b_0 \not{u}$ ,

$$b_0 = \frac{4G_F\epsilon_S}{\sqrt{2}} \left( J_1^{(\nu)} - \frac{8\omega}{3m_\phi^2} J_2^{(\nu)} \right). \quad (\text{C.37})$$

From the calculation of  $J_n^{(\nu)}$  provided in the end,

$$b_0 = \frac{4G_F}{\sqrt{2}} \epsilon_S \left[ \frac{1}{2} (n_\nu - n_{\bar{\nu}}) - \frac{8\omega}{3m_\phi^2} \cdot \frac{1}{2} (n_\nu \langle E_\nu \rangle + n_{\bar{\nu}} \langle E_{\bar{\nu}} \rangle) \right] \quad (\text{C.38})$$

The first term becomes zero if we assume lepton symmetric universe. Then scalar NSSI thermal potential at the lowest order in  $\omega$ ,

$$\mathcal{V}_S = -\frac{7\sqrt{2}\pi^2 G_F\epsilon_S}{45m_\phi^2} \cdot \omega T^4 \quad (\text{C.39})$$

Similarly for an axial vector NSSI with  $\Gamma_A = \gamma_\mu \gamma^5$ ,

$$\mathcal{V}_A = -\frac{14\sqrt{2}\pi^2 G_F\epsilon_A}{45m_\phi^2} \cdot \omega T^4, \quad (\text{C.40})$$

and a pseudoscalar NSSI with  $\Gamma_P = i\gamma^5$ ,

$$\mathcal{V}_P = -\frac{7\sqrt{2}\pi^2 G_F\epsilon_P}{45m_\phi^2} \cdot \omega T^4. \quad (\text{C.41})$$

**Evaluating  $J_n^{(f)}$**

$$J_n^{(f)} = \int \frac{d^4 p}{(2\pi)^3} \delta(p^2 - m_f^2) \eta(p \cdot u) (p \cdot u)^n, \quad (\text{C.42})$$

with

$$\eta(p \cdot u) = \frac{\theta(p \cdot u)}{\exp(\frac{p \cdot u - \mu}{T}) + 1} + \frac{\theta(-p \cdot u)}{\exp(-\frac{p \cdot u - \mu}{T}) + 1}. \quad (\text{C.43})$$

In the rest frame of the medium  $u_\mu = (1, 0, 0, 0)$ ,

$$\eta(p \cdot u) = \frac{\theta(p_0)}{\exp(\frac{p_0 - \mu}{T}) + 1} + \frac{\theta(-p_0)}{\exp(-\frac{p_0 - \mu}{T}) + 1} = \theta(p_0) f_f(p_0) + \theta(-p_0) f_{\bar{f}}(-p_0), \quad (\text{C.44})$$

where,  $f_{f,\bar{f}}$  represent the particle and antiparticle momentum distributions

$$f_{f,\bar{f}}(E) = \frac{1}{e^{\beta(E \mp \mu)} + 1}$$

with number density

$$n_{f,\bar{f}} = g_f \int \frac{d^3 \mathbf{p}}{(2\pi)^3} f_{f,\bar{f}},$$

and thermal average of a quantity  $\mathcal{E}^n$ ,

$$\langle \mathcal{E}_{f,\bar{f}}^n \rangle \equiv \frac{g_f}{n_{f,\bar{f}}} \int \frac{d^3 \mathbf{p}}{(2\pi)^3} \mathcal{E}^n f_{f,\bar{f}}.$$

Restructuring Dirac- $\delta$  function,

$$\begin{aligned} \delta(p^2 - m_f^2) &= \delta((p - m_f)(p + m_f)) = \delta(p_0^2 - \mathbf{p}^2 - m_f^2) = \delta(p_0^2 - \omega_p^2) = \delta((p_0 - \omega_p)(p_0 + \omega_p)) \\ &= \frac{1}{2\omega_p} (\delta(p_0 - \omega_p) + \delta(p_0 + \omega_p)), \text{ where } \omega_p = \sqrt{\mathbf{p}^2 + m_f^2} = E_p \end{aligned}$$

Now  $J_n^{(f)}$  can be written as

$$\begin{aligned} J_n^{(f)} &= \int \frac{d^4 p}{(2\pi)^3} \delta(p^2 - m_f^2) \eta(p \cdot u) (p \cdot u)^n \\ &= \int \frac{d^3 \mathbf{p} dp_0}{(2\pi)^3} \frac{1}{2\omega_p} (\delta(p_0 - \omega_p) + \delta(p_0 + \omega_p)) (\theta(p_0) f_f(p_0) + \theta(-p_0) f_{\bar{f}}(-p_0)) (p_0)^n \\ &= \int \frac{d^3 \mathbf{p}}{(2\pi)^3} \left( \frac{\omega_p^n}{2\omega_p} f_f(\omega_p) + \frac{(-\omega_p)^n}{2\omega_p} f_{\bar{f}}(\omega_p) \right) \\ &= \frac{1}{2} \int \frac{d^3 \mathbf{p}}{(2\pi)^3} \left( E_f^{n-1} f_f(E_p) + (-1)^n E_{\bar{f}}^{n-1} f_{\bar{f}}(E_p) \right) \\ &= \frac{1}{2} \left( \frac{n_f}{g_f} \langle E_f^{n-1} \rangle + (-1)^n \frac{n_{\bar{f}}}{g_{\bar{f}}} \langle E_{\bar{f}}^{n-1} \rangle \right). \end{aligned} \quad (\text{C.45})$$

For neutrinos with  $g_\nu = g_{\bar{\nu}} = 1$ ,

$$J_1^{(\nu)} = \frac{1}{2} \left( \frac{n_\nu}{g_\nu} - \frac{n_{\bar{\nu}}}{g_{\bar{\nu}}} \right) = \frac{1}{2} (n_\nu - n_{\bar{\nu}}), \quad (\text{C.46})$$

$$J_2^{(\nu)} = \frac{1}{2} (n_\nu \langle E_\nu \rangle + n_{\bar{\nu}} \langle E_{\bar{\nu}} \rangle) = \frac{7\pi^2 T^4}{240}, \quad (\text{C.47})$$

where number density and average energies are numerically calculated for a massless fermion.

# Bibliography

- [1] Howard E. Haber and Gordon L. Kane. “The Search for Supersymmetry: Probing Physics Beyond the Standard Model”. In: *Phys. Rept.* 117 (1985), pp. 75–263. DOI: [10.1016/0370-1573\(85\)90051-1](https://doi.org/10.1016/0370-1573(85)90051-1).
- [2] N. Aghanim et al. “Planck 2018 results. VI. Cosmological parameters”. In: *Astron. Astrophys.* 641 (2020). [Erratum: *Astron. Astrophys.* 652, C4 (2021)], A6. DOI: [10.1051/0004-6361/201833910](https://doi.org/10.1051/0004-6361/201833910). arXiv: [1807.06209 \[astro-ph.CO\]](https://arxiv.org/abs/1807.06209).
- [3] Henri Poincaré. “The milky way and the theory of gases”. In: *Popular Astronomy* 14 (1906), pp. 475–488.
- [4] Fritz Zwicky. “Die rotverschiebung von extragalaktischen nebeln”. In: *Helvetica physica acta* 6 (1933), pp. 110–127.
- [5] Gianfranco Bertone and Dan Hooper. “History of dark matter”. In: *Reviews of Modern Physics* 90.4 (2018). ISSN: 1539-0756. DOI: [10.1103/revmodphys.90.045002](https://doi.org/10.1103/revmodphys.90.045002). URL: <http://dx.doi.org/10.1103/RevModPhys.90.045002>.
- [6] M. Markevitch et al. “Direct Constraints on the Dark Matter SelfInteraction Cross Section from the Merging Galaxy Cluster 1E 065756”. In: *The Astrophysical Journal* 606.2 (2004), pp. 819824. ISSN: 1538-4357. DOI: [10.1086/383178](https://doi.org/10.1086/383178). URL: <http://dx.doi.org/10.1086/383178>.
- [7] Marco Taoso, Gianfranco Bertone, and Antonio Masiero. “Dark matter candidates: a ten-point test”. In: *Journal of Cosmology and Astroparticle Physics* 2008.03 (2008), p. 022. ISSN: 1475-7516. DOI: [10.1088/1475-7516/2008/03/022](https://doi.org/10.1088/1475-7516/2008/03/022). URL: <http://dx.doi.org/10.1088/1475-7516/2008/03/022>.
- [8] Benjamin W. Lee and Steven Weinberg. “Cosmological Lower Bound on Heavy-Neutrino Masses”. In: *Phys. Rev. Lett.* 39 (4 1977), pp. 165–168. DOI: [10.1103/PhysRevLett.39.165](https://doi.org/10.1103/PhysRevLett.39.165). URL: <https://link.aps.org/doi/10.1103/PhysRevLett.39.165>.
- [9] Giorgio Arcadi et al. “The waning of the WIMP? A review of models, searches, and constraints”. In: *The European Physical Journal C* 78.3 (2018). ISSN: 1434-6052. DOI: [10.1140/epjc/s10052-018-5662-y](https://doi.org/10.1140/epjc/s10052-018-5662-y). URL: <http://dx.doi.org/10.1140/epjc/s10052-018-5662-y>.
- [10] Francesca Chadha-Day, John Ellis, and David J. E. Marsh. *Axion Dark Matter: What is it and Why Now?* 2021. arXiv: [2105.01406 \[hep-ph\]](https://arxiv.org/abs/2105.01406).
- [11] Alexander Merle. *Sterile Neutrino Dark Matter*. IOP, Mar. 2017. ISBN: 978-1-68174-480-3, 978-1-68174-481-0. DOI: [10.1088/978-1-6817-4481-0](https://doi.org/10.1088/978-1-6817-4481-0).
- [12] B Pontecorvo. “Inverse  $\beta$ -processes and lepton charge nonconservation”. In: *Zh. Eksp. Teor. Fiz.* 34 (1958), p. 247.
- [13] Bruno Pontecorvo. “Mesonium and antimesonium”. In: *Soviet Journal of Experimental and Theoretical Physics* 6 (1958), p. 429.

- [14] M.C. Gonzalez-Garcia, Michele Maltoni, and Thomas Schwetz. “Global analyses of neutrino oscillation experiments”. In: *Nuclear Physics B* 908 (2016), pp. 199217. ISSN: 0550-3213. DOI: [10.1016/j.nuclphysb.2016.02.033](https://doi.org/10.1016/j.nuclphysb.2016.02.033). URL: <http://dx.doi.org/10.1016/j.nuclphysb.2016.02.033>.
- [15] R N Mohapatra et al. “Theory of neutrinos: a white paper”. In: *Reports on Progress in Physics* 70.11 (2007), pp. 17571867. ISSN: 1361-6633. DOI: [10.1088/0034-4885/70/11/r02](https://doi.org/10.1088/0034-4885/70/11/r02). URL: <http://dx.doi.org/10.1088/0034-4885/70/11/R02>.
- [16] Joachim Wolf. “The KATRIN neutrino mass experiment”. In: *Nuclear Instruments and Methods in Physics Research Section A: Accelerators, Spectrometers, Detectors and Associated Equipment* 623.1 (2010), pp. 442444. ISSN: 0168-9002. DOI: [10.1016/j.nima.2010.03.030](https://doi.org/10.1016/j.nima.2010.03.030). URL: <http://dx.doi.org/10.1016/j.nima.2010.03.030>.
- [17] Susanne Mertens et al. “A novel detector system for KATRIN to search for keV-scale sterile neutrinos”. In: *J. Phys. G* 46.6 (2019), p. 065203. DOI: [10.1088/1361-6471/ab12fe](https://doi.org/10.1088/1361-6471/ab12fe). arXiv: [1810.06711 \[physics.ins-det\]](https://arxiv.org/abs/1810.06711).
- [18] L. Gastaldo et al. “The electron capture in<sup>163</sup>Ho experiment – ECHo”. In: *Eur. Phys. J. ST* 226.8 (2017), pp. 1623–1694. DOI: [10.1140/epjst/e2017-70071-y](https://doi.org/10.1140/epjst/e2017-70071-y).
- [19] CJ Martoff et al. “HUNTER: precision massive-neutrino search based on a laser cooled atomic source”. In: *Quantum Science and Technology* 6.2 (2021), p. 024008.
- [20] Cristina Benso et al. “Prospects for finding sterile neutrino dark matter at KATRIN”. In: *Physical Review D* 100.11 (2019). ISSN: 2470-0029. DOI: [10.1103/physrevd.100.115035](https://doi.org/10.1103/physrevd.100.115035). URL: <http://dx.doi.org/10.1103/PhysRevD.100.115035>.
- [21] Joachim Kopp. “Sterile Neutrinos as Dark Matter Candidates”. In: *Les Houches summer school on Dark Matter*. Sept. 2021. arXiv: [2109.00767 \[hep-ph\]](https://arxiv.org/abs/2109.00767).
- [22] Esra Bulbul et al. “Detection of An Unidentified Emission Line in the Stacked X-ray spectrum of Galaxy Clusters”. In: *Astrophys. J.* 789 (2014), p. 13. DOI: [10.1088/0004-637X/789/1/13](https://doi.org/10.1088/0004-637X/789/1/13). arXiv: [1402.2301 \[astro-ph.CO\]](https://arxiv.org/abs/1402.2301).
- [23] Alexey Boyarsky et al. “Unidentified Line in X-Ray Spectra of the Andromeda Galaxy and Perseus Galaxy Cluster”. In: *Phys. Rev. Lett.* 113 (2014), p. 251301. DOI: [10.1103/PhysRevLett.113.251301](https://doi.org/10.1103/PhysRevLett.113.251301). arXiv: [1402.4119 \[astro-ph.CO\]](https://arxiv.org/abs/1402.4119).
- [24] Laurie M Brown. “The idea of the neutrino”. In: *Physics Today* 31.9 (1978), p. 23.
- [25] E. Giannetto et al. “Are Muon Neutrinos Faster Than Light Particles?: Possible Consequences for Neutrino Oscillations”. In: *Phys. Lett. B* 178 (1986), pp. 115–120. DOI: [10.1016/0370-2693\(86\)90480-6](https://doi.org/10.1016/0370-2693(86)90480-6).
- [26] Y. Fukuda et al. “Neutrino-induced upward stopping muons in Super-Kamiokande”. In: *Physics Letters B* 467.3-4 (1999), pp. 185193. ISSN: 0370-2693. DOI: [10.1016/s0370-2693\(99\)01188-0](https://doi.org/10.1016/s0370-2693(99)01188-0). URL: [http://dx.doi.org/10.1016/S0370-2693\(99\)01188-0](http://dx.doi.org/10.1016/S0370-2693(99)01188-0).
- [27] Q. R. Ahmad et al. “Direct Evidence for Neutrino Flavor Transformation from Neutral-Current Interactions in the Sudbury Neutrino Observatory”. In: *Physical Review Letters* 89.1 (2002). ISSN: 1079-7114. DOI: [10.1103/physrevlett.89.011301](https://doi.org/10.1103/physrevlett.89.011301). URL: <http://dx.doi.org/10.1103/PhysRevLett.89.011301>.

- [28] Ivan Esteban et al. “The fate of hints: updated global analysis of three-flavor neutrino oscillations”. In: *Journal of High Energy Physics* 2020.9 (2020). ISSN: 1029-8479. DOI: [10.1007/jhep09\(2020\)178](https://doi.org/10.1007/jhep09(2020)178). URL: [http://dx.doi.org/10.1007/JHEP09\(2020\)178](http://dx.doi.org/10.1007/JHEP09(2020)178).
- [29] Carlo Giunti and Chung W. Kim. *Fundamentals of Neutrino Physics and Astrophysics*. 2007. ISBN: 978-0-19-850871-7.
- [30] Particle Data Group et al. “Review of particle physics”. In: *Progress of Theoretical and Experimental Physics* 2020.8 (2020), p. 083C01.
- [31] Palash B. Pal. “Dirac, Majorana, and Weyl fermions”. In: *American Journal of Physics* 79.5 (2011), pp. 485498. ISSN: 1943-2909. DOI: [10.1119/1.3549729](https://doi.org/10.1119/1.3549729). URL: <http://dx.doi.org/10.1119/1.3549729>.
- [32] Kevork N Abazajian et al. “Light sterile neutrinos: a white paper”. In: *arXiv preprint arXiv:1204.5379* (2012).
- [33] M. Drewes et al. “A White Paper on keV Sterile Neutrino Dark Matter”. In: *JCAP* 01 (2017), p. 025. DOI: [10.1088/1475-7516/2017/01/025](https://doi.org/10.1088/1475-7516/2017/01/025). arXiv: [1602.04816 \[hep-ph\]](https://arxiv.org/abs/1602.04816).
- [34] Marco Drewes. “The Phenomenology of Right Handed Neutrinos”. In: *Int. J. Mod. Phys. E* 22 (2013), p. 1330019. DOI: [10.1142/S0218301313300191](https://doi.org/10.1142/S0218301313300191). arXiv: [1303.6912 \[hep-ph\]](https://arxiv.org/abs/1303.6912).
- [35] Marco Drewes et al. “Leptogenesis with GeV-Scale Right-Handed Neutrinos”. In: *Journal of Physics: Conference Series*. Vol. 873. 1. IOP Publishing. 2017, p. 012027.
- [36] S. M. Bilenky and C. Giunti. “Neutrinoless Double-Beta Decay: a Probe of Physics Beyond the Standard Model”. In: *Int. J. Mod. Phys. A* 30.04n05 (2015), p. 1530001. DOI: [10.1142/S0217751X1530001X](https://doi.org/10.1142/S0217751X1530001X). arXiv: [1411.4791 \[hep-ph\]](https://arxiv.org/abs/1411.4791).
- [37] Pablo F de Salas et al. “Neutrino mass ordering from oscillations and beyond: 2018 status and future prospects”. In: *Frontiers in Astronomy and Space Sciences* 5 (2018), p. 36.
- [38] Lincoln Wolfenstein. “Neutrino oscillations in matter”. In: *Physical Review D* 17.9 (1978), p. 2369.
- [39] S. P. Mikheyev and A. Yu. Smirnov. “Resonance Amplification of Oscillations in Matter and Spectroscopy of Solar Neutrinos”. In: *Sov. J. Nucl. Phys.* 42 (1985), pp. 913–917.
- [40] S. P. Rosen and J. M. Gelb. “Mikheyev-Smirnov-Wolfenstein enhancement of oscillations as a possible solution to the solar-neutrino problem”. In: *Phys. Rev. D* 34 (4 1986), pp. 969–979. DOI: [10.1103/PhysRevD.34.969](https://doi.org/10.1103/PhysRevD.34.969). URL: <https://link.aps.org/doi/10.1103/PhysRevD.34.969>.
- [41] Edward W. Kolb and Michael S. Turner. *The Early Universe*. Vol. 69. 1990. ISBN: 978-0-201-62674-2.
- [42] R. Cowsik and J. McClelland. “An Upper Limit on the Neutrino Rest Mass”. In: *Phys. Rev. Lett.* 29 (1972), pp. 669–670. DOI: [10.1103/PhysRevLett.29.669](https://doi.org/10.1103/PhysRevLett.29.669).
- [43] Lawrence J. Hall et al. “Freeze-In Production of FIMP Dark Matter”. In: *JHEP* 03 (2010), p. 080. DOI: [10.1007/JHEP03\(2010\)080](https://doi.org/10.1007/JHEP03(2010)080). arXiv: [0911.1120 \[hep-ph\]](https://arxiv.org/abs/0911.1120).
- [44] Paul Langacker. “On the cosmological production of light sterile-neutrinos”. In: *Report UPR-0401T* (1989).

- [45] Scott Dodelson and Lawrence M. Widrow. “Sterile neutrinos as dark matter”. In: *Physical Review Letters* 72.1 (1994), pp. 1720. ISSN: 0031-9007. DOI: [10.1103/physrevlett.72.17](https://doi.org/10.1103/physrevlett.72.17). URL: <http://dx.doi.org/10.1103/PhysRevLett.72.17>.
- [46] Kerstin Perez et al. “Almost closing the  $\nu$ MSM sterile neutrino dark matter window with NuSTAR”. In: *Phys. Rev. D* 95.12 (2017), p. 123002. DOI: [10.1103/PhysRevD.95.123002](https://doi.org/10.1103/PhysRevD.95.123002). arXiv: [1609.00667 \[astro-ph.HE\]](https://arxiv.org/abs/1609.00667).
- [47] Kenny C. Y. Ng et al. “New Constraints on Sterile Neutrino Dark Matter from *NuSTAR* M31 Observations”. In: *Phys. Rev. D* 99 (2019), p. 083005. DOI: [10.1103/PhysRevD.99.083005](https://doi.org/10.1103/PhysRevD.99.083005). arXiv: [1901.01262 \[astro-ph.HE\]](https://arxiv.org/abs/1901.01262).
- [48] Alexander Merle, Aurel Schneider, and Maximilian Totzauer. “Dodelson-Widrow production of sterile neutrino Dark Matter with non-trivial initial abundance”. In: *Journal of Cosmology and Astroparticle Physics* 2016.04 (2016), pp. 003003. ISSN: 1475-7516. DOI: [10.1088/1475-7516/2016/04/003](https://doi.org/10.1088/1475-7516/2016/04/003). URL: <http://dx.doi.org/10.1088/1475-7516/2016/04/003>.
- [49] K. Enqvist, K. Kainulainen, and J. Maalampi. “Refraction and Oscillations of Neutrinos in the Early Universe”. In: *Nucl. Phys. B* 349 (1991), pp. 754–790. DOI: [10.1016/0550-3213\(91\)90397-G](https://doi.org/10.1016/0550-3213(91)90397-G).
- [50] Kari Enqvist, K Kainulainen, and Jukka Maalampi. “Resonant neutrino transitions and nucleosynthesis”. In: *Physics Letters B* 249.3-4 (1990), pp. 531–534.
- [51] Xiangdong Shi and George M Fuller. “New dark matter candidate: Nonthermal sterile neutrinos”. In: *Physical Review Letters* 82.14 (1999), p. 2832.
- [52] Sacha Davidson, Enrico Nardi, and Yosef Nir. “Leptogenesis”. In: *Physics Reports* 466.4-5 (2008), pp. 105–177.
- [53] Apostolos Pilaftsis. “The little review on leptogenesis”. In: *Journal of Physics: Conference Series*. Vol. 171. 1. IOP Publishing. 2009, p. 012017.
- [54] Alexander Kusenko. “Sterile neutrinos, dark matter, and the pulsar velocities in models with a Higgs singlet”. In: *Phys. Rev. Lett.* 97 (2006), p. 241301. DOI: [10.1103/PhysRevLett.97.241301](https://doi.org/10.1103/PhysRevLett.97.241301). arXiv: [hep-ph/0609081](https://arxiv.org/abs/hep-ph/0609081).
- [55] Takehiko Asaka, Mikko Laine, and Mikhail Shaposhnikov. “On the hadronic contribution to sterile neutrino production”. In: *JHEP* 06 (2006), p. 053. DOI: [10.1088/1126-6708/2006/06/053](https://doi.org/10.1088/1126-6708/2006/06/053). arXiv: [hep-ph/0605209](https://arxiv.org/abs/hep-ph/0605209).
- [56] Michele Frigerio and Carlos E. Yaguna. “Sterile Neutrino Dark Matter and Low Scale Leptogenesis from a Charged Scalar”. In: *Eur. Phys. J. C* 75.1 (2015), p. 31. DOI: [10.1140/epjc/s10052-014-3252-1](https://doi.org/10.1140/epjc/s10052-014-3252-1). arXiv: [1409.0659 \[hep-ph\]](https://arxiv.org/abs/1409.0659).
- [57] Brian Shuve and Itay Yavin. “Dark matter progenitor: Light vector boson decay into sterile neutrinos”. In: *Phys. Rev. D* 89.11 (2014), p. 113004. DOI: [10.1103/PhysRevD.89.113004](https://doi.org/10.1103/PhysRevD.89.113004). arXiv: [1403.2727 \[hep-ph\]](https://arxiv.org/abs/1403.2727).
- [58] Asmaa Abada, Giorgio Arcadi, and Michele Lucente. “Dark Matter in the minimal Inverse Seesaw mechanism”. In: *JCAP* 10 (2014), p. 001. DOI: [10.1088/1475-7516/2014/10/001](https://doi.org/10.1088/1475-7516/2014/10/001). arXiv: [1406.6556 \[hep-ph\]](https://arxiv.org/abs/1406.6556).
- [59] M. G. Betti et al. “Neutrino physics with the PTOLEMY project: active neutrino properties and the light sterile case”. In: *JCAP* 07 (2019), p. 047. DOI: [10.1088/1475-7516/2019/07/047](https://doi.org/10.1088/1475-7516/2019/07/047). arXiv: [1902.05508 \[astro-ph.CO\]](https://arxiv.org/abs/1902.05508).

- [60] S. Friedrich et al. “Limits on the Existence of sub-MeV Sterile Neutrinos from the Decay of  ${}^7\text{Be}$  in Superconducting Quantum Sensors”. In: *Phys. Rev. Lett.* 126.2 (2021), p. 021803. DOI: [10.1103/PhysRevLett.126.021803](https://doi.org/10.1103/PhysRevLett.126.021803). arXiv: [2010.09603 \[nucl-ex\]](https://arxiv.org/abs/2010.09603).
- [61] A. Nucciotti et al. “Status of the HOLMES Experiment to Directly Measure the Neutrino Mass”. In: *J. Low Temp. Phys.* 193.5-6 (2018), pp. 1137–1145. DOI: [10.1007/s10909-018-2025-x](https://doi.org/10.1007/s10909-018-2025-x). arXiv: [1807.09269 \[physics.ins-det\]](https://arxiv.org/abs/1807.09269).
- [62] Mathieu Guigue. “Status of the Project 8 Phase II”. In: *J. Phys. Conf. Ser.* 1342.1 (2020). Ed. by Ken Clark et al., p. 012025. DOI: [10.1088/1742-6596/1342/1/012025](https://doi.org/10.1088/1742-6596/1342/1/012025). arXiv: [1710.01827 \[physics.ins-det\]](https://arxiv.org/abs/1710.01827).
- [63] Nicholas Steinbrink et al. “keV-Scale sterile neutrino sensitivity estimation with time-of-flight spectroscopy in KATRIN using self-consistent approximate Monte Carlo”. In: *The European Physical Journal C* 78 (2017), pp. 1–14.
- [64] O. Moreno, E. Moya de Guerra, and M. Ramón Medrano. “Warm dark matter sterile neutrinos in electron capture and beta decay spectra”. In: *Adv. High Energy Phys.* 2016 (2016), p. 6318102. DOI: [10.1155/2016/6318102](https://doi.org/10.1155/2016/6318102). arXiv: [1607.02931 \[hep-ph\]](https://arxiv.org/abs/1607.02931).
- [65] *Neutrino Non-Standard Interactions: A Status Report*. Vol. 2. 2019, p. 001. DOI: [10.21468/SciPostPhysProc.2.001](https://doi.org/10.21468/SciPostPhysProc.2.001). arXiv: [1907.00991 \[hep-ph\]](https://arxiv.org/abs/1907.00991).
- [66] Ivan Esteban et al. “Updated constraints on non-standard interactions from global analysis of oscillation data”. In: *JHEP* 08 (2018). [Addendum: *JHEP* 12, 152 (2020)], p. 180. DOI: [10.1007/JHEP08\(2018\)180](https://doi.org/10.1007/JHEP08(2018)180). arXiv: [1805.04530 \[hep-ph\]](https://arxiv.org/abs/1805.04530).
- [67] Pilar Coloma et al. “Improved global fit to Non-Standard neutrino Interactions using COHERENT energy and timing data”. In: *JHEP* 02 (2020). [Addendum: *JHEP* 12, 071 (2020)], p. 023. DOI: [10.1007/JHEP02\(2020\)023](https://doi.org/10.1007/JHEP02(2020)023). arXiv: [1911.09109 \[hep-ph\]](https://arxiv.org/abs/1911.09109).
- [68] Ingolf Bischer and Werner Rodejohann. “General neutrino interactions from an effective field theory perspective”. In: *Nuclear Physics B* 947 (2019), p. 114746. ISSN: 0550-3213. DOI: [10.1016/j.nuclphysb.2019.114746](https://doi.org/10.1016/j.nuclphysb.2019.114746). URL: <http://dx.doi.org/10.1016/j.nuclphysb.2019.114746>.
- [69] Nikita Blinov et al. “Constraining the Self-Interacting Neutrino Interpretation of the Hubble Tension”. In: *Phys. Rev. Lett.* 123.19 (2019), p. 191102. DOI: [10.1103/PhysRevLett.123.191102](https://doi.org/10.1103/PhysRevLett.123.191102). arXiv: [1905.02727 \[astro-ph.CO\]](https://arxiv.org/abs/1905.02727).
- [70] Mikhail S. Bilenky, Samoil M. Bilenky, and A. Santamaria. “Invisible width of the Z boson and ‘secret’ neutrino-neutrino interactions”. In: *Phys. Lett. B* 301 (1993), pp. 287–291. DOI: [10.1016/0370-2693\(93\)90703-K](https://doi.org/10.1016/0370-2693(93)90703-K).
- [71] Kevork Abazajian, George M. Fuller, and Mitesh Patel. “Sterile neutrino hot, warm, and cold dark matter”. In: *Phys. Rev. D* 64 (2001), p. 023501. DOI: [10.1103/PhysRevD.64.023501](https://doi.org/10.1103/PhysRevD.64.023501). arXiv: [astro-ph/0101524](https://arxiv.org/abs/astro-ph/0101524).
- [72] Tejaswi Venumadhav et al. “Sterile neutrino dark matter: Weak interactions in the strong coupling epoch”. In: *Physical Review D* 94.4 (2016). ISSN: 2470-0029. DOI: [10.1103/physrevd.94.043515](https://doi.org/10.1103/physrevd.94.043515). URL: <http://dx.doi.org/10.1103/PhysRevD.94.043515>.
- [73] Jeremy Bernstein. *Kinetic Theory in the Expanding Universe*. Cambridge Monographs on Mathematical Physics. Cambridge University Press, 1988. DOI: [10.1017/CBO9780511564185](https://doi.org/10.1017/CBO9780511564185).

- [74] Bruce H. J. McKellar and Mark J. Thomson. “Oscillating neutrinos in the early Universe”. In: *Phys. Rev. D* 49 (6 1994), pp. 2710–2728. DOI: [10.1103/PhysRevD.49.2710](https://doi.org/10.1103/PhysRevD.49.2710). URL: <https://link.aps.org/doi/10.1103/PhysRevD.49.2710>.
- [75] G. Sigl and G. Raffelt. “General kinetic description of relativistic mixed neutrinos”. In: *Nucl. Phys. B* 406 (1993), pp. 423–451. DOI: [10.1016/0550-3213\(93\)90175-0](https://doi.org/10.1016/0550-3213(93)90175-0).
- [76] Lucas Johns. “Derivation of the sterile neutrino Boltzmann equation from quantum kinetics”. In: *Phys. Rev. D* 100.8 (2019), p. 083536. DOI: [10.1103/PhysRevD.100.083536](https://doi.org/10.1103/PhysRevD.100.083536). arXiv: [1908.04244 \[hep-ph\]](https://arxiv.org/abs/1908.04244).
- [77] D. Boyanovsky and Chiu Man Ho. “Sterile neutrino production via active-sterile oscillations: The Quantum Zeno effect”. In: *JHEP* 07 (2007), p. 030. DOI: [10.1088/1126-6708/2007/07/030](https://doi.org/10.1088/1126-6708/2007/07/030). arXiv: [hep-ph/0612092](https://arxiv.org/abs/hep-ph/0612092).
- [78] J. Baur. “Determining the mass of cosmological neutrinos using Lyman-alpha forests”. In: 2017.
- [79] Kevin J. Kelly et al. “Origin of sterile neutrino dark matter via secret neutrino interactions with vector bosons”. In: *Physical Review D* 101.11 (2020). ISSN: 2470-0029. DOI: [10.1103/physrevd.101.115031](https://doi.org/10.1103/physrevd.101.115031). URL: <http://dx.doi.org/10.1103/PhysRevD.101.115031>.
- [80] Mirco Cannoni. “Lorentz invariant relative velocity and relativistic binary collisions”. In: *Int. J. Mod. Phys. A* 32.02n03 (2017), p. 1730002. DOI: [10.1142/S0217751X17300022](https://doi.org/10.1142/S0217751X17300022). arXiv: [1605.00569 \[hep-ph\]](https://arxiv.org/abs/1605.00569).
- [81] Takehiko Asaka, Mikko Laine, and Mikhail Shaposhnikov. “Lightest sterile neutrino abundance within the nuMSM”. In: *JHEP* 01 (2007). [Erratum: *JHEP* 02, 028 (2015)], p. 091. DOI: [10.1088/1126-6708/2007/01/091](https://doi.org/10.1088/1126-6708/2007/01/091). arXiv: [hep-ph/0612182](https://arxiv.org/abs/hep-ph/0612182).
- [82] H. Arthur Weldon. “Effective Fermion Masses of Order  $gT$  in High Temperature Gauge Theories with Exact Chiral Invariance”. In: *Phys. Rev. D* 26 (1982), p. 2789. DOI: [10.1103/PhysRevD.26.2789](https://doi.org/10.1103/PhysRevD.26.2789).
- [83] Dirk Notzold and Georg Raffelt. “Neutrino Dispersion at Finite Temperature and Density”. In: *Nucl. Phys. B* 307 (1988), pp. 924–936. DOI: [10.1016/0550-3213\(88\)90113-7](https://doi.org/10.1016/0550-3213(88)90113-7).
- [84] Juan Carlos D’Olivo, Jose F. Nieves, and Manuel Torres. “Finite temperature corrections to the effective potential of neutrinos in a medium”. In: *Phys. Rev. D* 46 (1992), pp. 1172–1179. DOI: [10.1103/PhysRevD.46.1172](https://doi.org/10.1103/PhysRevD.46.1172).
- [85] Julien Lesgourgues. “The Cosmic Linear Anisotropy Solving System (CLASS) I: Overview”. In: (Apr. 2011). arXiv: [1104.2932 \[astro-ph.IM\]](https://arxiv.org/abs/1104.2932).
- [86] Antony Lewis, Anthony Challinor, and Anthony Lasenby. “Efficient computation of CMB anisotropies in closed FRW models”. In: *Astrophys. J.* 538 (2000), pp. 473–476. DOI: [10.1086/309179](https://doi.org/10.1086/309179). arXiv: [astro-ph/9911177](https://arxiv.org/abs/astro-ph/9911177).
- [87] Steen Hannestad, Rasmus Sloth Hansen, and Thomas Tram. “Can active-sterile neutrino oscillations lead to chaotic behavior of the cosmological lepton asymmetry?” In: *JCAP* 04 (2013), p. 032. DOI: [10.1088/1475-7516/2013/04/032](https://doi.org/10.1088/1475-7516/2013/04/032). arXiv: [1302.7279 \[astro-ph.CO\]](https://arxiv.org/abs/1302.7279).

- [88] Lucas Johns and George M. Fuller. “Self-interacting sterile neutrino dark matter: The heavy-mediator case”. In: *Phys. Rev. D* 100 (2 2019), p. 023533. DOI: [10.1103/PhysRevD.100.023533](https://doi.org/10.1103/PhysRevD.100.023533). URL: <https://link.aps.org/doi/10.1103/PhysRevD.100.023533>.
- [89] André de Gouvêa et al. “Dodelson-Widrow Mechanism in the Presence of Self-Interacting Neutrinos”. In: *Physical Review Letters* 124.8 (2020). ISSN: 1079-7114. DOI: [10.1103/physrevlett.124.081802](https://doi.org/10.1103/physrevlett.124.081802). URL: <http://dx.doi.org/10.1103/PhysRevLett.124.081802>.
- [90] M. Paraskevas. “Dirac and Majorana Feynman Rules with four-fermions”. In: (Feb. 2018). arXiv: [1802.02657 \[hep-ph\]](https://arxiv.org/abs/1802.02657).
- [91] Vladyslav Shtabovenko, Rolf Mertig, and Frederik Orellana. “New Developments in FeynCalc 9.0”. In: *Comput. Phys. Commun.* 207 (2016), pp. 432–444. DOI: [10.1016/j.cpc.2016.06.008](https://doi.org/10.1016/j.cpc.2016.06.008). arXiv: [1601.01167 \[hep-ph\]](https://arxiv.org/abs/1601.01167).
- [92] Kevork Abazajian et al. “The Nonlinear cosmological matter power spectrum with massive neutrinos. 1. The Halo model”. In: *Phys. Rev. D* 71 (2005), p. 043507. DOI: [10.1103/PhysRevD.71.043507](https://doi.org/10.1103/PhysRevD.71.043507). arXiv: [astro-ph/0411552](https://arxiv.org/abs/astro-ph/0411552).
- [93] E. M. Silich et al. “A Search for the 3.5 keV Line from the Milky Way’s Dark Matter Halo with HaloSat”. In: *Astrophys. J.* 916.1 (2021), p. 2. DOI: [10.3847/1538-4357/ac043b](https://doi.org/10.3847/1538-4357/ac043b). arXiv: [2105.12252 \[astro-ph.HE\]](https://arxiv.org/abs/2105.12252).
- [94] Evgeny Akhmedov. *Majorana neutrinos and other Majorana particles: Theory and experiment*. 2014. arXiv: [1412.3320 \[hep-ph\]](https://arxiv.org/abs/1412.3320).
- [95] David J Griffiths. *Introduction to elementary particles; 2nd rev. version*. Physics textbook. New York, NY: Wiley, 2008. URL: <https://cds.cern.ch/record/111880>.



## *Acknowledgements*

I would like to thank Prof. Dr. Achim Stahl and Dr. Werner Rodejohann for giving me an opportunity to work on an interesting topic and guiding me with patience. A big thanks to Cristina Benso for her immense support, which was integral to this thesis. I would also like to thank Dr. Manibrata Sen for the collaboration and for sharing his expertise in the field.

Thanks to Valentina for the valuable comments on the draft.

Finally, thanks to my parents for their unconditional support and encouragement to pursue my interests.